New ex vivo models to study the mechanical interplay between muscle cells and their microenvironment

Nicolas Rose

Sorbonne Université

École doctorale 515 : Complexité du Vivant
Programme doctoral Interface Pour le Vivant

Thèse de Doctorat

New *ex vivo* models to study the mechanical interplay between muscle cells and their microenvironment

Par Nicolas ROSE

Réalisée au Centre de Recherche en Myologie
et à l'Institut Jacques Monod

Dirigée par	Dr. Léa TRICHET	Encadrante de thèse
	Dr. Fabien LE GRAND	Directeur de thèse
	Pr. Benoît LADOUX	Co-directeur de thèse

Présentée et soutenue publiquement le 19 Mars 2021
devant le jury composé de :

Président :	Pr. Delphine DUPREZ	Sorbonne Université
Rapporteurs :	Pr. Sylvie HENON	Université de Paris
	Dr. Vincent GACHE	Université Lyon 1
Examinateurs :	Dr. Vanessa RIBES	Université de Paris
	Pr. Edoardo MALFATTI	UPEC / AP-HP
Direction de thèse :	Dr. Léa TRICHET	Sorbonne Université
	Dr. Fabien LE GRAND	Sorbonne Université
	Pr. Benoît LADOUX	Université de Paris

TABLE OF CONTENTS

INTRODUCTION

Chapter A: Key challenges facing *in vitro* study of muscle

A.1 | Bioethical, legal and economic stakes of *in vitro* models

Biology, the study of living organisms and its underlying mechanisms, is essential to the advance of medicine and human understanding of nature. As an experimental science, biological research relies on a systemic approach consisting in testing hypothesis through empirical observations. From Claudius Galenus (129-210) in Antiquity to Leonardo da Vinci (1452-1519) and Andreas Vesalius (1514-1564) during the Renaissance until nowadays, physicians and biologists have been establishing scientific theories on anatomy and physiology based on animal experimentation. This to comprehend the organisation of biological systems, their functional features and reactivity to external stimuli. In these eras, regards were not always given to the fate of the model organisms, as the french physiologist Claude Bernard (1813-1878), one of the father of modern animal experimentation, stated in his Introduction à la médecine expérimentale (Baillière 1865):

« It is essentially moral to do experiences, albeit painful and dangerous, on animals, if it can be useful for mankind. […] The physiologist is not a man of the world; he is a scholar […] he does not hear the cries of animals […] he only sees his idea […] he only perceives organisms hiding from him problems he wants to solve."

Over the XVIIth century, concerns for animal sensitivity grew among biologists. Humphrey Primatt authored in 1776 "A Dissertation on the Duty of Mercy and Sin of Cruelty to Brute Animals", preaching against the infliction of pain to animals, leading to the creation of the Royal Society For the Prevention of Cruelty to Animals in 1824. In France the Société Protectrice des Animaux is founded in 1845, and the Loi Grammont, penalizing any form of cruelty toward animals, is voted in 1850.

The evolution of biologists' perception on animal welfare brought up the question of our legitimacy as subjects conscious of animal nociception and capable of empathy, to use pain sensitive subjects as model for experimental procedures. To solve the dilemma between the necessity to use model organisms for the progress of science and medicine and the moral issue of inflicting suffering to sensitive animals, the scientific community adopted a doctrine based on Utilitarianism as a foundation of an ethical practice of animal experimentation. As developed by Jeremy Bentham in "An Introduction to the Principles of Morals and Legislation (1738)", utility is understood as the principle under which any action must be considered regarding its tendency to increase or decrease the happiness of parties affected by the action. These utilitarian ethics were first implemented to animal experimentation in 1926 by the Universities Federation for Animal Welfare, and eventually theorized by William M. S. Russel and Rex L. Burch in the 1959 "Principles of Humane Experimental Technique" (Methuen, London) and summed up in the "Three Rs". The three Rs (Replacement, Refinement, Reduction) rule consist in : Replacing methods using animals by substitutive ones (*in vitro* methods, computer modelling) or using animals considered "lower" to mammals (e. g. invertebrates) ; Reducing the number of animals used by optimizing experimental design, statistical exploitation and non-invasive imaging to extract more information from a given number of animals ; Refining the experimental protocols to improve the welfare of animals and minimize the stress and pain inflicted.

The IASP (International Association for the Study of Pain) defines pain as an unpleasant sensory and emotional experience associated with actual or potential tissue damage, or described in terms of such damage. Nociception as the neural process of encoding noxious stimuli (automatically e. g. elevated blood pressure, or behaviorally with motor withdrawal reflex and more complex nocifensive behavior) (https://www.iasp-pain.org). The pain can be organic (with identified lesions) or not. Research on nociception in animals has considerably advanced, today the scientific consensus recognizing the capacity to suffer for every species of Mammals and birds (Recognition and Alleviation of Pain in Laboratory Animals p.21). There is also nociception evidence regarding fishes (Sneddon *et al.* 2003) and crustaceans (Elwood *et al.* 2009).

According to the report for the French parliament (9 December 2009) from the Evaluation Office of scientific and technological choices, 12 million animals were used for scientific purposes in Europe during 2009, this value was estimated to be between 22 and 25 million in the United States of America. In 2005, a survey performed on 956 individuals from the United Kingdom revealed that 52% of interrogated people were convinced that scientists did not cause useless suffering to animals. This percentage was in growth compared to 2002 (40%) and 1999 (29%), showing an increase of the trust from the public to the scientific community. According to a Ministère de l'Enseignement Superieur et de la Recherche study: Usage of animals for scientific purposes in French institutions (statistical investigation 2017), in 2016, 1 918 481 animals have been used in France for scientific research, 59.6% of which are mice. These animals have been used for fundamental research (43%) ; Human and veterinary medicine (26%) ; Security, production and quality control of pharmaceutical products (25%) ; Maintenance of genetically modified lineage with deleterious phenotype (3%) ; Teaching and formation (2%) ; Research for species conservation (1%).

There is a permanent call into question from society of the legitimacy, efficiency and control of animal experimentation, which translates into more restrictive regulatory framework from institutional actors defining scientific and ethical evaluations in the last decades. In France, charters were separately signed by public (Charte des comités régionaux d'éthique en expérimentation animale, 2001) and private (Charte du Groupe de réflexion interprofessionnel sur les comités d'éthique appliqués à l'expérimentation animale, 1992) research institutions, before to be fused under a unified agreement (Charte nationale portant sur l'éthique de l'expérimentation animale, 2008) and to be surveyed by a national committee (Comité National de Réflexion Ethique en Expérimentation Animale, 2005). Local ethics committees are also multiplicating within diverse institutions. The Three Rs rule have been included in the European parliament 2010/63 directive **(Figure 1)** and constitute the basis of future scientific projects in regards of their authorization to be pursued. This legislation applies to all vertebrates, from autonomous larvae or fœtal forms at the last third of their development.

DIRECTIVE 2010/63/EU OF THE EUROPEAN PARLIAMENT AND OF THE COUNCIL of 22 September 2010 on the protection of animals used for scientific purposes

Article 4

Principle of replacement, reduction and refinement

1. Member States shall ensure that, wherever possible, a scientifically satisfactory method or testing strategy, not entailing the use of live animals, shall be used instead of a procedure.

2. Member States shall ensure that the number of animals used in projects is reduced to a minimum without compromising the objectives of the project.

3. Member States shall ensure refinement of breeding, accommodation and care, and of methods used in procedures, eliminating or reducing to the minimum any possible pain, suffering, distress or lasting harm to the animals.

4. This Article shall, in the choice of methods, be implemented in accordance with Article 13.

Article 13

Choice of methods

1. Without prejudice to national legislation prohibiting certain types of methods, Member States shall ensure that a procedure is not carried out if another method or testing strategy for obtaining the result sought, not entailing the use of a live animal, is recognised under the legislation of the Union.

2. In choosing between procedures, those which to the greatest extent meet the following requirements shall be selected:

(a) use the minimum number of animals;

(b) involve animals with the lowest capacity to experience pain, suffering, distress or lasting harm;

(c) cause the least pain, suffering, distress or lasting harm;

and are most likely to provide satisfactory results.

3. Death as the end-point of a procedure shall be avoided as far as possible and replaced by early and humane end-points. Where death as the end-point is unavoidable, the procedure shall be designed so as to:

(a) result in the deaths of as few animals as possible; and

(b) reduce the duration and intensity of suffering to the animal to the minimum possible and, as far as possible, ensure a painless death.

Figure 1: Articles 4 and 13 from the directive 2010/63/EU of the European parliament (22/09/2010) on the protection of animals used for scientific purposes.

Cosmetic products (defined as any substance or preparation intended to be applied on various superficial parts of the body or on the teeth and oral mucosae, in order to, exclusively and mainly, wash, perfume, or modify their aspect and/or correct corporal scent and/or protect and maintain them) cannot be tested on animals since 2009, even though there is no alternative method available. This interdiction is also applied in the rest of the EU, in the USA, Israel and India. These standards are on the way to be internationalized.

Because of the legal restrictions, academic research laboratories and the biotechnology industries have to adapt and create new ways to carry out their scientific investigations. This legal necessity also represents a strategic opportunity for these institutions to substantially alleviate the financial costs and logistics related to animal experimentation. Indeed, during 2009 in Switzerland, an animal facility of 40 000 rodents were estimated to cost 8 to 12 million swiss francs (7.57 to 11.36 million euros) per year for maintenance and personnel spendings. The cost of gathered rodent animal facilities from swiss public institutions raise to 82 millions of swiss francs (77.59 millions euros) per year. The hosting of murine subjects also generates logistic limitations due to the rodents' time of maturation, frequency of mating, catering, transport and euthanasia. From all these perspectives it appears crucial to develop new *in vitro* tools to diminish experimental procedures on animals and increase outcomes from sacrificed ones, since *in vivo* and *in vitro* both rely mainly on animal models (*in vitro* often implying a sacrifice to collect tissues) and are complementary.

In vitro methods consist in using cells, organelles and analytical chemistry methods, whereas *ex vivo* methods consist in using organs, tissues and cells samples from an animal. An alternative method is a method which satisfies at least one principle of the Three Rs rule. A substitutive method is an alternative method which replaces animal experimentation. The collection of tissue from a deceased animal not being considered as an experimentation procedure in the French law, most *in vitro* and *ex vivo* methods fall into that last category. *In vitro* methods cannot replace whole organisms since they do not provide a full physiological context. However, these tools are particularly useful as testing platforms to investigate the toxicity or a therapeutical effect toward a given

type of target cells (Worth *et al.* 2014). They can therefore be used upstream of *in vivo* pre-clinical studies.

Tissue engineering is an interesting compromise since it provides 3D structure and a good level of cellular differentiation and diversity approaching *in vivo* tissue conditions. Depending on the biological question investigated, these methods can offer fewer complex models to be analyzed with substantially decreased variability between samples, in addition to important regenerative medicine potential (Clevers 2016). Some promising organoid systems have been developed recently, such as cancer spheres for oncology pharmaceutical research (Weiswald, 2014 ; Cancer spheres, Neoplasia. 2015 Jan; 17(1): 1-15) or artificial skin for the cosmetic industry (L'Oréal Journal of the American Academy of Dermatology, Volume 58, Issue 5, Supplement 2, May 2008, pages S155-S159). There still remains to this day a lack of validated substitution methods compared to the needs of public and private research institutions, hence the challenge of developing new relevant methods to study more features of living organisms more efficiently.

A.2 | Adult Skeletal Muscle

Skeletal muscles are the most prevalent tissues in the human body and represent the majority of our corporal mass. They are attached to the bones by tendons, and are composed by a beam of giant cylindrical multinucleated cells (up to over 1000 nuclei) referred as myofibers (from ancient greek myo-: muscle) **(Figure 2A)**. Skeletal muscles provided metazoans with a tremendously advantageous evolutionary adaptation: the capacity to move in space and generate force *(OpenStax Anatomy and Physiology,* published on May 18, 2016). This function is under the control of the central nervous system and relies on the contractile features of myofibers, allowing to bring tendinous insertions closer, and therefore to attract the osseous segments they are linked to.

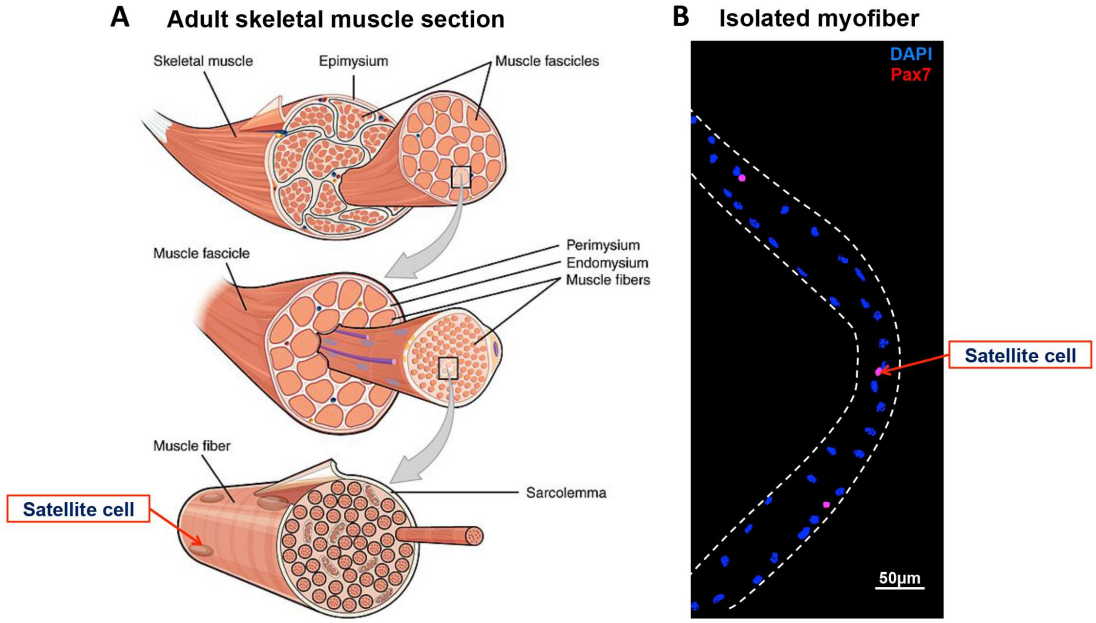

Figure 2: Skeletal muscle anatomy. **A.** Schematic representation of an adult skeletal muscle adapted from the textbook *OpenStax Anatomy and Physiology* (published on May 18, 2016). **B.** Image of an immunofluorescent staining of an isolated mouse myofiber (image from Fabien Le Grand) with satellite cells in red (defined in part A3). Scale bar = 50 µm.

The electrical input from the central nervous system transits via the motoneuron and is transmitted to the muscle fiber by the neuromuscular junction (NMJ) (Schiaffino and Reggiani 2011). This synaptic communication is key for voluntary contraction and thus to our capacity to move freely. Depolarized motoneuron releases a neurotransmitter called Acetylcholine (Ach) in the NMJ. The sarcolemma (from ancient greek sarco-: flesh, and –lemma: sheath), the membrane of the myofiber containing its cytoplasmic content

or sarcoplasm, is covered with Acetylcholine transmembrane receptors (AchR). Sarcolemma porosity to ions allows the potentialization of the myofiber membrane, which is regulated, at rest, by Chloride and Potassium channels (respectively responsible for 70% and 30% of the fiber conductance), and during excitation by Sodium, Calcium channels, Sodium-Potassium and Calcium pumps. Interaction of Ach and AchR in the NMJ is subsequently followed by Sodium influx and Potassium efflux in the sarcoplasm, causing a depolarization in the myofiber (Schiaffino and Reggiani 2011). Once this depolarization reaches a certain threshold, L-type voltage-gated Calcium channels directly trigger an intracellular release of Calcium by Ryanodine receptors (RyR, Calcium channels) from the Sarcoplasmic reticulum, a structure similar to endoplasmic reticulum, storing the Ca2+ to be released in the sarcoplasm, a phenomenon called the "Calcium spark" (a transient and intense increase of Ca2+ cytosolic free concentration), playing a central role in the Excitation-Contraction coupling.

Calcium acts as a multitask intracellular messenger within the myofiber (Schiaffino and Reggiani 2011). Calcium ions bind to Troponin to trigger contraction, to Calmodulin to activate protein phosphorylation/dephosphorylation and to Calcium-dependent proteases to activate proteolysis. Interacting with C-troponin, T-troponin, I-troponin and tropomyosin, which form a regulatory complex, Ca2+ ions increase their ability to activate strong binding between actin and myosin.

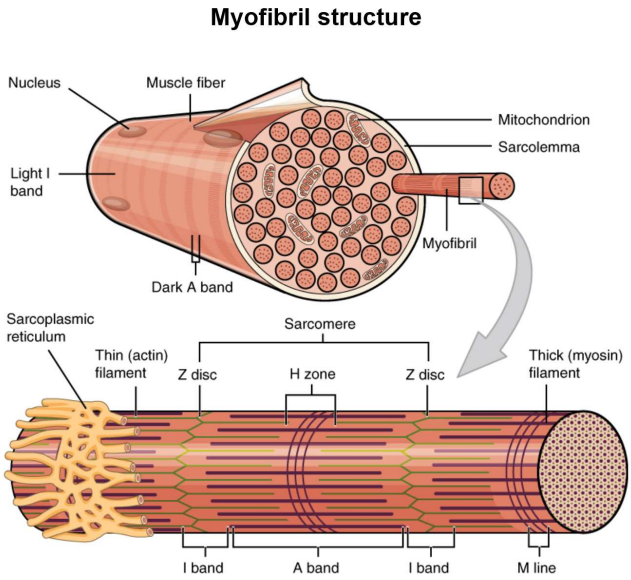

Figure 3: Myofibril structure. Schematic representation of a myofibril from the textbook *OpenStax Anatomy and Physiology* (published on May 18, 2016).

Myofibrils are the contractile apparatus running along the myofiber, organised in periodic segments called sarcomeres, which consist in an overlap of Myosin and Actin filaments **(Figure 3)** *(OpenStax Anatomy and Physiology*, published on May 18, 2016). These filaments are crossed both longitudinally by titin (binding to Myosin) and Nebulin (binding to actin) and transversally by Z disks (actin hubs) and M bands (myosin hubs) **(Figure 5A)**. Sarcomeres are connected to sarcolemma, mitochondria and myofibers' nuclei by extramyofibrillar cytoskeleton composed of Desmin, γ-actin, Plectin and Filamin C. The contractile function of the sarcomere is mediated by the interaction of Actin and Myosin filaments controlled by Ca2+ concentration through regulatory complex (Troponin-Tropomyosin) associated to Actin filaments. The Myosin scaffold acts as an engine that converts ATP chemical bond into movement, whereas Actin acts as a rail track to guide along Myosin advance. Sarcomeric Myosin is an hexamer composed of a tail, which can self-assemble to form thick filaments, and two globular domains ("heads"). These domains have ATP- and Actin-binding sites. In a periodic process, a Myosin molecule binds to ATP, breaks the acto-myosin link ("the rigor complex"), hydrolyses the ATP into ADP+Pi, rebinds to Actin a notch ahead on the thin filament, releases the free Pi and displaces itself to the newly formed rigor complex (Schiaffino and Reggiani 2011) **(Figure 5A)**. This generates movement at the

supramolecular level, which converts into sarcomere shortening by filament sliding. Combined, these sarcomeric shortenings result in muscle contraction.

A motor unit is composed by a motoneuron associated to several myofibers with the same phenotype. The heterogeneity of motor units within a muscle allows it to generate various contraction patterns (Schiaffino and Reggiani 2011). The different fiber phenotypes were first identified by histological coloration, and divided in two types depending on their metabolism. The oxidative metabolism type I “slow fibers”, specialized in low intensity postural function, and the glycolytic metabolism type II “fast fibers”, specialized in faster and more intense contraction. Today, the fiber type is mainly identified regarding the expression of Myosin Heavy Chain (MyHC) isoform, leading to the discovery of new type II phenotypes such as IIa, specialized in repetitive medium contractions, the type IIb, found in rodents but not in humans and specialized in sudden and maximal response, and the types IId and IIx, with intermediate contraction patterns between IIa and IIb. There can be pure or hybrid fiber types hosting different MyHC isoforms. The proportion of fiber phenotypes varies between muscle groups and species, it can also change depending on the neural input and hormonal context to adapt to an external stimulus.

These highly specialized phenotypes present differences in almost all steps of the contraction process and in every actors associated to it, from the NMJ to the myofibril apparatus. First, more Ach is released in type II synapses, increasing the potential amplitude. Acetylcholinesterase, the enzyme degrading the Ach in the NMJ is more active in type II, reducing the length of the contracting stimulus. Fast fibers have higher densities of AchR and voltage-dependent sodium channels, which allows them to respond more rapidly to motor neuron discharge, but also to causing a precocious fatigability.

Then, type II fibers also present more Chloride channels (being both more expressed and less enzymatically degraded than in type I fibers), which explains the difference in values for the resting level of membrane potential (in human type I = -85 mV ; type II = -95 mV) and resistance/unit area (in rats type I = 358 Ω/cm2 ; type II = 588 Ω/cm2). The amplitude of the contraction twitch is determined by the amplitude of the calcium

transient. At rest, the Ca2+ concentration is higher in type I fibers (in rodents, 60nM in type I vs 30nM in type II). Following an action potential, the Ca2+ concentration transient peak is twice as high in fast fibers (19µM vs 9µM and in rats; 2.4µM vs 1.3µM in mouse), conjugated with a twice as fast rate of decline in fast fibers (because of a greater sarcoplasmic reticulum volume for the Calcium uptake). This is notably due to the fact that there are five times more Calcium channels, and twice more RyR which are also more coupled with L-type voltage-gated Calcium channels. Finally, different Myosin Heavy Chain isoforms are expressed in each fiber type, which greatly affects their power generation capacity (Schiaffino and Reggiani 2011). To give a particularly striking representative idea of this difference: the rate of ATP hydrolysis is 22 per second for a "slow" myosin against 131 per second for a "fast" myosin, which also makes this last one run out of ATP much faster.

The muscle fibers are surrounded by connective tissue secreting the extracellular matrix (ECM) which provides an essential structure for its proper function (Gillies and Lieber, 2011), and is subdivided in four layers **(Figure 2A)**:
-Firstly, the basal lamina (constituting the basement membrane with the sarcolemma).
-Secondly, the endomysium, surrounding individual fibers, highly organised in terms of protein composition, with a longitudinal periodicity corresponding to the sarcomeres.
-Thirdly, the perimysium, a thicker Collagen-rich layer surrounding groups of fibers.
-Fourthly, the epimysium surrounding the entire muscle.

Collagen is the major structural protein of skeletal muscle ECM (1-10% of muscle mass dry weight), the spatial distribution of the different isoforms varies depending on the layer (Gillies and Lieber, 2011). The basal lamina is mainly composed of type IV Collagen networks (even though it also contains type VI, XV and XVIII). Glycoproteins like Laminins act as linkers between Collagen IV and the sarcolemma through Integrins, α-dystroglycans and Fibronectin. The endomysium and epimysium are composed evenly by type I and III Collagens, whereas the type I predominates in the perimysium (along with type XII and XIV). Collagen type V associates with the types I and III to form a core and give the rigid feature of the connective tissue.

The ECM is also populated with proteoglycans (PGs) interacting with the collagens to maintain the organization of the matrix (Gillies and Lieber, 2011). They are mainly small leucine-rich PGs (Decorin and Biglycan, binding to Collagen I in the perimysium to inhibit the fibrillogenesis) and heparan sulfate PGs, like Agrin, which is secreted by axons to activate AchR clustering at the NMJ. The ECM is constantly remodelled by synthesis, or digestive enzymes such as Matrix Metalloproteinases (MMPs), which degrade Collagens, Fibronectin, Proteoglycans and Laminin, or Tissue Inhibitors of MMPs (TIMP), which counterbalance MMPs to maintain ECM homeostasis and functional efficiency.

Tendons are collagen-rich (60 to 85% of dry mass) connective tissues arranged in a fibrillary organization, for compartimentalization of damage, able to sustain high tension. The stretching capacity of tendons varies greatly between species and muscle groups (transient increase reaching 16% of total length in rabbit Achilles tendon) (Kjaer 2003). They are essentially constituted of a network of collagens, the type I being the most represented in proportion (60%), followed by the type III (up to 10%). Types IV, V and VI are also present. Tendons also contain proteins like Elastin (2% of the dry mass) and PGs, such as Decorin, Cartilage oligomeric matrix protein, Fibromodulin, Biglycan and Lumican), which promote collagen fibrillogenesis and lubrication of the structure. This tissue is highly supplied in fibroblasts, which support maintenance and reinforcement in case of exercise, but is poor in vasculature compared to the muscle.

In addition to the multinucleated myofibers, there are also various mononucleated cell populations within the muscle associated with diverse types of tissues (Giordani *et al.* 2019). In the connective tissues, fibroblasts produce the majority of the ECM, whereas fibro-adipogenic progenitors (FAPs) and tenocytes are respectively responsible for the maintenance of muscle and tendon homeostasis. The nerves, constituted by motoneurons, have glial cells for support. The immune system, particularly active during regeneration, is effective through B cells, T cells, macrophages and neutrophils. Blood vessels are supported by endothelial cells and perivascular cells (pericytes and smooth muscle cells). Finally, and most importantly, the satellite cells (cells expressing α7-integrin and Vcam1), first observed by Alexander Mauro in 1961 using electronic microscopy examination of frog myofibers (Mauro 1961), were called that way due to

their peripheral location around the fibers **(Figure 2B)**. They are the key actor of muscle regeneration (detailed in the next section).

A.3 | Muscle regeneration

After an acute injury or a mechanical overload, satellite cells are the myogenic progenitors in charge of myofiber reconstitution, a process called myogenesis **(Figure 4)**. These cells (representing 2 to 7% of nuclei in skeletal muscle) have an extraordinary regenerative potential: it was shown that in a radiation ablated muscle (disabling resident satellite cells), the transplant of one myofiber containing only 7 satellite cells was enough to give rise to a hundred new myofibers within the damaged muscle and recreate the satellite cell pool through self-renewal within a week (Collins 2005).

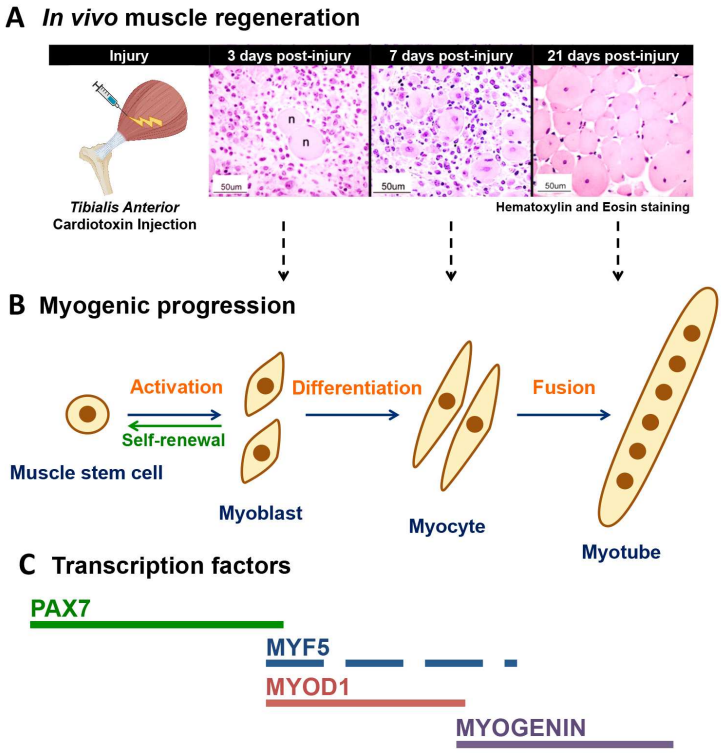

Figure 4: Adult Muscle Regeneration. A. Histological transversal sections of a murine *Tibialis anterior* following a cardiotoxin-induced acute injury, stained with Hematoxylin and Eosin through various timepoints of regeneration (images from Fabien Le Grand, drawing created with BioRender.com). Scale bars = 50 µm. **B.** Schematic representation of a muscle stem cell progression through myogenic differentiation. **C.** Associated transcription factors.

In addition to their primary function in the innate response to infectious or cancerous antigenes, the immune cells such as macrophages, monocytes, neutrophils, eosinophils or T cells are attracted to the wounded tissue by cytokines. They play an important role in muscle regeneration through the inflammatory response rapidly following the muscle necrosis: first by phagocytosis of cell debris, then by promotion of ECM remodelling and angiogenesis (Juban and Chazaud 2017). The latter also regulates myogenesis, generating a complex but essential interplay between these biological processes. Muscle resident and monocyte-derived macrophages intervene in two distinct phases of muscle regeneration. Ly6C-positive pro-inflammatory macrophages are involved in the phagocytosis of necrosed fibers and promote the expansion of proliferating satellite cell descendants called myoblasts and of FAPs **(Figure 4B)**. Ly6C-negative anti-inflammatory macrophages promote the myoblasts exit of cell cycle, their commitment into differentiated myogenic cells called myocytes and their fusion to recreate multinucleated myofibers.

The importance of the ECM remodelling for proper muscle regeneration has been known for a long time (Lluis *et al.* 2001). As an example, damage in muscle tissue is followed by polymerization of circulating Fibrinogen into a Fibrin clot, triggering the inflammatory response. The inactivation of proteases such as urokinase-type plasminogen activator (uPA) in mice causes delayed accumulation of fibrin in the site of injury that leads to impaired regeneration, highlighting the importance of the fibrinolysis step.

During the inflammatory response, the fibroblasts (that originate from FAPs) migrate toward the site of injury and proliferate. They produce new ECM proteins providing both a chemical stimulation and a structural support for myogenesis and NMJs formation (Mann *et al.* 2011). Satellite cells are also capable to produce their own ECM to a lesser extent (mainly collagens I and III). MMPs degrade the remaining ECM of necrosed myofibers, allowing the migration of satellites cells to the wounded site. ECM remodelling is also necessary for angiogenesis.

Satellite cells reside along the myofiber between the sarcolemma and the basal lamina in a microenvironment referred as the “niche”, in an active state of quiescence, maintained

by intracellular signalling pathways. This metabolic state, widespread among unicellular organisms to survive hostile external conditions, is also observed in mammals, allowing stem cell reservoirs to persist and ensure tissue regeneration and homeostasis throughout lifetime. Under the control of external stimuli, satellite cells have the capacity to leave their quiescent state and "activate", entering cell cycle to proliferate and expand in number (Cheung and Rando 2013). The potentiality of quiescent satellite cell activation can vary depending on environmental conditions. Indeed, it is thought that an injury to the muscle induces satellite cells located apart from the damaged tissue to sense systemic stress signals, which leads to a transitory phenotype with distinct morphology (increased cell size), transcriptional profile, metabolism (increased mitochondrial activity), displaying increased activation ability (through mTORC1 pathway), called "GAlert", as opposed to G0 quiescent state (Rodgers *et al.* 2014).

To identify and isolate satellite cells, we search for the expression of specific markers such as the paired-box transcription factor Pax7. Reliable cell surface markers that can be used for Flow cytometry and/or immunolocalization are the following: α7-integrin, Vascular Cell Adhesion Molecule 1 (VCAM-1), the tyrosine-protein kinase Met, M-cadherin, Neural Cell Adhesion Molecule 1 (NCAM1), CD34, CD82 and Syndecan 4 (SDC4). Pax7 is expressed by satellite cells from quiescence to proliferation until they commit to myogenic differentiation **(Figure 4C)**. Pax7 has been shown to be necessary for the regenerative capacity of the satellite cell pool, as the depletion of Pax7-positive cells leads to impaired muscle regeneration (Lepper *et al.* 2011)(Sambasivan *et al.* 2011).

A bHLH transcription factors group composed by Myod1, Myf5, Myogenin and Myf6, also referred as the myogenic regulatory factors (MRFs) regulate the differentiation of myoblasts into myocytes and eventually into new myofibers. Both MYF5 and MYOD1 are expressed during myoblasts proliferation whereas MYOGENIN expression increases during differentiation (while MYOD1 and MRF5 expressions decrease) **(Figure 4C)**. Myf6, like muscle Creatin Kinase, is a late differentiation marker (Rudnicki *et al.* 2008) that controls the niche capacity of mature myofibers (Lazure *et al.* 2020). The myogenic progression of satellite cells into a mature myofibers is self-orchestrated by these regulators. PAX7 upregulates *Myf5* expression (by recruiting histone methyltransferase

complex to *Myf5* locus, leading to histone 3 K4 trimethylation (McKinnell *et al.* 2008)) and MYOD1, although inhibited by PAX7, upregulates *Myogenin expression*, which is essential for terminal differentiation of myoblasts (Comai and Tajbakhsh 2014).

Analyses of isolated single myofibers of Myf5-Cre mice crossed with ROSA-lox-stop-lox-YFP reporter mice showed that 10% of satellite cells never engaged in myogenic commitment and that the division of Pax7+/Myf5- satellite cells gave rise to 2 subpopulations: Pax7+/Myf5- stem cells (mainly from planar symmetric division) and Pax7+/Myf5+ myogenic progenitors (mainly from apical-basal asymmetric division) (Kuang *et al.* 2007). Transplantation of these 2 populations also showed that Pax7+/Myf5- satellite cells had a higher regenerative potential since more satellite cells were observed in the muscle receiving this population compared to the ones receiving Pax7+/Myf5+ cells. The symmetry of satellite stem cell divisions is promoted by Wnt7a-Frizzled7, which plays an essential regulating role in the self-renewal of satellite cells and the maintenance of the stem cell reservoir (Le Grand *et al.* 2009).

The final maturation of a functional myofiber is completed with the assembly of the Actomyosin motors of the contractile myofibril network through a biological process called sarcomerogenesis, which relies on transient microtubule scaffolds and Titin guidance (Braun and Gautel 2011). The Actin filaments and associated proteins (α-actinin and the Z-disk portion of Titin) get first assembled, then the M-line scaffold of Titin and Myomesin is added, and eventually the Myosin filaments are integrated. This process is under the control of the Serum Response Factor (SRF), which controls the transcription of Troponin C, a key regulator of Actin filaments, and of the late differentiation factor MEF2C, which promotes the expression of Myosin filaments and M-line proteins.

The satellite cell contribution to the muscle regeneration process is tightly regulated by physical and chemical constraints of the niche, whether at the immediate environment level or at a further systemic level. First, there are autocrine and paracrine interactions with the adjacent myofibers and neighboring cells. This intercellular dialogue is mainly mediated by Wnt and Notch signaling pathways. The myofiber serves as a basal anchor for the satellite cells with the sarcolemma but also communicates by cell-cell contact

(via Laminins 2, 4 and Dystroglycans) and promotes quiescence through Notch signalling. Cadherins are key components of the adhesive junction between the satellite cells and the adjacent myofiber since depletion of M- cadherin and N-cadherin induces partial activation of satellite cells (Goel *et al.* 2017). On the apical side of the satellite cell immediate surrounding, the basal lamina provides a structural substrate for α7β1 integrins tethering and transmission of physical stimuli from the ECM to the Actin cytoskeleton, triggering activation inter alia. This niche molecule has been shown to be necessary for proper muscle regeneration by knock out in satellite cells (Rozo *et al.* 2016).

Myogenesis is influenced by physiological stimuli from the whole muscle tissue: innervation, vasculature, and connective tissue. Indeed, there are important paracrine exchanges between muscle-resident cells (other myogenic progenitors, motoneurons, interstitial, glial and endothelial cells) and the satellite cells proteoglycans, through the secretion of Wnt glycoproteins or various growth factors such as HGF, fibroblast-secreted FGFs (among which basic fibroblast growth factor (bFGF), a powerful mitogen agent), epidermal growth factor (EGF), Vascular endothelial growth factor (VEGF), insulin-like growth factor isoforms (IGF-I, IGF-II). Motoneurons activate proliferation and inhibit apoptosis of satellite cells, while denervation leads to a decline in satellite cells number. The angiogenesis and myogenesis phenomena are synchronized, endothelial cells promote expansion and then differentiation whereas pericytes and smooth muscle cells promote the return to quiescence. Satellite cells are also sensitive to systemic signals delivered by the vascular network, such as hormones and nutrients, circulating in the organism (Yin *et al.* 2013). Once the formation of myofibril network is effective, the muscle needs mechanical stimulation to properly develop and acquire its structural and physical features to efficiently transmit the generated force (Powell *et al.* 2002).

A.4 | Mechanics of Muscle Contraction

In the last 20 years, the perception of force transmission within the skeletal muscle and how the muscular function is actually carried out from a mechanical standpoint has greatly evolved. For a long time, the generated force was thought to be exclusively transmitted through longitudinal pulling of the myofibril network to the MTJs, but anatomical dissection studies revealed that among mammals, myofibers do not systematically reach the MTJ and are inserted intrafascicularly within the muscle (even though it is not observed in humans), which led the myologists to speculate on an alternative force transmission pathway distributing the tension laterally between contractile fibers (Grounds *et al.* 2005). Ever since, accumulating evidence leads to the hypothesis of a transmission circuit within the muscle, relying on the ECM to transmit the shortenings of sarcomeres.

The slack length of sarcomeres is usually between 1.9 and 2.4µm (Schiaffino and Reggiani 2011). When stretched further than 0.5µm per sarcomere, a relaxed muscle will generate a resistance force referred as the resting tension. The optimum length of a sarcomere to generate an active tension corresponds to the complete overlap of actin and myosin filaments. The further the sarcomere length is from this value, the lesser is the contracting potential. Fast fibers having shorter thin filaments, the most operational length corresponds to smaller sarcomere length in comparison to slow fibers.

A primary transmission chain of the actomyosin-generated force passes by the tendons toward the bone insertions. This tendon-based mechanical scheme is referred as longitudinal force transmission. A secondary force transmission chain relies on sarcolemmal structures called “costameres” (Bloch and Gonzalez-Serratos 2003). Costameres are periodic elements that were observed by electronic microscopy as “rib-like” structures (hence the latin prefix costa-, rib) at the myofiber membrane level above Actin network hubs (Z lines), and Myosin M lines **(Figure 5B)**. These protein complexes are essential links between the contractile apparatus and the sarcolemma, transmitting the movement of each sarcomere to the basement membrane, and manifesting themselves by the appearance of distortions (“bulges”) on the sarcolemma during muscle contraction. These small periodic distortions are key for the force transmission

along the muscle ECM also referred as Lateral Force Transmission (LFT). In addition to their force transmission functions, costameres also have a protective function to avoid excessive stress on the sarcolemma and the myofibril network.

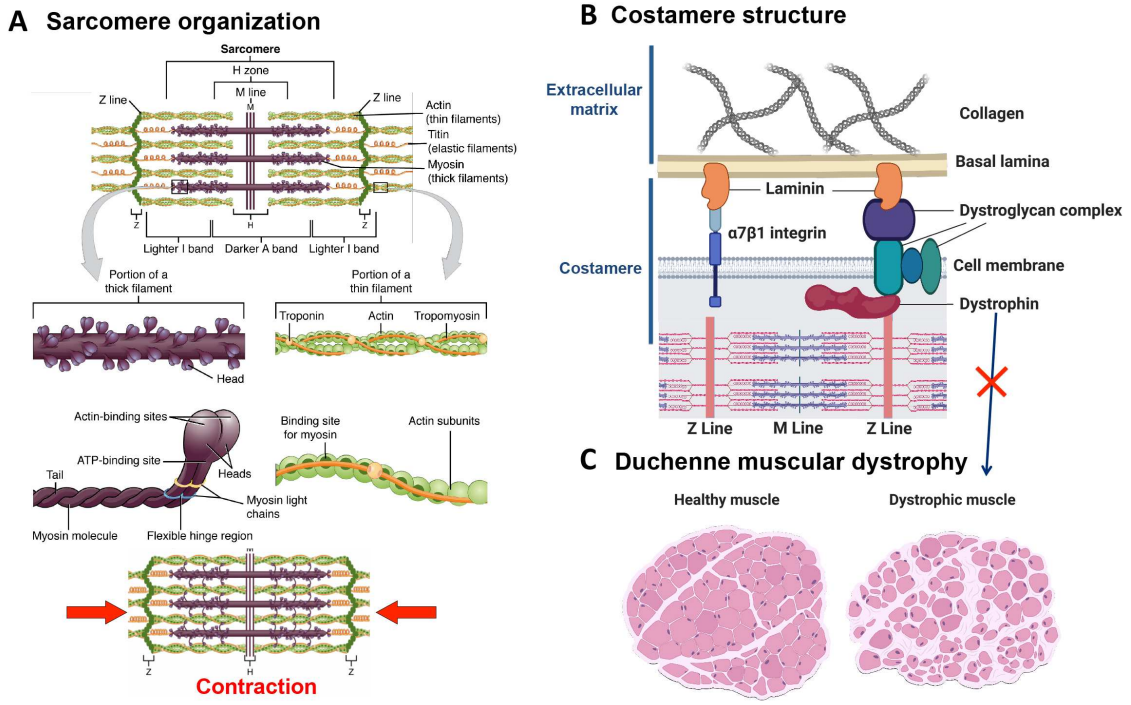

Figure 5: Sarcomere structure and muscle contraction. A. Schematic representation of a sarcomere from the textbook *OpenStax Anatomy and Physiology* (published on May 18, 2016). **B.** Schematic representation of costamere transmembrane protein complex (adaptation created with BioRender.com from *Bloch and Gonzalez 2003*). **C.** Schematic representation of muscle cross sections from healthy (left) and patient with Duchenne muscular dystrophy (right) created with BioRender.com.

Sarcomere Z lines of the Actin network are linked to the sarcolemma transmembrane β-dystroglycan and α7β1 integrins by sarcoplasmic proteins such as α-actinin, Desmin, Cytokeratin, Spectrin, Vinculin, Ankyrin 3 and most importantly, Dystrophin. α-actinin is a crucial protein for the LFT since it constitutes a binder between the different myofibrils to move together and combine their forces **(Figure 5B)**. Along with other transmembrane proteins forming the costamere complex (Sarcospan and Sarcoglycan complex), α7β1 integrins and β-dystroglycans (associated with an α-dystroglycan unit) interact with the laminin residing in the basal lamina, allowing the transmission of force through the basement membrane to the ECM collagen scaffold in the endomysium (Kjaer 2003).

Force measurement on frog single myofibers showed that the force generated was linearly proportional to the radius and not the cross-section area of the fiber, which suggested that the force depends on the perimeter, and therefore on the sarcolemma surface rather than on the sarcoplasmic area that defines the amount of myofibrillar content (Bloch and Gonzalez-Serratos 2003). The LFT was finally proved by a tenotomy (ablation of the tendon) on an isolated rat extensor digitorum longus (EDL) (Zhang and Gao 2014). A silk suture was tied to the distal edge and the muscle clamped on a contractile testing device. The performed force assessment revealed no significant difference of contraction force after the tenotomy, contrarily to the force observed after partial myotomy of the EDL fasciae, proving the prevalence of ECM-borne force transmission throughout the muscle. It has been proposed that more than 50% of the force generated by skeletal muscles is carried to the bones through LFT (Grounds *et al.* 2005).

Arising from the structural and kinetic crucial role of the costamere complex, an impairment in a constitutive protein causes tragically deleterious consequences, like in muscular dystrophies. A mutation in the genes coding for laminins, integrins or dystrophins, making them dysfunctional, causes a deterioration of the costamere apparatus, which inflicts a reduction of the contractile function and injury to the myofibers (Grounds *et al.* 2005) **(Figure 5C)**. This repetitive degeneration-regeneration cycle leads to the exhaustion of the satellite cell reservoir and causes progressive locomotion disability in the long-term. Interestingly, overexpression of α7β1 integrins improves conditions of dystrophin-deficient mice, suggesting a functional redundancy with Dystrophin (Grounds *et al.* 2005). Collagen defects are also sources of myopathic symptoms. Age-related fibrosis (expansion and composition switch of connective tissue) is deleterious to muscle function and regeneration, most likely because of the ECM role in force transmission (Kjaer 2003).

The study of myogenic progression, late maturation, contraction and force transmission in the muscle is facilitated by the use of *in vitro* models (as evoked above, Powell *et al.* 2002).

A.5 | Evolution of Muscle Regeneration Study *in vitro*

In opposition to *in vivo* experiments, happening in a living organism (Cambridge Dictionary), *in vitro* experiments are taking place outside the body (Cambridge Dictionary), literally borrowed from the latin "in glass". Cell extraction from their original tissue of residence, followed by culture in an external medium, to observe survival, amplification or differentiation in order to study their biological properties and functions has been processed since the early 20th century. The first *in vitro* experiment recorded in the scientific literature has controversially been attributed either to Leo Loeb in 1902, who cultivated guinea pig embryo skin-derived epithelial cells and retransplanted them to adults, or to R. G. Harrison in 1907, who produced neural branching from a frog embryo in lymph plasmatic medium (Carrel and Burrows 1911).

In the myology field, an important innovation of *in vitro* muscle regeneration study was the isolation of single myofibers from rat hindlimb skeletal muscle, associated with the culture of mononucleated myogenic precursors, to directly observe the early steps of myogenesis (Bischoff 1975). Nowadays, antibody-based isolation techniques, such as Magnetic-activated cell sorting (MACS) and Fluorescence-activated cell sorting (FACS), which are used in this doctoral research project (Liu *et al.* 2015), allow us to obtain cell populations expressing specific markers, such as satellite cells, with relatively high purity for *ex vivo* experiments, while making abstraction of other systemic and micro-environmental physiological parameters and interactions with other cell types. Moreover, cell isolation allows the exponential amplification of satellite cells into millions of primary myoblasts. These cells can then be used to study myogenic progression from stem cell activation and self-renewal to myocyte fusion (Girardi *et al.* 2020). Our capacity to identify and isolate cell subpopulations is constantly increasing with cutting edge technologies such as mass cytometry (CyTOF) and single-cell RNA-sequencing (scRNA-seq) (Giordani *et al.*2019).

Recently developed models such as Traction Force Microscopy (TFM) or micropatterned substrates allow to study the mechanical properties and mechanosensitivity of single cells (Plotnikov *et al.* 2014 ; Trichet *et al.* 2012). Likewise, the evaluation of forces generated by 3D organoids can be done for various types of tissues (Kural and Billiar

2013). In muscle, which is an organ whose primary function is to physically generate force, it seems crucial to appreciate mechanical stresses involved and to control the physical features of the environment, more than in any other branches of biology research. The challenge is to integrate the interactions between environmental mechanical constraints and muscle cells during myogenesis, hence the necessity to use new *in vitro* systems **(Figure 6)** to study: 1) the physical influences of the niche on satellite cells, which remains mainly unknown, and more precisely the mechanosensitivity of quiescence as described in the **chapter B**. 2) the maturated myotubes mechanics, at stages of development where it has the greatest impact on the environment through resting tension and active contraction, as described in the **chapter C**.

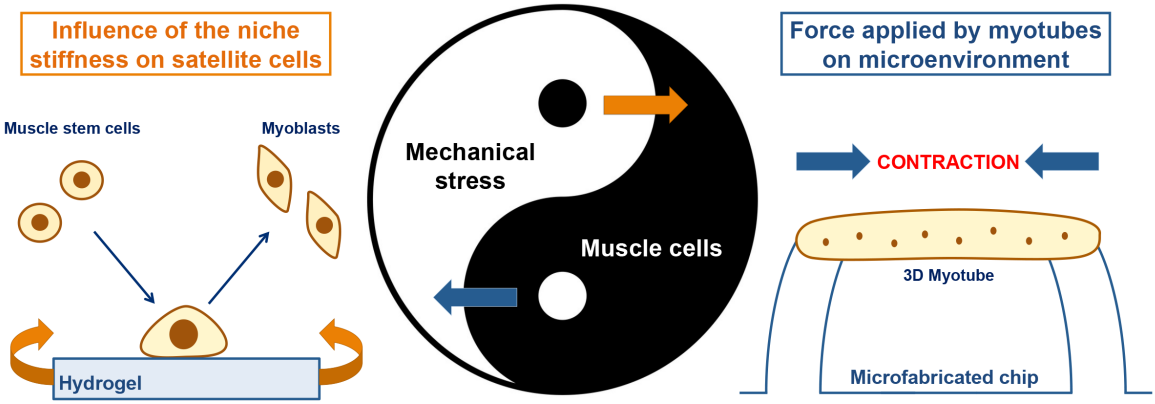

Figure 6: New *ex vivo* models to study the mechanical interplay between muscle cells and their microenvironment.

Chapter B: Mechanotransduction and Muscle Regeneration

B.1 | Mechanotransduction

First observed in cancerology in the 1950s, the mechanotransduction process, defined in Iskratsch *et al.* 2014 as the conversion of mechanical stimuli (substrate rigidity, stretching or shear stress) into chemical signals to regulate cell behaviour and function, is present in every tissue (Iskratch *et al.* 2014). This biological process can be separated in distinct steps **(Figure 7)**. The mechanical input, whether it comes from the ECM or neighboring cells, is transmitted across the plasma membrane to the cytoskeleton respectively by focal adhesions and intercellular junctions, crucial elements on which relies the mechanobiology of living cells. The signal is then "mechanosensed" by stretchable (thanks to conformational changes) proteins such as Talin, Vinculin, Bcar1, Focal Adhesion Kinase (FAK) or Csrp3, and integrated into the nucleus through mechanosignalling pathways (Myocardin-related transcription factor A, Yes-associated protein, LIM proteins…). Once translocated within the nucleus by various factors, the signal will cause variation in the gene expression, leading the cells to adapt to the environment in response to the physical stimulus.

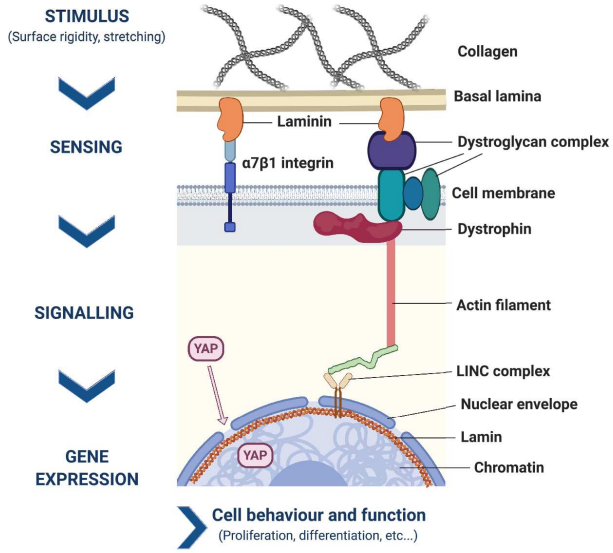

Figure 7: Schematic representation of mechanotransduction steps and its main effectors in muscle cells (Created with BioRender.com).

As mentioned above, cadherins and integrins are two absolute mainstays of mechanotransduction. Cadherin both ensures the adhesion and the diffusion of mechanical cues between cells in contact, it is therefore essential to homeostasis within soft tissues (Leckband and Rooij 2014). While the extracellular domain of the protein carries on the intercellular adhesive function, the cytoplasmic domain interacts with α-, β-, γ- and p120-catenins, forming a complex that connects with the actin cytoskeleton. This complex works for both inside-out and outside-in communications since it can be remodelled from internal cytoskeleton pulling. The cadherin/catenin complex is linked to F-actin by α-catenin, which plays a crucial role in cadherin-mediated mechanotransduction. Cadherin responds to external force by phosphorylating p120-catenin, but also acts as a mechanosensor by exerting a traction force leading to a conformational switch of α-catenin. Vinculin is an effector of the tension-dependent conformational regulation of α-catenin by cadherins, which affects the actomyosin organization downstream.

Integrins are heterodimeric transmembrane receptors composed of α and β subunits (specifically α7 and β1 isoforms in satellite cells) that bind to ECM proteins (each isoform being specific to different ECM components) and are responsible of tensile force mechanotransmission to the cytoskeleton (Sun. 2016). Integrins can be activated to have a higher affinity with the ECM through a conformational shift triggered by Kindlin and Talin. Following the binding with a ligand, they recruit a set of proteins to form a focal adhesion (containing Talin and Vinculin inter alia), which connects to the actomyosin network and transmits mechanic tension. This complex is referred as a "molecular clutch" since it mediates the forces sensed by integrins from the ECM, but also transfers back to the ECM a retrograde traction caused by actin polymerization against the membrane and actomyosin generated force. Just as a clutch, the focal adhesion harnesses actomyosin "engine", can be engaged or disengaged on this cytoskeletal motor and can slip if the mechanical loading is too high due to an excess of external surface rigidity. Downstream, mechanically induced conformational changes of Csrp3 or Bcar1 trigger various signalling pathways, among which FAK and YAP ones.

Polymerization of the actomyosin network controls the chromatin condensation state, notably through Serum response factor (SRF) and Nuclear factor-KB (NF-KB) pathways

(respectively with SRF and p95 transcription factors) by regulating the accessibility of certain loci for the transcriptional machinery (Uhler and Shivashankar 2017). The mechanotransduction of the external stimulus to the nucleus is mainly mediated by the translocation of these transcription factors following the activation of intracellular cascades. However, growing evidence (nuclei aspiration by micropipetting experiments) is supporting the hypothesis according to which the nucleoskeleton (nuclear matrix mainly composed by lamin filaments) would be mechanically stimulated by the cytoskeleton (Guilluy and Burridge 2015). The Linker of Nucleoskeleton and Cytoskeleton (LINC) proteins constitute a transmembrane complex across the nuclear envelope, which regulates nucleus shape, movements within the cytoplasm and ensures physical state coherency with the rest of the cell **(Figure 7)**. This nuclear mechanotranslocation may even directly impact gene expression by affecting chromatin structure through Lamin A/C. Indeed, analysis of nuclear content by fluorescence in situ hybridization showed that a downregulation of Lamin A/C was disturbing chromosomes location within the nucleus (Uhler and Shivashankar 2017). This repositioning substantially modifies the exposure of chromosomal regions to polymerases for their transcriptional activity.

Mechanotransduction is a common mechanism shared by most cell types in a vast range of species, and metazoan stem cells are not an exception to it. As examples, the niche stiffness has been shown to regulate the differentiation fate of mesenchymal stem cells (Steward and Kelly 2015), vascular stem cells (Potter *et al.* 2014) and epidermal stem cells (Strzyz 2016), by epigenetic modifications (chromatin condensation state for mesenchymal stem cells) that remain as marks encoding mechanical memory in the gene expression (Heo *et al.* 2015). The physical properties of skeletal muscle and its mechanobiology regarding satellite cells will be discussed further.

B.2 | Physical features of muscles

There are diverging estimations of the skeletal muscle stiffness **(Figure 8A)**, which could eventually be mechanosensed by satellite cells and regulate their functional behaviour. First, there is a significant difference between the Young's modulus (Elasticity constant value) of a myofiber, measured with or without the external layer of ECM, especially whether the perimysium surrounding fiber bundles gets included or not (around 10 kPa for single mouse myofibers and small fiber groups, around 40 kPa for fiber bundles) (Gillies and Lieber 2011). Considering that satellite cells reside between the sarcolemma and basal lamina, it can be postulated that the rigidity they feel is closer to the myofiber's one. In contradiction, isolated myofiber stiffness has been estimated by Trensz *et al.* using atomic force microscopy (AFM). The measured Young's modulus was comprised between 0.5 and 2kPa (whether the basement membrane was intact or collapsed). These relatively low values might be due to the isolation of the fiber, which may be less subject to internal forces and to the ECM sheath effect than a myofiber integrated within the muscle.

A

Sources	Stiffness	Methods of measurement
Gillies and Lieber 2011	10 kPa	Single myofiber compressive load testing
Trensz *et al.* 2015	2 kPa	Atomic force microscopy on an isolated myofiber
Urciuolo *et al.* 2013	12 kPa	Compressive load-unload cycling device on a whole *Tibialis anterior*
Engler *et al.* 2004	12 kPa	Atomic force microscopy on *Extensor digitorum longus*
Safaee *et al.* 2017	12 kPa	Bulk *Tibialis anterior* compression testing

B

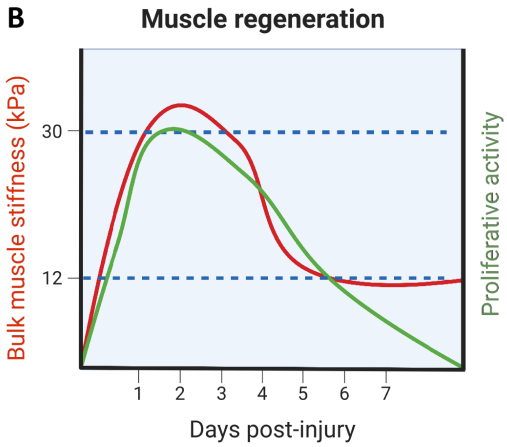

Figure 8: Physical features of muscle in mouse model. A. Table of measured mouse muscle stiffness in the literature (Created with BioRender.com).**B.** Schematic representation of bulk murine muscle stiffness and proliferative activity throughout early muscle regeneration (Modified from Safaee et al).

Using compressive load-unload cycling device on mice Tibialis anterior, Urciuolo *et al.* measured a whole muscle Young's modulus of 12 kPa, which partially relies on collagen IV predominance in the basal lamina, since Col6a1 knocked-out murine Tibialis anterior

showed a Young's modulus of 7 kPa (Urciuolo *et al.* 2013). Consistently, Engler *et al.* also measured mouse (Extensor digitorum longus) EDL elasticity with AFM to be approximately 12 kPa, the EDL of mdx dystrophic mice approaching 18 kPa (Engler *et al.* 2004). However, the most interesting estimation was performed by Safaee *et al.* who assessed the evolution of whole Tibialis anterior rigidity following muscle injury by compression testing over a week (Safaee *et al.* 2017). The Young's modulus of 12 kPa before injury was quickly increasing to more than 30 kPa in the first 3 days of regeneration, and decreasing back to normal in the last 4 days of assessing **(Figure 8B)**. These results are consistent with the 16 kPa elasticity value measured 4 days post injury in Urciuolo *et al.* 2013, and are most likely due to a transient switch in ECM content in proteins. Indeed, in the first 3 days following injury, an excess of type I collagen deposition is observed (Safaee *et al.* 2017). The influence of substrate elasticity on myogenic progenitors has been recently studied (detailed below), nevertheless the impact of injury-induced ECM remodelling causing a transient increase of muscle bulk stiffness on satellite cells remains mainly unknown.

B.3 | Muscle mechanobiology

Mechanotransduction is an important mechanism for skeletal muscle homeostasis conservation and regeneration following an injury. As previously mentioned, mechanical stimulation in the late stages of myogenesis is essential for proper muscle tissue formation and functionalization (Powell *et al.* 2002). Even though underlying molecular processes are not fully listed, the protein synthesis allowing muscle hypertrophy is regulated by external mechanical overload through activation of the IGF1-Akt-mTOR pathway (Goodman *et al.* 2005), acting in balance with the AMPK pathway (Mounier *et al.* 2009) which inhibits anabolic processes that consume ATP.

Yes-associated protein (YAP) is a central effector **(Figure 9)** of mechanotransduction in skeletal muscle, for homeostasis of the mature organ, but also during myogenesis (Fisher *et al.* 2016). This transcription co-activator bears an activation domain that can be phosphorylated (inactive form) for the protein to remain in the cytoplasm, or dephosphorylated (active form) for nuclear translocation where it interacts with other transcription factors and promotes the expression of various genes. YAP is involved in a vast variety of biological processes since it acts as a multi-integrated cross-talk messenger regulated by different intracellular cascades. Indeed, YAP is activated by the Hippo pathway (regulating contact inhibition of proliferation), interacts with adherens junctions, which regulates its cytoplasmic location and is also involved in IGF1-Akt-mTOR and an alternative Wnt (through FZD/ROR) pathways (Fischer *et al.* 2016). YAP signalling crosstalks with mechanosensitive pathways such as TGFβ/BMP signalling through SMAD1, Wnt canonical pathway by inhibiting β-catenin translocation, and could also be directly converting mechanical stimulation into biochemical information since its activation is correlated with actin stress fibers and its nuclear translocation dependent on the LINC complex (Fischer *et al.* 2016).

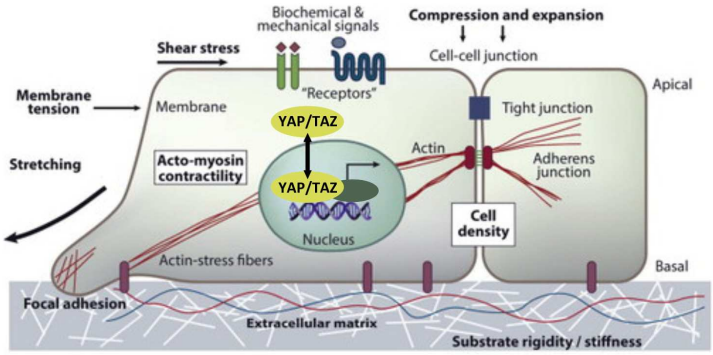

Figure 9: Yes-associated protein, a key effector of mechanotransduction. Schematic representation of YAP-TAZ-mediated mechanotransduction. When translocated to the nucleus, YAP-TAZ associates to transcription factors to regulate gene expression (adapted from Low *et al.* 2014).

Protein synthesis and organ size being regulated respectively by IGF1-Akt-mTOR and the Hippo pathways, YAP plays a central role in muscle mass conservation (Fisher *et al.* 2016). Furthermore, it also controls the expression of contractile apparatus proteins such as Myosin Heavy Chain, and α-actinin, and therefore influences the fiber phenotype. The myogenic progression is also tightly regulated by YAP level of activation. Indeed, YAP activation increases the transcription of MRFs like Myf5, and reduces Myogenin and Myf6 ones. Cell cycle regulators are also under the control of YAP (Cyclin D1 is upregulated whereas p21 is downregulated). These effects on target genes expression lead YAP activation to be associated with myoblasts proliferation, and YAP inactivation to be required for inducing differentiation.

Muscle mechanotransduction is severely impacted in dystrophies (Jaalouk and Lammerding 2009). The disruption of costameric complexes does not only induce damage to the sarcolemma, but also threatens interactions between the ECM and transmembrane mechano-transmitting proteins. The mechanical constraints being both increased due to fibrosis, and misread due to the dislocation of the mechanosensing system, they provoke an increase of the MAPK extracellular regulated kinase 1/2 (ERK1/2) signalling activation, further disturbing cell function. The membrane impairment allows external calcium invasion into the myofiber, causing excessive recruitment of the contractile apparatus. These parasite contractions induce severe damages, in addition to increased exerted tractions, and impeach mechanotransduction to take place successfully.

B.4 | Mechanosensitivity of Myogenesis

Biochemical and physical constraints of the microenvironment hosting muscle stem cells (MuSC) play an important role in the regulation of their regenerative function. Most studies investigating mechanotransduction in stem cells use hydrogels with an adjustable polymerization level to control substrate elasticity and mimic tissue stiffness (Gilbert and Weaver 2017). More and more innovative materials are being used to get closer to physical and chemical conditions of the niche, respectively by means of hyaluronin gels, collagen and fibrin scaffolds and by a combination of these latter with Matrigel coating and hormone-rich media.

Regarding muscle progenitors progression through myogenesis, normal muscle-like stiffness (12 kPa) facilitates myocyte alignment, myotubes formation and striation compared to softer (2-5 kPa) or stiffer substrates (17 kPa) (Engler *et al.* 2004 ; Romanazzo *et al.* 2012). More recently, a growing interest has been brought to earlier phases of myogenesis. Disturbance of the endomysium integrity affects its structural physical properties, which could modify myoblasts proliferation (Trensz *et al.* 2015). It is suspected that a change in the niche mechanical properties is needed for proper myoblasts expansion, knowing that a transient increase in the muscle stiffness was measured in the first 3 days of regeneration (Safaee *et al.* 2017 – See chapter B.2), concomitantly to the highest mitotic activity among progenitor cells.

The dependence of MuSCs regenerative potential on mechanical constraints has been brilliantly proven by Gilbert *et al.* in a study published in 2010, in which GFP+ mouse satellite cells were cultured on hydrogels of various stiffnesses, and retransplanted in injured muscles (Gilbert *et al.* 2010). The cell survival on hydrogels, engraftment and capacity to generate new myofibers in transplanted muscles were increased when the isolated cells were cultured at 12 kPa for 7 days, compared to 2kPa, and to 42 kPa, this higher rigidity being even less favourable. The decade that followed saw the rise of artificial niche mimicking models designed to resemble its physical and biochemical context, in order to maintain the quiescent state (Quarta *et al.* 2016), or even attempt to "rejuvenate" aged MuSCs (Cosgrove *et al.* 2014).

A method to culture human primary myoblasts on variable elasticity was developed in Picart lab (Monge *et al.* 2017), using hybrid hydrogels composed of Poly-L-Lysine (PLL), hyaluronan, and defined quantities of the cross-linking agents 1-ethyl-3-(3-(dimethylamino)-propyl)carbodiimide (EDC) and N-hydroxysulfosuccinimide (s-NHS), to tune the Young's modulus of the substrate (Schneider *et al.* 2006). In addition to observing morphological adaptations of myoblasts to the substrate stiffness, this study made the demonstration of two absolutely crucial points for the conception of the present doctoral research project. First, myoblasts' Pax7 expression is mechanosensitive to substrate elasticity. Second, this phenomenon is reversible, since the expression patterns depend on current substrate stiffness regardless of the previous hosting substrate (Monge *et al.* 2017). This last fact is of a great importance for experimental design since it allows to use primary myoblasts amplified on stiffer substrates (e. g. simply plastic), and replated on soft hydrogels, to study the mechanosensitivity of quiescence.

However, the differential expression of Pax7 was assessed by immunofluorescence between ECD10 and ECD70 gels, which have respectively Young's modulus of more than 150kPa and 350 kPa (Schneider *et al.* 2006). These values do not match muscle-like rigidity. This leads us wondering if the MuSCs quiescent state is differentially impacted by muscle-like elasticities (ranging from 12kPa to more than 30kPa) through the transient switch of tissue stiffness following injury-induced regeneration. The purposes of the present project is to determine the role of this transient switch in MuSCs activation and to understand the underlying molecular mechanisms at the transcriptional level.

Chapter C: Functional muscle culture on chip

C.1 | From clinical to *in vitro* evaluation of strength

In complementation of physiological symptoms analysis, there is a medical need to assess the muscle function of patients suffering neurological and muscular pathologies or other types of diseases, for healthcare and research purposes (Iaizzo and Durfee 2011). Indeed, the quantification of skeletal muscle functional strength is essential to diagnose and monitor the evolution of myopathies and neuromuscular diseases, or to estimate the outcomes of therapeutic procedures. Clinical tests triggering various types of contraction patterns (isometric, isotonic, isokinetic, concentric, eccentric) allow to consider the global muscle performance, including strength, power, and endurance indicators. After normalization of muscle length, and subject's joints position, the resulting data can be assembled for public health and clinical studies.

To assess the strength generated by a patient's muscle group, the easiest method, called the manual muscle test, consists in scoring an effort within a determined range of motion, induced by a voluntary contraction against a certain resistance in standardized conditions (Iaizzo and Durfee 2011) **(Figure 10A)**. This most widely used technique relying on assessor's applied force, palpation and subjective evaluation, is limited in accuracy and reproducibility. In order to diminish the inaccuracy issues of manual muscle tests and have more control on the measurement parameters, dynamometer-based instruments have been developed to read out precise values of muscle performance **(Figure 10B)**. For example, a commonly used dynamometer to follow patients suffering myopathies on the long term is the Jamar Hand Dynamometer, which consists in two plates arranged in a handle that presses on a portative dynamometer.

In vivo force assessment on isolated muscle from sacrificed mice are used in fundamental myology research and pre-clinical studies to monitor muscle performance, but also to get more insights on functional aspects such as dynamic, kinematic, and fatigue components **(Figure 10C)**. This technique has the major quality to give a complete control on the electrical input transmitted to the analysed muscle and the contractile apparatus of the myofibers. The dissection of the muscle also allows the

advantageous ablation of surrounding connective tissues and joints that bias measurements between individuals.

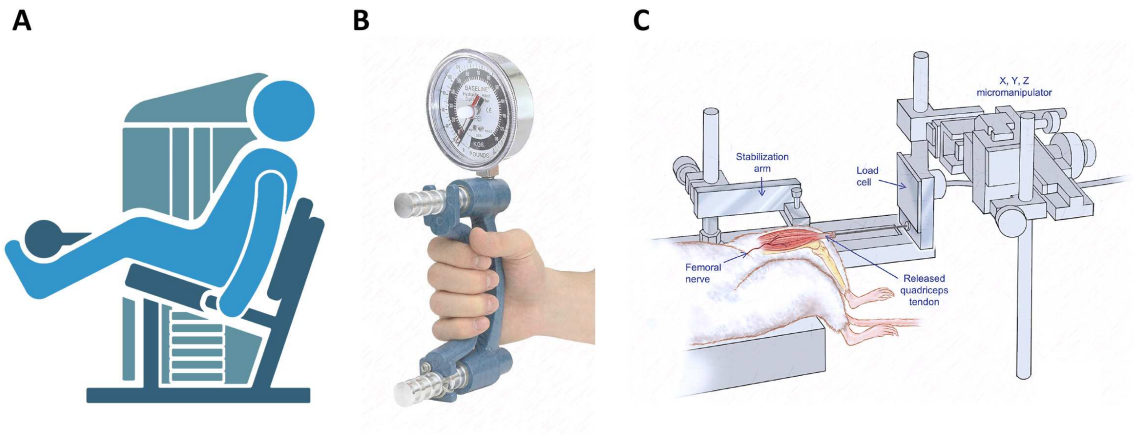

Figure 10: Methods of force measurement. A. Schematic representation of a leg extension force-measurement machine (created with BioRender.com). **B.** Picture of a Baseline 300lb hydraulic hand dynamometer (Adapted from Amazon.com). **C.** Drawing representing an *in situ* force measurement of a mouse quadriceps (adapted from Pratt and Lovering, *Journal of Biological Methods* 2014).

For the study of muscle regeneration, the isolation and analysis of a distinct muscle rather than a muscle group or a whole segment is particularly interesting in post-injury experiments to avoid strength compensation. These protocols usually consist in attaching isolated muscle's tendon to a force-sensing device that converts the physical input into informatics signal. On the other edge, the muscle receives electrical stimulations from an electrode, which also give the great experimental freedom to choose among a wide range of contraction patterns. For neurological studies, additional electrodes can also be placed to record the electrical activity of the muscle and produce an electromyogram (EMG).

The most commonly used *in vitro* model to study muscle regeneration is the culture of myoblasts on plastic dishes in a monolayer fashion. These models allow to study early phases of myogenesis, from satellite cell activation to myocytes fusion. Efficient and ergonomic protocols have been developed to measure the forces generated by single cells in 2D, such as the Traction Force Microscopy (Martiel *et al.* 2015). However, when myotubes reach a certain level of maturation, they start to contract and detach from the substrate. To allow the assessment of myotube contraction and proceed force

measurement, there is a need for 3D organoids models which permit anchoring of the newly formed myotubes. Such force sensitive 3D models have undergone an important development in the last decades for other tissue types (Kural and Billiar 2013).

C.2 | The emergence of organoids

In vitro culture of cells has been practised in biology research for over a century. However, this type of experiment does not enable to reproduce a vast range of physiological parameters compared to *in vivo* models, beginning with the three-dimensional structure of studied organisms. To overcome this main defect, organ-mimicking 3D constructs called organoids have been engineered **(Figure 11)**. There are as many definitions of an organoid as there are organoid developers, nevertheless it could be summed up as a self-organized 3D structure issued from progenitor cells of a specific lineage (Simian and Bissell 2017) and which reproduces the function of the imitated organ.

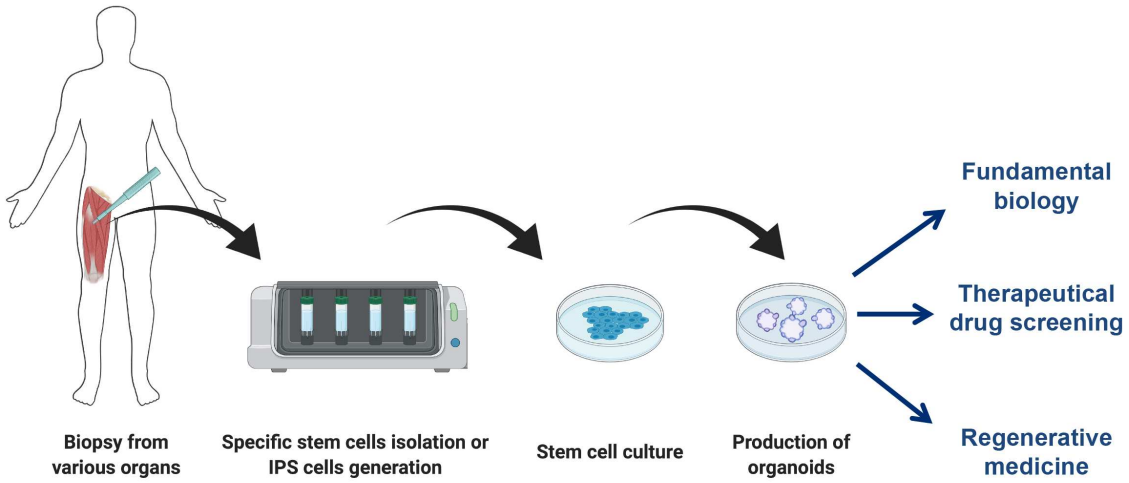

Figure 11: Organoids technology and its applications. Schematic representation of Human organoids generation process and the potential applications for this technology (Created with BioRender.com).

Starting from *ex vivo* culture of tissue explants in gel suspensions, organoids evolved toward stem cells generated complex multicellular structures. The first organoid-like construct published in the literature can be traced back to 1989 when Barcellos-Hoff *et al.* reconstituted mammary gland alveoli from primary mammary epithelial cells (Barcellos-Hoff *et al.* 1989).

Nowadays, organoids overflow biology research in all fields (Passier *et al.* 2016) and exist for almost every tissue type. In addition to the mammary glands, the digestive system (Esophagus, salivary glands, stomach, intestine and colon), as well as organs such as liver, kidney, pancreas, prostate and even Fallopian tube have been modelled (Clevers 2016). Vascular constructs from rat endothelial and aortic smooth muscle cells (Cummings *et al.* 2004), or respiratory structures made from human lung epithelial, mesenchymal and microvascular endothelial cells (Tan *et al.* 2017) are brilliant examples of complex organoids derived from a mix of different progenitor lineages.

Outstandingly, entire brain regions, such as the adenohypophysis, cerebellum or the hippocampus could be recreated (Clevers 2016). Embryonic stem cells from human could be turned into retinal stratified structure (Nakano *et al.* 2012), and more fascinating, induced pluripotent stem cells gave rise to a cerebral organoids mimicking the multiregional organization of the brain (Lancaster *et al.* 2013). At the edge of the nervous system, the neuromuscular junction described previously has also been imitated by human organoids using neuromesodermal progenitors (Martins *et al.* 2020).

Organoids provided an extraordinary new insight on morphogenesis and organogenesis, and are now increasingly used to assess various functional features, and establish test platforms to model pathologies for pharmaceutical drug screening. There are countless applications for organoids as they can also serve as models to study infections of target cells by viruses (Clevers 2016). Patient or mutant progenitor cells generate organoids modelling diseases to test cures and toxicology. 3D tumoral organoids can also be developed from cancer cells. Eventually, organoids could be used for retransplantation procedures following corrective gene editing of patients' induced Pluripotent Stem cells.
Organoids culture also represents a powerful tool to answer numerous fundamental biology questions. It aims at getting closer to *in vivo* conditions regarding tissue spatial organization and ECM layering structure and composition (Shamir and Ewald 2014). Organotypic models also have the capacity to reach further stages of maturation as compared to their equivalent 2D culture systems. For the monitoring of tissues' mechanobiology, the embedment within 3D ECM matrix (most commonly constituted by Matrigel), the fine-tuned mechanical properties and the configuration of the culture

substrate allow to have a tight control over biochemical and physical constraints applied to the organoids (Eyckmans and Chen 2017).

Bioengineering of organoids is still trending in the academic research and biotechnology industry. Among many possible evolutions, there are two features for which future models can substantially improve. First, the development of mechanosensitive models to assess tensile forces applied by the organoid on its environment. Second, the development of “organ-on-chip” or “tissue-on-chip” technologies allowing to reduce the biological material prerequisite, which is often a limiting element, by rescaling the dimensions of the organoid and expanding the number of replicates made from a constant initial sample size.

C.3 | Skeletal muscle constructs

Skeletal muscle organoids engineering has first been attempted in the early 1990's with quail myoblasts culture on a scratched membrane, combined to tendon fibroblasts added to wax pins placed to provide an anchorage (Swadison and Mayne 1992). Once transferred in a collagen suspension, this muscle bundle-like construct would present sarcomeric striations under electronic microscopy after 3 weeks of culture. Three-dimensional 12mm long constructs from rat myoblasts referred as "myooids" were then developed (Dennis and Kosnik 2000). These mini-muscles contracted both spontaneously and under electrical stimulation. However, the resulting specific force measured was not consistent with the one observed *in vivo* on rat muscles. The first human skeletal muscle construct was recreated from primary human myogenic precursors issued from healthy patient biopsies in a collagen-matrigel mix suspension (Powell *et al.* 2002). This 18mm model both allowed to induce mechanical input and to monitor generated force output from the tissue. It greatly helped to prove the necessity of mechanical stimulations for optimal hypertrophy during myogenesis.

The skeletal muscle organoids field has been revived ten years ago by the Bursac lab. Since then, they have been developing alveolar PDMS (Polydimethylsiloxane) culture substrates to implement monitoring of various functional aspects using modern molecular biology techniques (Immunofluorescent live imaging, confocal microscopy, transcriptomics, etc…) (Bian *et al.* 2009). The 14x14mm silicone molds could receive rat myogenic progenitors or immortalized myoblasts cell lines (C2C12) to fuse into a tissue network expressing maturation markers such as Myogenin, α-actinin, Vimentin (Bian and Bursac 2009). In larger wells (25mm) associated to Velcro anchorage, this research team obtained bioartificial constructs able to exert contraction that could even be vascularized once re-transplanted to mice (Juhas *et al.* 2014). Similar results were obtained recently in this lab using human pluripotent stem cells that could be cultured for a month, forming maturated myofiber bundles *in vitro* (Rao *et al.* 2018).

Most 3D skeletal muscle *in vitro* models are borne by gel-based scaffolds providing a structural support for cells to fuse and spread in all three spatial dimensions. The

hosting matrix can be composed of various ECM components to imitate the microenvironment, such as fibrin gels (Chiron *et al.* 2012), fibronectin-gelatin nanofilms (Gribova *et al.* 2016), and most interestingly collagen-Matrigel mix (Mills *et al.* 2018). This last *in vitro* platform is particularly efficient to observe and analyse maturated myotubes in 3D. However, the erratic fiber bundles orientation and various volume of muscle cellular content within the gel deeply bias force measurement when comparing different replicates.

Gel scaffold-borne muscle tissues represent a promising opportunity for future therapeutic approach to a wide spectrum of myopathies. For example, the culture of human primary muscle progenitor cells in a 3D bioprinted fibrin/gelatin gel gave excellent retransplantation outcomes in rodent's Tibialis anterior (Kim *et al.* 2018). Another brilliant example of a system with a high potential in biomedical research is the iPSC-derived artificial skeletal muscle from Tedesco lab, providing both a model to study organoids from individual patients (notably suffering Duchenne dystrophy), but also offering the perspective of a highly HLA immunocompatible re-transplantation material (Maffioletti *et al.* 2018).

C.4 | Microfabrication and micropatterning applied to muscle cells

Nowadays, sophisticated systems allow to study the mechanical interplay between cells and their microenvironment. For instance, submicrometric pillars chip models in PDMS (Polydimethylsiloxane), an elastomer compatible with fluorescence imaging (Ravasio *et al.* 2012), can both serve for measuring traction forces as well as monitoring cell mechanosensing in relation to local rheology variations (Ghibaudo *et al.* 2011 ; Trichet *et al.* 2012).

Skeletal muscle microtissues present a unique technical challenge compared to other organoids due to their very specific contractile function. Indeed, it turns out to be difficult to spatially control the self-organization of the tissue through fusion and maturation, in addition to contain the resting tension and active generated forces in targeted areas within the culture substrate. These problematic tensions can already be observed in the early stages of myocytes differentiation (Griffin *et al.* 2004). The interplay between myotube's early contractility and substrate compliance is essential to the proper reorganization of the actomyosin cytoskeleton, in order to achieve a functional striated shape.

To that regard, both the chemical composition and the topographical parameters of the microenvironment have to be optimized to promote myogenesis and ensure myotube stability. Indeed, crucial components of the ECM have been shown to be required for muscle cells to proceed myogenic progression (Penton *et al.* 2016). Matrigel, a gelatinous protein mixture secreted by Engelbreth-Holm-Swarm mouse sarcoma, seems to be offering the best deal to install a niche-mimicking coating in culture substrates, by providing a vast spectrum of ECM proteins such as laminins, which have been proven to increase myoblasts expansion and fusion into myotubes (in particular laminin 521). Utilized with higher concentrations, Matrigel can also act as a sheath to restrain myotube movements throughout the later phases of maturation, once the generated forces have largely induced detachment from the substrate, in addition to promoting myotube maturation (Pimentel *et al.* 2017). The positioning of cells also plays an

important role since pre-coating of laminin linear tracks increases myotubes adhesion, fusion and viability (Clarks and al. 1997).

Micropatterning of substrate's shape and adhesive proteins distribution is a powerful tool to spatially constrain myotube fusion and development. Various microscaled shapes of substrates have been tested for myoblasts optimal alignment, from circular to linear wells (Charest *et al.* 2007). Lined up striations helping myocytes to orientate in parallel for the branching step of fusion have been preferentially used for the micropatterning of *in vitro* culture models (Lam *et al.* 2006). Wave-like incurvations under 6µm (or around 3µm) inducing orientation angles closer to 0° between plated myoblasts in the first 72 hours of culture, we decided to use this pattern in the present doctoral project. Juxtaposition of myoblasts on striations significantly increases the early myotube formation (Huang *et al.* 2010). At a larger scale, parallel orientation of myotubes within a microtissue is conserved during later stages of differentiation to obtain a muscle bundle-like beam of myofibers organization. Alignment could also be obtained by other methods, although less accessible and convertible, using poly(ε-caprolactone)/collagen nanofiber meshes network (Choi *et al.* 2008) and magnetically labelled cell sheets on 3D layout (Akiyama *et al.* 2009). The results confirmed that alignment is consistently helping myotube formation.

Most common adhesive proteins micropatterning techniques rely on a stamping approach to print out shapes on surfaces. However, these methods do not comply to the culture on substrates with complex 3D topographies like micropillars, since the printing step present the risk to damage the substrate shaping and miss out targeted areas of coating due to restricted access. Hopefully, alternative micropatterning technologies have been developed, dodging these technical obstacles. The one used in this doctoral research project, called Light-induced molecular adsorption **(Figure 12)**, consists in combining PLL-PEG polymers substrate passivization with UV local restoration of surface adhesion (Strale *et al.* 2015). The Poly-L-lysine backbone interacts electrostatically with the substrate while the PEG (Polyethylene glycol) side chains block protein and cell adhesion to the surface, making it "passive". After addition of a light-sensitive photoinitiator, exposure to a given UV dose can locally cancel PEG's passive features, allowing proteins to attach in treated areas.

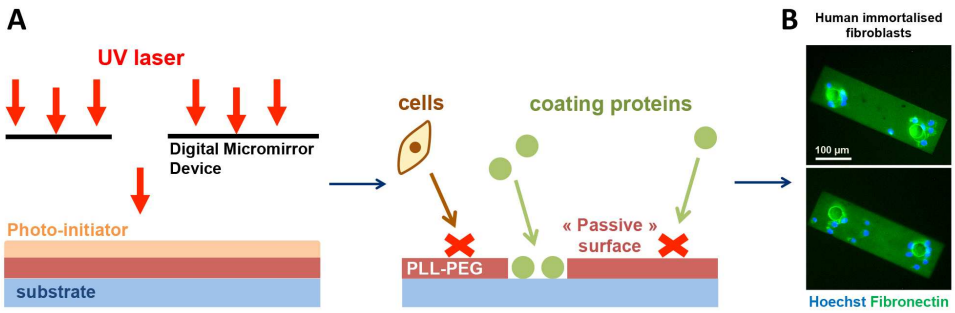

Figure 12: Micropatterning of coating proteins with light induced molecular adsorption. A. Schematic representation of light induced molecular adsorption technique. **B.** Images of immunostained human immortalized fibroblasts nuclei (blue) plated on microsubstrates with FN-Cy5-labeled fibronectin (green). Scale bar = 100 µm.

The power of this technology relies on the use of digital micromirror devices, each micromirror converting a pixel from the numeric mask into a projected beam of light. Associating three fluorescent-labelled proteins, this technique efficiently reproduced, at the microscopic level (425 µm x 275µm), such a complex and precise combination of shapes as the Botticelli's masterpiece "The Birth of Venus" painting (Strale *et al.* 2015). This tool can be combined to different material with various rheologies (glass, plastic, hydrogels, ECM gels…) and topographies (pillars, wells, striations…) to recreate an artificial 3D niche, while controlling the biochemical and biophysical characteristics of the microenvironment (Stoecklin *et al.* 2018). It has recently been used to reproduce a niche to study contraction and force transmission in human airways smooth muscle cells (Polio *et al.* 2019). This represents a promising technology for organ-on-chip bioengineering and has not been yet implemented to skeletal muscle 3D organoids development.

C.5 | Limitations of current muscle tissue technology

Today, the two worldwide reference models in the field of skeletal muscle organoids are the Tedesco lab's iPSC-derived artificial skeletal muscle (Maffioletti *et al.* 2018), previously described, and the ingenious MyoTACTIC system from the Gilbert lab (Afshar *et al.* 2020). This 96 well-plate platform allows to culture human primary myoblasts for several weeks until they form a muscle tissue between pillar duos. The pillar's deflection monitoring is used to calculate applied forces during spontaneous contractions or Ach stimulations, leading to voluntary contractions thanks to Ach receptors clusters expressed on the fibers. Co-culture with motoneurons can turn this technology into a NMJ model to study neuromuscular pathologies (Bakooshli *et al.* 2019). These two models are very powerful tools to perform therapeutical analysis, but their important sizes (1cm long for the iPSC-derived artificial skeletal muscle and around 25mm long for MyoTACTIC) require a high number of myoblasts to generate organoids (1 million cells per construct for the iPSC-derived artificial skeletal muscle and 15 million suspended cells per mL of hydrogel mixture for MyoTACTIC). To reduce biological material cost and substantially increase the drug screening capacity, there is a need to improve the cell/construct ratio by developing "organ-on-chip" or "tissue-on-chip" technology for skeletal muscle, as it exists for other tissue types such as lung, skin or tumors (Ronaldson-Bouchard and Vunjak-Novakovic 2018).

Bioengineering research for such technology has already been performed **(Figure 13)**, drastically reducing the cell/construct ratio (Sakar *et al.* 2012; Cvetkovic *et al.* 2014; Mills *et al.* 2018). However, problematic technical cues would arise from these models, mainly due to the fact that the myogenic progenitors are pre-suspended in a gel mixture of collagen I and Matrigel before being put into differentiation, leading to the erratic formation of unfused myotubes within the gel. The generated myotubes would not be arranged in parallel, leaving important gaps within the constructs, and sometimes not even connecting the two pillars holding it. Moreover, the fidelity of force measurement between each replicate could be questioned due to the difference in myotube's number, angles and orientation within the gel construct.

The best organ-on-chip skeletal muscle microtissue engineered to this day is the microfluidic device from the Massachusetts Institute of Technology (Osaki *et al.* 2019). This brilliant 3D neuromuscular model generated from optogenetically controllable iPSC-derived motoneurons and iPSC-derived myoblasts allows to study a vast range of diseases, but is of a high complexity with medium reservoir, injection ports, air channels and pillar caps (technically challenging to produce). Indeed, there is a need for a much more accessible, fast and easy-to-use protocol to simply observe high number of 3D myotubes and their contractions. We propose a well-free model to reduce the size needed for a single tissue, increasing the pillar density of the chip (from 4 per chip in Osaki *et al.* 2019 to >100 per chip) and to improve the 84k cells per microtissue ratio (Calculations = using 1.25% of cells from an 80% confluent T75 to generate 80 microtissues ; according to Thermofisher, 80% confluent T75 = 6.72 million cells).

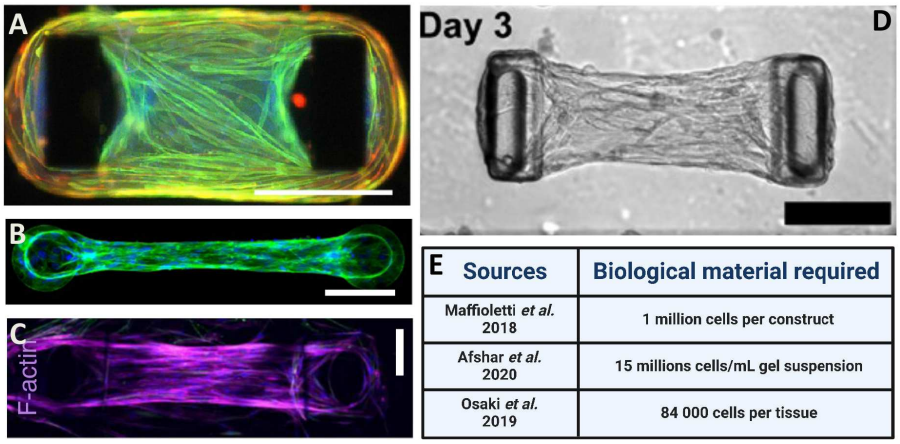

E Sources	Biological material required
Maffioletti *et al.* 2018	1 million cells per construct
Afshar *et al.* 2020	15 millions cells/mL gel suspension
Osaki *et al.* 2019	84 000 cells per tissue

Figure 13: Muscle microtissues, a state of the art. A. Image of an immunostained muscle microtissue from Mills *et al.* 2018 (Desmin (red), Titin (green), nuclei (blue), scale bar = 500 µm). **B.** Image of an immunostained fibroblast microtissue from Kalman *et al.* 2016 (Actin (green), nuclei (blue), scale bar = 100 µm). **C.** Image of an immunostained muscle microtissue from Osaki *et al.* 2019 (F-actin (purple) scale bar = 100 µm). **D.** Image of an immunostained muscle microtissue from Kalman *et al.* 2015 transmitted light, scale bar = 200 µm). **E.** Table comparing the quantity of myoblasts required a single microtissue in existing systems (created with BioRender.com).

Inspiring systems have been developed for other cell types such as cardiac microtissues (Boudou *et al.* 2012), or immortalized (3T3) fibroblasts-based microtissues arrays (Kalman *et al.* 2016), microtissue vacuum-actuated stretcher (Walker *et al.* 2018) or microfabricated substrate (Legant *et al.* 2009) models. By implementing substrate

topographical patterning and light-induced molecular adsorption proteins patterning techniques, our goal is to create such “tissue-on-chip” microtissue technology for skeletal muscle to propose a reduced-scale model allowing to exploit small sized biological samples for functional 3D myotube analysis.

GOALS OF THE PROJECTS

As presented in the introduction, there are growing bioethical, legal and economic interests in developing *ex vivo* systems to study biology for academic research and biotech industry. To better understand how the skeletal muscles operate and regenerate, there is a need for mature myotube analysis platforms and unconventional muscle stem cell culture tools to incorporate the mechanical constraint component.

Main project | Bioengineering a 3D myotube culture chip with contraction monitoring for therapeutical research. (p.47-73)

As described in the Chapter C (Introduction), there is a medical need to assess the muscle function of patients suffering myopathies to estimate the outcomes of therapeutic procedures (Iaizzo and Durfee 2011). Development of skeletal muscle organoids is a promising technology which has been spreading in recent years (Rao *et al.* 2018 ; Mills *et al.* 2018 ; Maffioletti *et al.* 2018 ; Osaki *et al.* 2019 ; Afshar *et al.* 2020). However, these technologies consume an important quantity of biological material (see introduction Figure 12). To solve this technical issue, there is a need to create miniaturized systems.

To study the mechanical interplay between cells and their microenvironment, PDMS pillars models have been developed in the Benoît Ladoux research team to measure cell-generated traction forces (Ghibaudo *et al.* 2011). This approach has also been used to culture fibroblasts microtissues between pillars in other labs (Legant *et al.* 2009). Léa Trichet adapted the technology to obtain C2C12-derived myotubes (immortalized murine myoblasts) (Fig. 0). However, the myotubes resulting from this lineage differs from human cells in terms of organization and contraction patterns.

For these reasons, the aim of this project is to adapt and optimize this method for human immortalized and primary myoblasts (available in the Myology institute), in order to obtain three-dimensional myotubes from healthy and diseased patients and observe resulting *ex vivo* contractions.

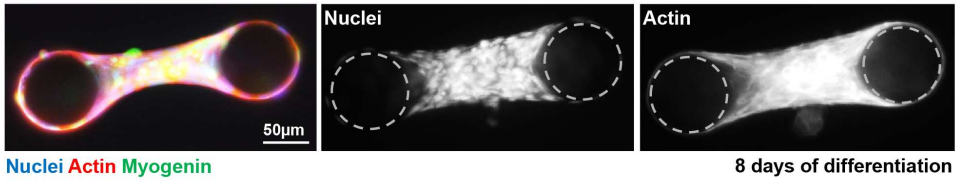

Figure 0: Preliminary results obtained with murine immortalized myoblasts (Léa Trichet). Image of immunofluorescent stained myotube obtained from C2C12 myoblasts after 8 days of differentiation (Myogenin (green), DAPI (blue), Actin (red), pillars are surrounded with dashes). C2C12 culture, myotube generation, immunostaining and imaging were performed by Léa Trichet before the beginning of my PhD.

Secondary project | Mechanosensitivity of Muscle stem cells quiescence. (p.74-84)

As described in the Chapter B (Introduction), mechanotransduction is processed by a vast range of cell types, including muscle progenitors (Fischer *et al.* 2016). Accumulating evidence demonstrates that muscle cells' function is impacted by external mechanical stimuli, from stem cell survival to myocyte differentiation and muscle hypertrophy (Gilbert *et al.* 2010 ; Engler *et al.* 2004 ; Romanazzo *et al.* 2012 ; Trensz *et al.* 2015 ; Powell *et al.* 2002 ; Goodman *et al.* 2005). Satellite cells quiescence has been shown to react to substrate's stiffness (Monge *et al.* 2017), using hydrogels with relatively high rigidities (Young's modulus of more than 150kPa and 350 kPa) (Schneider *et al.* 2006). Transient increase of skeletal muscle stiffness (switching from 12 kPa to more than 30 kPa Young's modulus) during the three initial days of muscle regeneration, which are associated to stem cell entering the cell cycle, has been observed in previous work from Penney Gilbert lab (Safaee *et al.* 2017).

Our aim is to use the hydrogel protocol (Davoudi and Gilbert 2017) to culture freshly FACS-isolated satellite cells (Liu *et al.* 2015) (a protocol currently performed in Fabien Le Grand lab) and study the effects of microenvironment elasticity variations on satellite cell activation.

Bioengineering a Miniaturized Contraction Monitoring Chip For 3D Myotube Analysis

Tentative list of authors (target journal : *eLife*)
Nicolas Rose, … , Gianluca Grenci, Anne Bigot, Antoine Muchir, Fabien Le Grand*, Benoit Ladoux*, Léa Trichet*

ABSTRACT

Quantification of skeletal muscle functional strength is essential to assess the outcomes of therapeutic procedures for muscular disorders. To this aim, several three-dimensional "Organ-on-chip" models have been developed. Yet, these technologies require a substantial amount of biological material, which is problematic in the context of limited patient sample. As a consequence, miniaturization of these technologies and creation of "Tissue-on-chip" devices are key steps to enable large-scale application of these systems. In this work a 3D myotube culture chip with contraction monitoring capacity was developed. Combination of light-induced molecular adsorption technology and optimized micropatterned substrate design, yet using simple microfabrication process, enabled to obtain high culture yields in tightly controlled physical and chemical microenvironments. Spontaneous twitch contractions in 3D myotubes derived from primary human myoblasts were observed, the generated force was measured and the contraction pattern characterized. In addition, the impact of three-dimensional culture on nuclear morphology was analyzed, confirming the similarity in organization between the obtained 3D myotubes and *in vivo* myofibers. Finally, the system enabled to model LMNA-related Congenital Muscular Dystrophy (L-CMD) with successful development of mutant 3D myotubes displaying a typical laminopathy phenotype. This technology shall be used for studying contraction characteristics, as well as for evaluating how specific diseases affect muscle organization and force generation. Furthermore, this downsized model might allow to substantially improve drug screening capability for therapeutic oriented research.

1. Introduction

Skeletal muscles constitute the most prevalent tissue in the human body, representing the majority of the corporal mass. Force generation relies on the contractile features of the myofibers. These are organized in periodic segments called sarcomeres, which consist in an overlap of Myosin and Actin filaments ensuring contractility. After an acute injury or a mechanical overload, Muscle stem cells (MuSC) contribute to the muscle regeneration in a process tightly regulated by physical and chemical constraints of the niche. As a complement to physiological symptoms analysis, there is a medical need to assess the muscle function of patients suffering muscular pathologies, for healthcare and research purposes (Iaizzo and Durfee, 2011). Indeed, the quantification of skeletal muscle functional strength is essential to estimate the outcomes of therapeutic procedures.

The most common *in vitro* model used to study muscle is dish culture of myoblast monolayers, allowing to study early phases of myogenesis until myotube formation. On the other hand, recently developed models such as Traction Force Microscopy or micropatterned substrates allow to study the mechanical properties and mechanosensitivity of single cells (Plotnikov et al., 2014) (Ghibaudo et al., 2011) (Trichet et al., 2012). When myotubes reach a certain level of maturation, contraction leads to detachment from the culture substrate. Hence, there is a need for 3D organoids models that permit anchoring of newly formed myotubes to allow assessment of myotube contraction and proceed force measurement. Such system should enable to study further stages of maturation. Force sensitive 3D models have undergone an important development in the last decades for other tissue types (Kural and Billiar 2013) (Boudou et al., 2012) (Kalman et al., 2016) (Walker et al., 2018) (Legant et al., 2009). In muscle, which primary function is to physically generate force, assessing involved mechanical stresses and controlling the physical features of the environment appear even more crucial.

Muscle contractile function, with resting tension and active generated forces, as well as myotube fusion process, make spatial control of the organoids within targeted areas in the culture substrate particularly challenging. Micropatterning of substrate's shape and

adhesive proteins distribution is a powerful tool to spatially constrain myotube fusion and development (Charest et al., 2007), while linear striations help myocytes to orientate in parallel for the branching step of fusion (Lam et al., 2006) (Huang et al., 2010). The most accessible adhesive proteins micropatterning techniques rely on a stamping approach to print out shapes on surfaces. However, these methods do not systematically comply with substrates presenting complex 3D topographies, and alternative micropatterning technologies have been developed, dodging these technical obstacles. Light-induced molecular adsorption consists in combining PLL-PEG polymers substrate passivization with UV local restoration of surface adhesion (Strale et al., 2016) and has not been yet implemented to skeletal muscle 3D organoids development.

Powerful tools to perform therapeutical analysis (Rao et al., 2018) (Maffioletti et al., 2018) (Afshar et al., 2020) already exist, but their important sizes require a high number of myoblasts to generate organoids. “Organ-on-chip” and “tissue-on-chip” technologies are trending in the academic research and biotechnology industry, as for other tissue types (Ronaldson-Bouchard and Vunjak-Novakovic, 2018). They allow to reduce the biological material prerequisite, which is often a limiting element, by rescaling the dimensions of the organoids and expanding the number of replicates made from a constant initial sample size. Bioengineering research for such technology has already been performed, which permitted to drastically reduce the amount of myoblasts required to obtain the same number of muscle constructs (Sakar et al., 2012) (Cvetkovic et al., 2014) (Mills et al., 2019) (Osaki et al., 2020).

In this work we propose a well-free model to diminish the size needed for a single tissue, and increase the pillar density of the chip. To do so, we optimized our silicone chip geometrical features and light-induced molecular adsorption proteins patterning technique to maximize the yields of 3D myotubes culture in a hydrogel matrix free condition. This system enabled to monitor spontaneous contractions of myotubes obtained from primary myoblasts and to study nuclei three-dimensional morphology in myotubes obtained from immortalized myoblasts of both healthy and L-CMD (LMNA-related Congenital Muscular Dystrophy) patients.

2. Materials & methods

The major project of my doctoral work mainly consisted in system development and protocol optimization, which is described in the Annex 1 (p.89)

- *2.1. Silicon wafer production and silanization*

Silicon wafers were provided by the Mechanobiology Institute (National University of Singapore). As illustrated in the Figure 1, pillar duos with varying geometries presented either a pattern of 6 µm periodic striations, with a height of 3.5 µm, in between the pillars (Fig. 3C) or no striation for the controls (Fig. 3B). Silicon wafer were placed in a vacuum bell with a drop of silane (1H,1H,2H,2H-perfluorooctyl-trichlorosilane 97%), degased for 15min and left for 2 hours for silane vapors deposition.

- *2.2. Polydimethylsiloxane chip molding*

PDMS Sylgard 184 silicone elastomere base was mixed with curing agent in a 1:10 ratio (Dow Corning, ref 01673921). The mixture was poured on the silicon wafer, degased (with vacuum) and heated at 80°C for 2 hours. PDMS was then disassembled from the silicon wafer and cut into individual chips.

- *2.3. Matrigel micropatterning*

As detailed in the Supplementary Figure S1, chips were hydrophilized by 5 min exposure to plasma cleaning. PLL-g-PEG (SuSoS Technology) was added to the chip surface for 1 hour and rinsed three times with Phosphate-Buffered Saline (PBS). Photoactivable reagent (Alvéole's Classic PLPP 14.5 mg/mL) was added on the chip and specific areas were exposed with 1200 mJ/mm^2, using PRIMO micropatterning device (Alvéole) on 20X objective, with Leonardo photopatterning software (Alvéole). Following the photopatterning step, Photoactivable reagent was vigorously rinsed away with PBS at least 5 times. Matrigel matrix (Corning ref 354230) solution (1mg/mL in DMEM) with 1:50 Cy5 dye-labeled fibronectin (conjugated in house using dialysis kit from Life technologies) was added on the chip and incubated for 1 hour at room temperature.

Matrigel solution was gently rinsed once with H_2O, and the patterned chips kept in sterile water at 4°C, plated in a multiwell-plate protected from the light.

- *2.4. Myoblasts lines and cell culture*

Myoblasts lineages were provided by the Myoline platform from the Institut de Myologie, Paris. The different cell lines are described in the Supplementary Table 1. Cells were amplified in proliferation medium composed of DMEM (high glucose, GlutaMAX(TM), ThermoFischer scientific) with 5% 199 medium (Medium 199, GlutaMAX™ Supplement, ThermoFischer scientific), supplemented with 20% Foetal Bovine Serum (Gibco ref 15750-037), 5 ng/ml human epithelial growth factor (Life Technologies), 0.5 ng/ml bFGF (Life Technologies), 0.2 mM dexamethasone (Sigma-Aldrich), 50 mg/ml fetuin (Life Technologies), 5 mg/ml insulin (Life Technologies) and 0.1 mg/mL Gentamicine (Gibco). Cells were cultured directly in plastic dishes and the passages were performed with 0.05% Trypsine-EDTA (1X) (Gibco). Human primary myoblasts were used within less than 30 divisions.

- *2.5. 3D myotube generation*

The chips were rinsed with sterile PBS, plated in new sterile multiwell plate and immersed with proliferation medium. Myoblasts were plated (100k to 200k cells per chip depending on cell type - primary or immortalized, control or mutant, etc…) directly above the chip in a 0.5 to 1mL proliferation medium drop. The chips were then spinned at 300g for 5 min, and left at 37°C for 1 hour. The medium covering the chips was then gently changed (while keeping the chip immersed) 3 to 4 times until the off-pattern cells would detach. The chip was kept in proliferating conditions overnight until a switch to differentiation medium (DMEM high glucose, GlutaMAX (TM) + 0.1 mg/mL Gentamicine), by removing 1mL from the culture well and adding 1mL of new medium (repeated 4 to 5 times). The chips were left in differentiation conditions for at least 6 days (partial medium change can be done every 2 days), and 0.4 µm/mL recombinant rat Agrin (R&D systems) in differentiation medium was then added to the 3D myotubes. Fresh differentiation medium (1mL) was gently added before contraction monitoring (performed after 7 to 14 days of differentiation).

- *2.6. Fixation and immunostaining*

Samples were fixed 10min with 4% Paraformaldehyde (formaldehyde) aqueous solution (Electronic Microscopy Sciences), blocked with 4% Bovine Serum Albumin (BSA) and permeabilized with 0.1% TritonX-100. The following primary antibodies (diluted in 4% BSA) were used for immunostaining: mouse IgG2b anti- Myosin Heavy Chain Type I MYH7 (DSHB, 1:50), rabbit monoclonal anti-Titin (DSHB 9D10-s, 1:500), mouse IgG1 anti-Sarcomeric Alpha Actinin (Abcam 9465, 1:500), rat monoclonal anti- Nicotinic Acetylcholine Receptor (Sigma-Aldrich, 1:800). The following secondary antibodies (diluted in PBS) were used for immunostaining: goat Alexa-Fluor-488/546/647-conjugated anti-mouse IgG1/IgG2b, anti-rabbit and anti-rat (Life Technologies, 1:500). Actin was stained with Phalloidin-tetramethylrhodamine conjugate (Santa-Cruz 362065, 1:500) and nuclei with Hoechst 33342 (Life technologies H3570, 1:10 000). Chips were mounting upside down on glass coverslip with Dako Fluorescence Mounting medium (ref 53023).

- *2.7. Microscopy imaging*

Transmitted light videomicroscopy for contraction monitoring was performed at 37°C and 5% CO_2 on Nikon eclipse Ti microscope with coolsnap HQ2 camera and 20X objective. Fluorescent imaging was acquired with EVOS FL Cell Imaging System microscope (Life Technologies). Contraction force was calculated using Saez et al. 2007 formula (Saez et al., 2007). Confocal and 3D imaging was acquired with Nikon Ti2 microscope equipped with a motorized stage and a Yokogawa CSU-W1 spinning disk head coupled with a Prime 95 sCMOS camera (Photometrics). Scanning electron microscopy was performed with Hitachi SU-70 High vacuum FESEM 1 kV or 0.5 kV (high magnification) without coating (We thank the Institut des Matériaux de Paris Centre (IMPC FR2482) for servicing FEGSEM & EDX instrumentation and Sorbonne Université, CNRS and C'Nano projects of the Région Ile-de-France for funding.)

- *2.8. Images and statistical analysis*

Images were acquired using Metamorph software and further treated with ImageJ/FIJI. Nuclear volumes were calculated by addition of all individually measured xy areas and multiplication with the confocal Z-step (zy or xz areas and ellipticities were not considered). All graphs and statistical analyses were performed with Prism software.

3. Results

- *3.1. Downsized model for in vitro functional skeletal muscle culture.*

In order to create a 3D myotube culture chip with contraction monitoring for therapeutical research, we developed the present system (Fig. 1A). This method consists in adding human myoblasts amplified from patients biopsies on micropatterned substrates made in PDMS (Polydimethylsiloxane), an elastomer compatible with fluorescence imaging (Ravasio et al., 2015). The pre-molded PDMS chip micro-substrates (10x10mm) (Fig. 1B) allow to culture micro-tissues between micropillar duos (Fig. 1C) at a high density (each chip can potentially bear 100 micro-tissues), providing numerous replicates while requiring relatively few myoblasts to be seeded (60k cells needed per chip). Different shapes, sizes and heights of the pillars were considered (Supplementary table 2). Depending on their geometry, the pillars have different spring constant values (Supplementary table 2), offering the possibility to perform studies on 3D myotubes while opposing different resistances.

Cells were plated directly on the substrates and put in differentiation condition (Fig. 1D). After fusion, the newly formed myotubes embrace the pillars. Interestingly, the lateral force exerted by the myotubes allows the myotube to migrate upward and caused the elastic pillars to bend toward each other. The pillars deflection can easily be observed from the top by transmitted light microscopy, allowing to estimate the generated force (Fig. 1D).

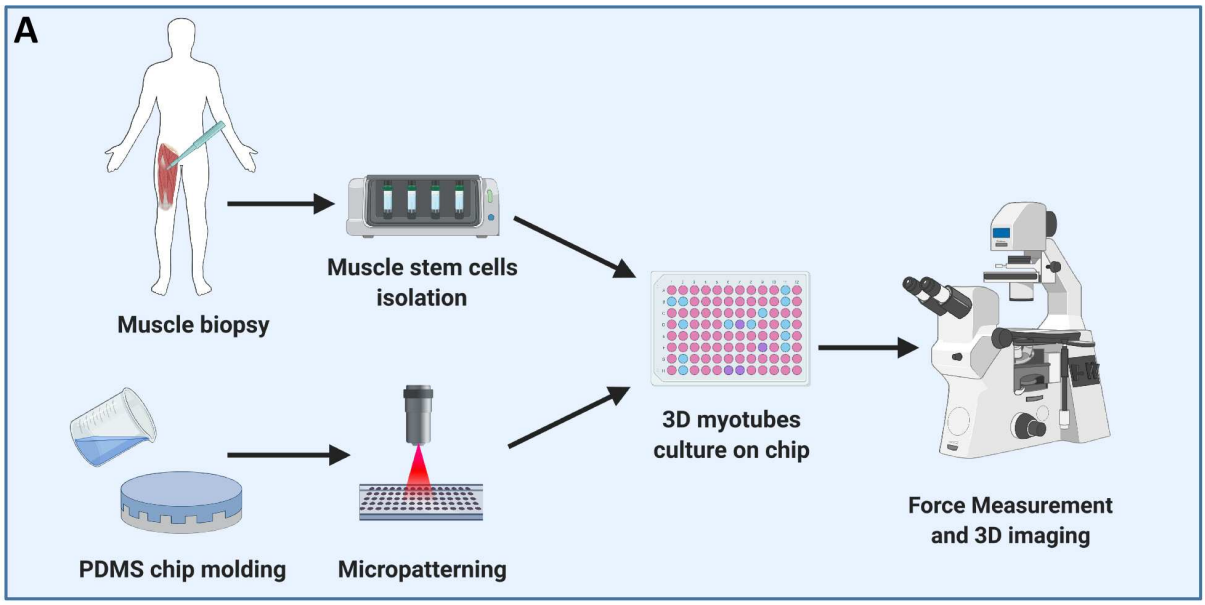

Silicone « Chip » microsubstrates

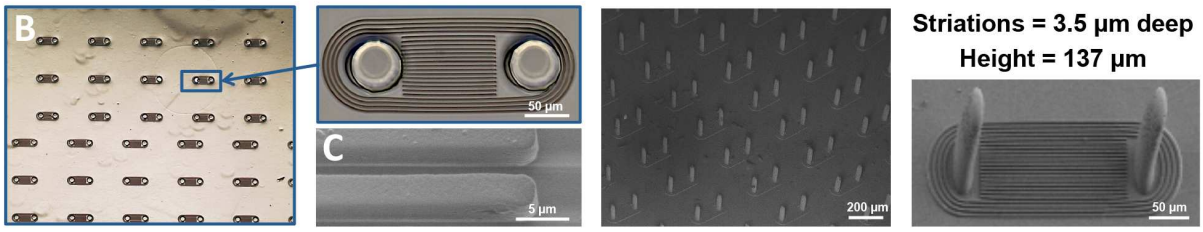

(1 Chip = 100-200 micropillar duos)

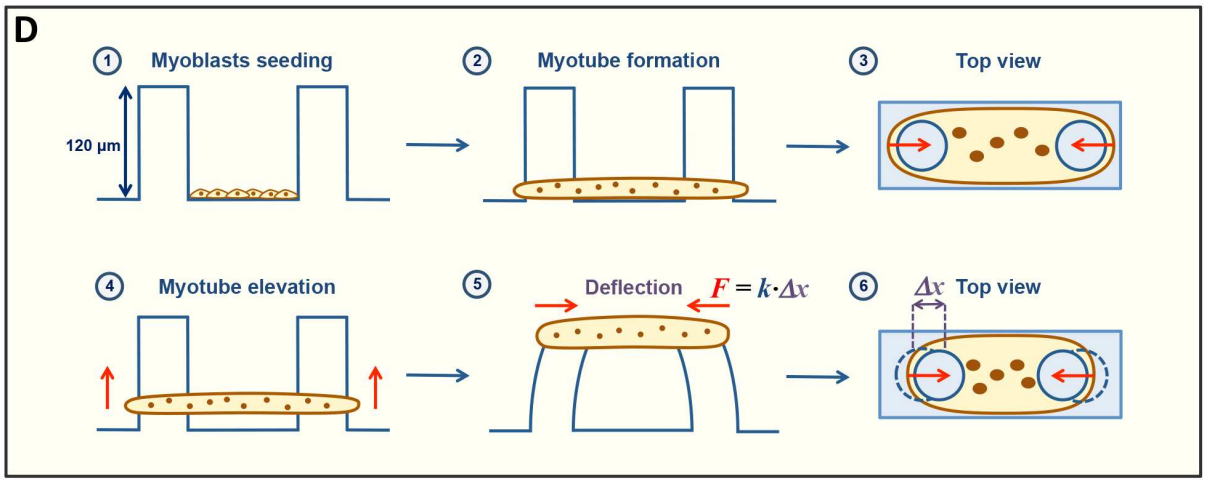

Figure 1: Developing a new *ex vivo* model of muscle microconstruct. A. Schematic representation of the method developed in the present project, combining photopatterning technique with culture of human muscle cells (PDMS=Polydimethylsiloxane) (Created with BioRender.com). **B.** Transmitted light microscopic image of a chip's topography. **C.** Tilted electronic microscopy images from few examples of the pillar types used in the present project. (striations (left), n°6 (middle), n°2 (right); see Table 2). **D**. Schematic representation of the 3D myotube generation and elevation, with observation of pillar deflection (associated to contraction force calculation formula from (Saez et al., 2007)).

- *3.2. Matrigel coating micropatterning*

In order to gain in 3D myotube density, micropillar duos were placed side by side on the chip without well to receive the seeded cells. We used Light-induced molecular adsorption technique (Fig. 2A) to avoid myoblast monolayer formation over the entire chip surface and restrict myoblasts adhesion in the inter-pillar area. This technique is based on the "passivization" of the substrate by PLL-PEG polymers. While the poly(L-lysine) backbone interacts electrostatically with the substrate, the poly(ethylene glycol) side chains block proteins or cell adhesion (Strale et al., 2016). Combined to a photo-initiator, local exposure to UV degrades PLL-PEG, creating a region permissive to cell adhesion (Fig. 2B).

Diverse technical parameters were optimized, such as the UV exposure (the required minimal dose being 1000 mJ/mm^2 for optimal patterning) of PLL-PEG polymers (Fig. 2C). The developed protocol (Supplementary Fig. S1) enables to obtain Matrigel-coated areas exclusively between the pillar duos (Fig. 2D), forcing the myoblasts to adhere in clusters and fuse into myotubes strictly in the axis of the pillars (Fig. 2E). The specificity of the Matrigel micropatterning was proved as cells would almost exclusively adhere to patterned areas from early proliferation phase to later stages of myotube maturation (Fig. 2F).

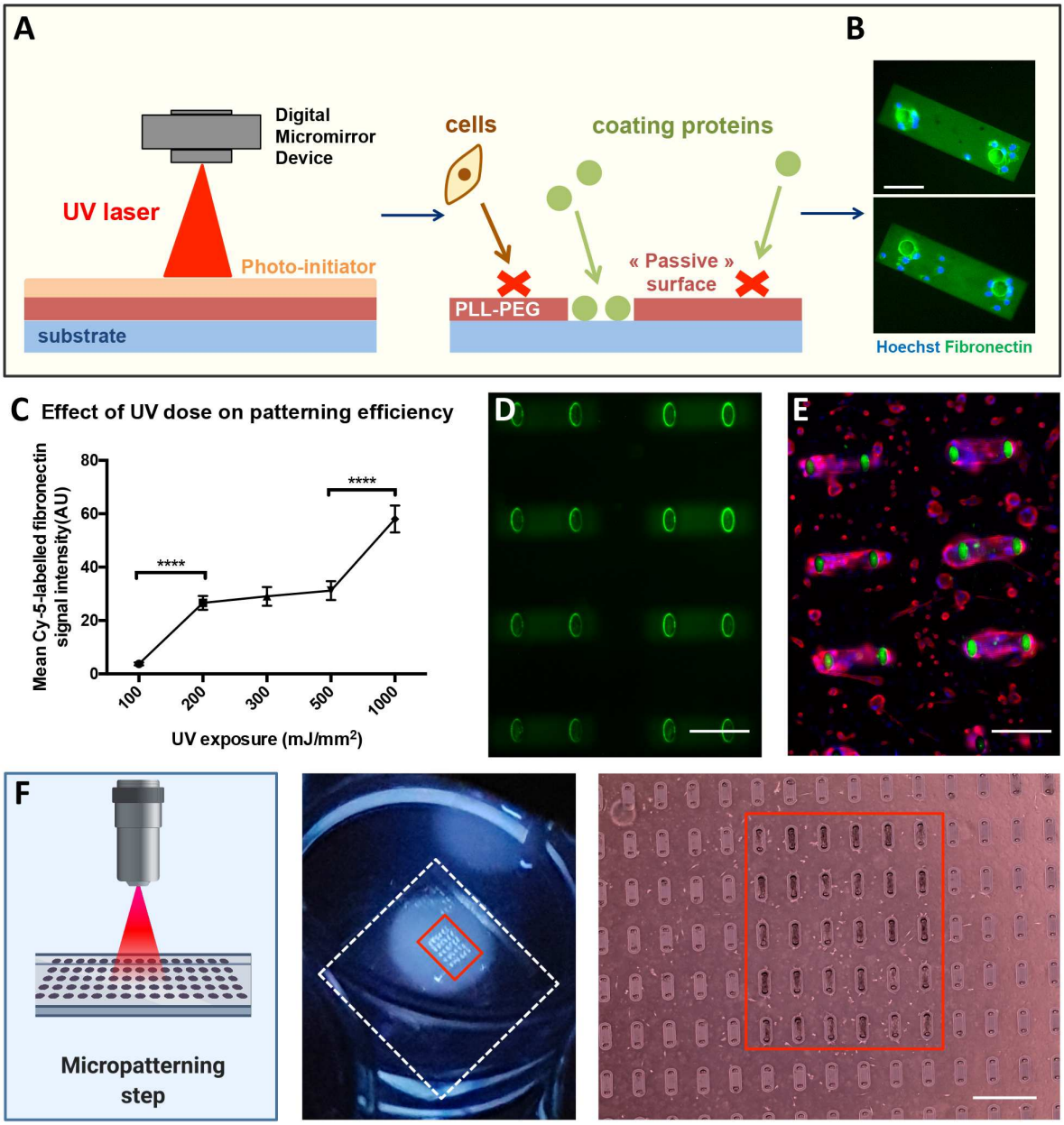
A
B
Digital
Micromirror
Device
UV laser
Photo-initiator
substrate
cells
coating proteins
« Passive »
surface
PLL-PEG
Hoechst Fibronectin
C Effect of UV dose on patterning efficiency
Mean Cy-5-labelled fibronectin
signal intensity(AU)
80
60
40
20
0
****
****
100
200
300
500
1000
UV exposure (mJ/mm²)
D
E
F
Micropatterning
step

Figure 2: Micropatterning 3D myotubes with light induced molecular adsorption. A. Schematic representation of light induced molecular adsorption technique. **B.** Images of immunostained human immortalized fibroblasts nuclei (blue) plated on microsubstrates with Cy5-labeled fibronectin (green). Scale bar = 100 µm. **C.** Mean Cy-5 labelled fibronectin fluorescent signal intensity ± s.e.m. measured on a spatial gradient of UV exposures. ****p<0.0001 (Unpaired t-test). **D.** Image of micropillars patterned with Fibronectin-Cy5/Matrigel mix (FN-Cy5 = green). Scale bar = 200 µm. **E.** Image of immunofluorescent staining of forming myotubes (from human immortalized (8220) myoblasts) after 7 days differentiation on micropillars patterned with FN-Cy5/Matrigel mix (Myosin heavy chain (red), FN-Cy5 (green), nuclei (blue) scale bar = 200 µm). **F.** From left to right: Schematic representation of photopatterning. Photograph of a chip (white dashes) in a 12 wells plate with 30 myotubes (from human immortalized (8220) myoblasts) constrained within patterned area (red rectangle) and exposed to UV light (reavealing Hoechst-stained nuclei (blue) from the myotubes). Transmitted light microscopic image of 30 microconstructs (from human immortalized (8220) myoblasts seeded the day before) forming within patterned area (red rectangle) (scale bar = 500 µm).

- *3.3. Optimization of chip geometrical settings.*

In order to facilitate myoblasts alignment, 6 µm periodic striations, with an height of 3.5 µm, were sculpted in between the micropillars duos, as this pattern was already shown to produce the most healthy, aligned myoblasts when comparing to 3 and 12 µm periodicity size (Lam et al., 2006). This topographical modification drastically improved 3D myotube yield (Fig. 3A-C), with a 6% myotube survival rate on flat substrate versus a 35% on striated ones, when considering different pillar geometries (Supplementary table 2: patterns n°3, 4, 7 and 8. Interestingly, we found the pillar major axis to be negatively correlated to the myotube survival rate (Fig. 3D). We set two optimal pillar shapes (Supplementary table 2: patterns n°5 and 6) that gave great 3D myotube yields, with survival rates reaching respectively 80% and 58% after 7 days of differentiation and 63 % and 58% after 10 days of differentiation (Fig. 3E). Regarding the pillar stiffness (Fig. 3F), which was calculated using Saez *et al.* 2007 formula (Fig. 3G), no correlation was found with the myotube survival rate (Supplementary table 2: n°1, 2, 4, 5, 6).

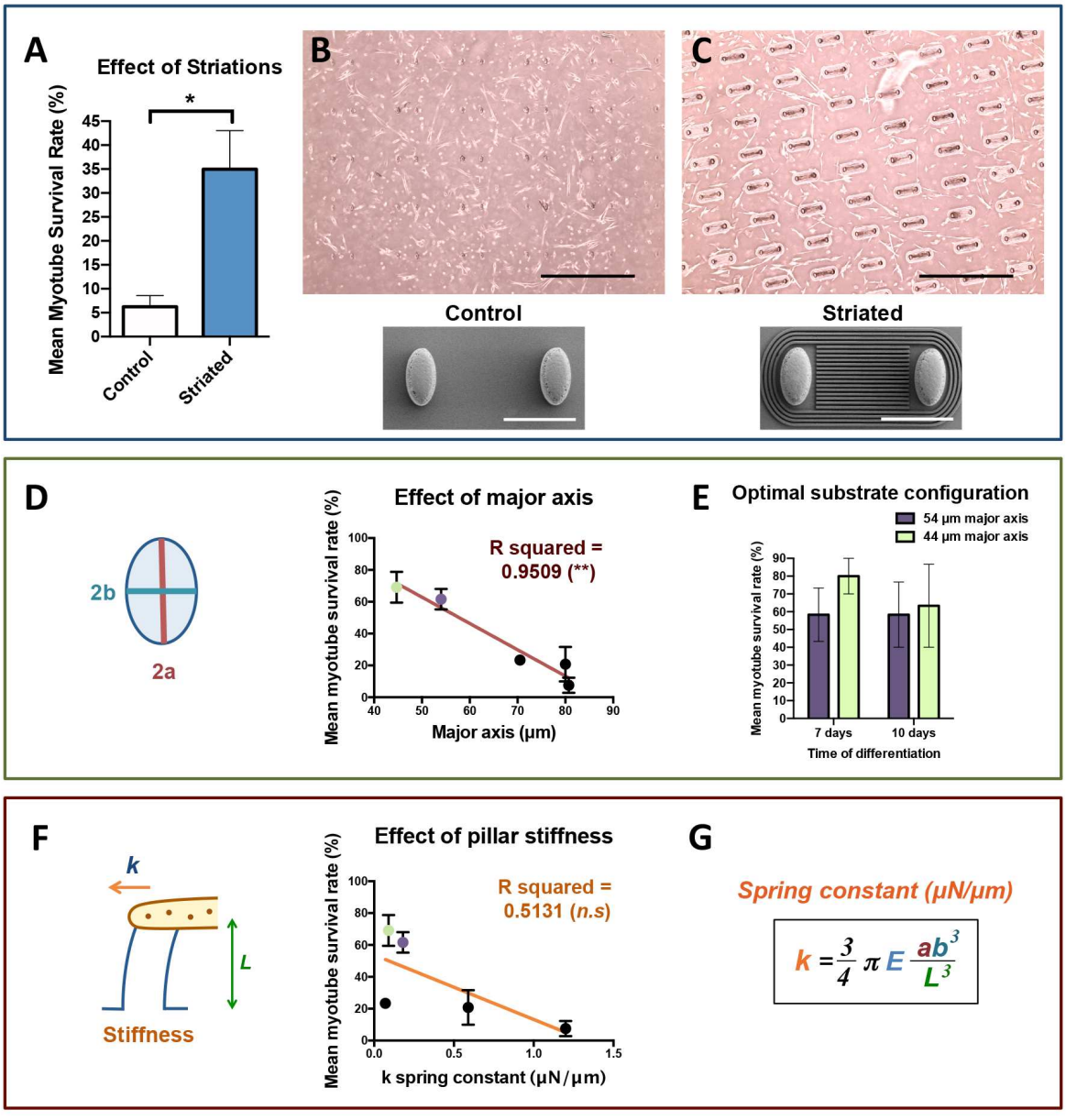
A
Effect of Striations
Mean Myotube Survival Rate (%)
*
Control
Striated
B
C
Control
Striated
D
2b
2a
Effect of major axis
Mean myotube survival rate (%)
R squared =
0.9509 (**)
Major axis (μm)
E
Optimal substrate configuration
54 μm major axis
44 μm major axis
Mean myotube survival rate (%)
7 days
10 days
Time of differentiation
F
k
L
Stiffness
Effect of pillar stiffness
Mean myotube survival rate (%)
R squared =
0.5131 (n.s)
k spring constant (μN/μm)
G
Spring constant (μN/μm)
k = 3/4 π E ab³/L³

Figure 3: Optimization of substrate configuration for myotube culture efficiency. A. Mean myotube (from human immortalized (8220 and AB1190) myoblasts) survival rate ± s.e.m. after 7 days of differentiation on patterned micropillars with or without 6 µm periodic striations (pillar n°3, n°4, n°7 and n°9. See Table 2). **p*<0.05 (Wilcoxon matched-pairs signed rank test), N=4. **B,C.** Transmitted light microscopic images of myotubes (from human immortalized myoblasts) after 7 days of differentiation and associated electronic microscopy images (n°7 and n°4 ; see Table 2. Scale bars = 100 µm) of non striated (B) and striated (C) identical micropillar duos. Scale bars = 600 µm. **D.** Mean myotube (from human immortalized (8220 and AB1190) myoblasts) survival rate after 7 days of differentiation on patterned micropillars with various major axis (pillar n°1, 2, 4, 5, 6 with 140 µm and 190 µm approximate interpillar distance. See Table 2). Linear regression (red line) and Pearson correlation test (***p*<0.01) and coefficient (R squared = 0.9509), N=4. **E.** Mean myotube (from human immortalized (8220 and AB1190) myoblasts) survival rate ± s.e.m. after 7 and 10 days of differentiation on patterned micropillars with the two most optimal substrate configurations (pillar n°5 in purple and n°6 in green. See Table 2), N=2. **F.** Mean myotube (from human immortalized (8220 and AB1190) myoblasts) survival rate after 7 days of differentiation on patterned micropillars with various stiffnesses (calculated from 3G formula, same pillars as 3D). Linear regression (orange line) and Pearson correlation test (*n.s* not significant) and coefficient (R squared = 0.5131), N=4. **G.** Pillars spring constant calculation formula (E: PDMS 1:10 Young's modulus = 1.8 MPa ; a: pillar semi-major axis ; b: pillar semi-minor axis ; L: pillar height) (Saez et al., 2007).

- *3.4. Hydrogel matrix free culture system.*

"Matrigel embedment" technique, which has been shown to promote myotubes maturation and restrain the myotube movements through later phases of maturation (Pimentel et al., 2017) was used both on 2D and 3D cultures. This method benefits were confirmed in 2D monolayer cultures (Supplementary Fig. S2 A-C), as the proportion of nuclei within sarcomeric α-actinin-expressing myotube (Fig. S2D) and sarcomeric network quantity (Fig. S2E) increased in embedded myotubes. Matrigel embedment was therefore thought to improve tissue stability and maturation if implemented to our 3D chip system (Fig. S2F). Unfortunately both pure Matrigel (Fig. S2G) and Matrigel/Collagen I mix (Fig. S2H) embedments displayed disastrous effects on 3D myotube culture yields (Fig. S2I). Indeed, hydrogel embedment seems to cancel micropatterning-based clustering of cells, allowing branching between myotubes. The system was kept gel-free with only silicone substrate and liquid medium to support 3D myotube culture.

- *3.5. Functional analysis of 3D myotubes.*

Maturated 3D myotubes from primary human myoblasts successfully developed a sarcomeric network (Fig. 4A), which spread spatially in a cylindrical fashion (Fig. 4B), conforming to the myotube shape, and expressing markers of the contractile apparatus (Fig. 4C and 4D) (titin and sarcomeric α-actinin respectively staining I-bands and Z-disks). The nuclei as well aligned themselves along the myotube at different height levels (Fig. 4E), similarly to myonuclei observed in isolated myofibers.

Following the formation of the contractile machinery, we observed input-free twitch contractions of our 3D myotubes (Movie 1) (Supplementary Figure S3) (Supplementary table 2: pattern n°6), which could be monitored by pillar deflection tracking (Fig. 4F-G). Unlike most preceding models using optogenetic or electrophysiological activation and modifications, our system easily relies on the monitoring of spontaneous contractions events automatically occurring once a certain maturation stage is passed. We observed a striking stability of the force generated through spontaneous contractions repeated measurements, at every step of the contraction pattern, notably the peak (Fig. 4H). This gives credit to the observation of spontaneous contractions as a reliable method of force assessment in these skeletal muscle constructs.

Spontaneous contraction observed on 44 monitored contractions phenomena systematically displayed a repetitive and stereotyped pattern within approximately 1.5 second (Fig. 4I). First exerting a fast force increase until the peak of the contraction (after 0.5 second), followed by a progressive force decrease (lasting 0.5 to 1 second). Relaxation of the resting tension would often be observed immediately surrounding the contraction event (with slight negative force measured before and/or afterward).

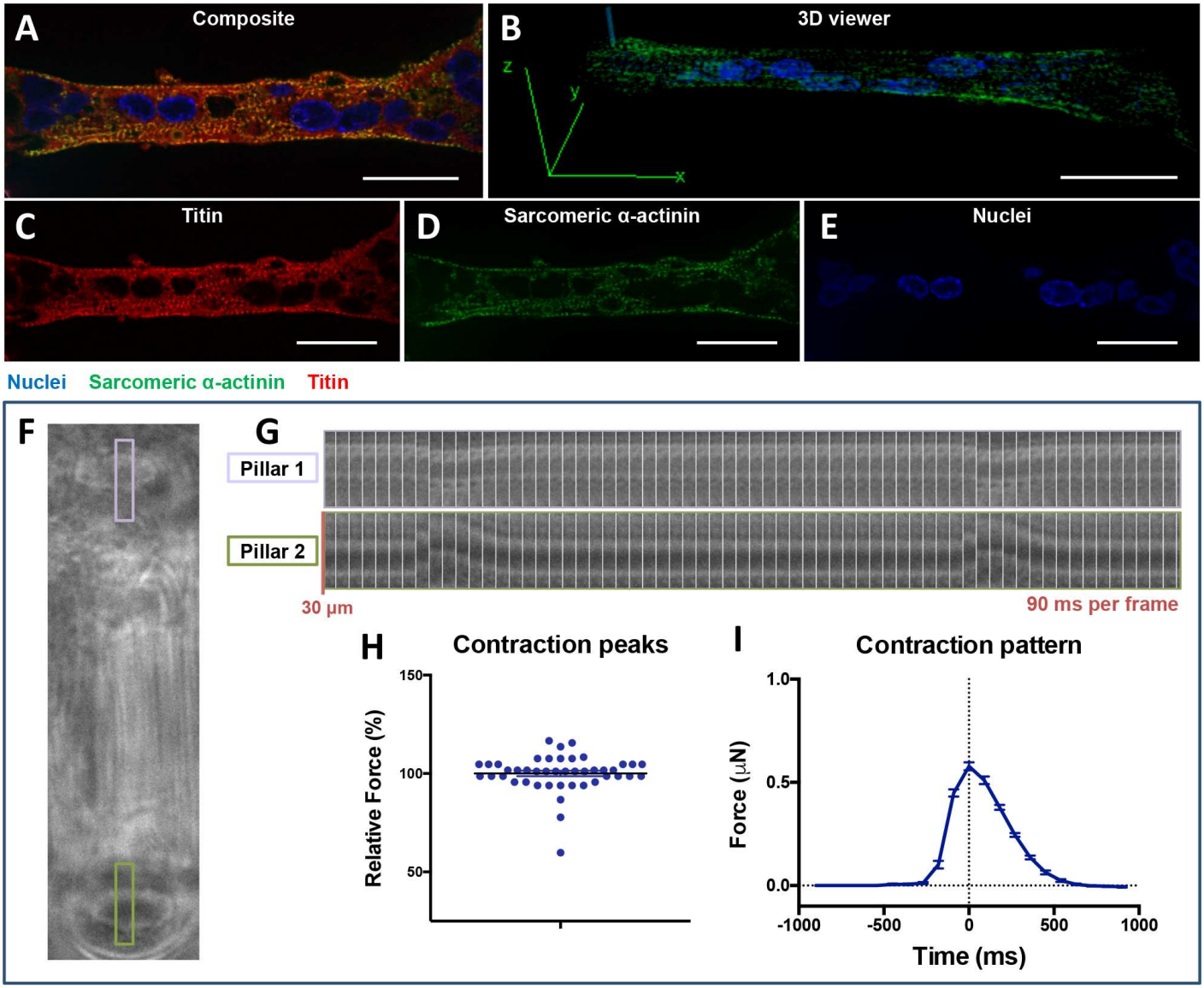

Figure 4: Monitoring of spontaneous contraction generated by mature 3D myotubes. A,B,C,D,E. Representative image of and immunofluorescent stained 3D myotube from human primary (AB678C53Q) myoblasts after 12 days of differentiation (Sarcomeric α-actinin (green), Hoechst (blue), Titin (red), scale bars = 25 µm) as a confocal section (A,C,D,E) and a three-dimensional view (B). **F,G.** Transmitted light microscopic images of a 3D myotube (F) from human primary (AB678C53Q) myoblasts after 9 days of differentiation and kymographs (G) of pillars over time. **H.** Relative forces of contraction peaks (normalized with mean peak contraction force) ± s.e.m. generated by 3D myotubes from human primary (AB678C53Q) myoblasts after 9 days of differentiation (N=2 ; 44 contractions (dots) observed) **I.** Mean relative contraction force over time (Normalized with nuclei number: Each force was multiplied by this nuclei ratio = (100 / nuclei number) to be standardized based on a 100 nuclei tissue) ± s.e.m. generated by 3D myotubes from human primary (AB678C53Q) myoblasts after 9 days of differentiation (N=2 ; 44 contractions observed).

- *3.6. Morphological impact of 3D culture on myonuclei.*

Diving into deeper scales of obtained 3D myotubes organization, we measured each nucleus projection area slice by slice on a vertical z axis, as well as the three-dimensional features, in order to apprehend the morphological impact of 3D culture on nuclei shape in comparison to 2D culture (Fig. 5A-D). In comparison to nuclei from 2D monolayers, nuclei from 3D myotubes had heights twice superior (respectively 3.2 µm and 7 µm) (Fig. 5F) but were less spread in length (Fig. 5G) (respectively 16.4 µm and 12.5 µm), and in width (Fig.5H) (respectively 9.7 µm and 7.7 µm). The flatter a nucleus is, the faster the slice areas that are located further away from the nucleus central slice will decease, compared to the maximal slice area (MSA). Comparing the distributions of nuclei slice areas normalized by the MSA is thus an indicator of nuclear flatness. Thereby the nuclei within 3D myotubes showed largely reduced flatness compared to nuclei from 2D monolayers (Fig. 5I). However, nuclei from 3D myotubes conserved a similar (xy) ellipticity (Fig. 5J), showing that the nuclear width and length evolved in the same proportions. In addition, 3D nuclei also exhibited decreased volume (Fig. 5K) compared to 2D nuclei (respectively 229 μm^3 and 285 μm^3).

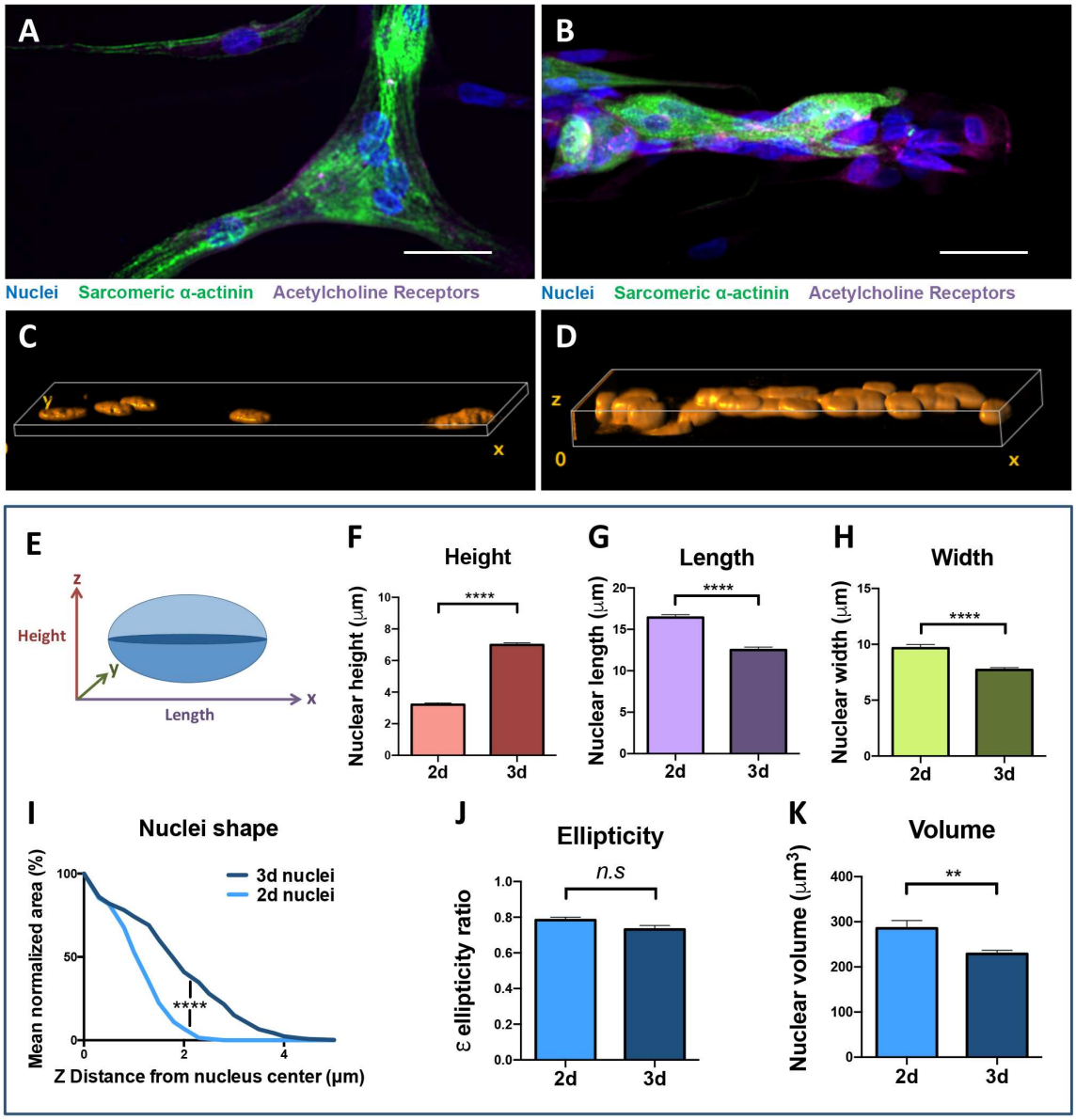

Figure 5: Shape and dimensions of nuclei within 2D monolayer and 3D myotubes. A,B. Representative (top view) images of immunofluorescent stained myotubes monolayer (A) and 3D myotube (B) from human primary (AB678C53Q) myoblasts after 7 days of differentiation (Sarcomeric α-actinin (green), Hoechst (blue), Acetylcholine receptors (magenta) scale bars = 25 µm). **C,D.** Volume viewer of Hoechst-stained nuclei from tilted representative images of myotubes monolayer (C) and 3D myotube (D) from human primary myoblasts after 7 days of differentiation (rotations : x=105 ; y=15 ; x=0). **E.** Schematic representations of mean 3D myotube nucleus. **F,G,H.** Mean nuclear height (F), length (G) and width (H) in 2D myotubes monolayer and 3D myotubes from human primary myoblasts after 7 days of differentiation. ****p<0.0001 (F,H : Unpaired t-test ; G : Mann-Whitney unpaired test), 2D = 35 nuclei ; 3D = 69 nuclei. **I.** Distributions of mean normalized areas calculated in 2D myotubes monolayers and 3D myotubes from human primary myoblasts after 7 days of differentiation. ****p<0.0001 (Wilcoxon matched-pairs signed rank test), 2D = 35 nuclei ; 3D = 69 nuclei. **J.** Mean nuclear (xy) ellipticity in 2D myotubes monolayer and 3D myotubes from human primary myoblasts after 7 days of differentiation. *n.s* not significant (Mann-Whitney unpaired test), 2D = 35 nuclei ; 3D = 69 nuclei. **K.** Mean nuclear volume in 2D myotubes monolayer and 3D myotubes from human primary myoblasts after 7 days of differentiation. **p<0.01 (Mann-Whitney unpaired test), 2D = 35 nuclei ; 3D = 69 nuclei. AB678C53Q myoblast line.

- *3.7. Expression of pathological phenotypes in patient 3D myotubes.*

Using the same approach as previously described, we cultured and analyzed 3D myotubes from healthy (Fig. 6A) and LMNA-related Congenital Muscular Dystrophy (Fig. 6B) patients immortalized myoblasts. As observed in 3D reconstitutions from confocal imaging (Fig. 6C and D), nuclei with LMNA mutation displayed morphological differences compared to control nuclei. First, LMNA mutation was associated to a significant increase of nuclear flatness (Fig. 6F), leading to a higher MSA value (87 μm^2) in comparison to control nuclei (54 μm^2). Furthermore, while maintaining a constant nuclear ellipticity (Fig. 3G), 3D myotubes issued from L-CMD patients also differed from control myotubes by presenting longer (Fig. 6H) (respectively 14.5 µm and 11.4 µm) and wider (Fig. 6I) (respectively 9.6 µm and 7.1 µm) nuclei. Confirming the relative flatness of LMNA mutated nuclei, the height (Fig. 6J) was slightly but significantly reduced compared to control nuclei (respectively 5.2 µm and 5.8 µm), despite the larger volume (Fig. 6K) of mutant nuclei (211 μm^3 against 162 μm^3 in control nuclei).

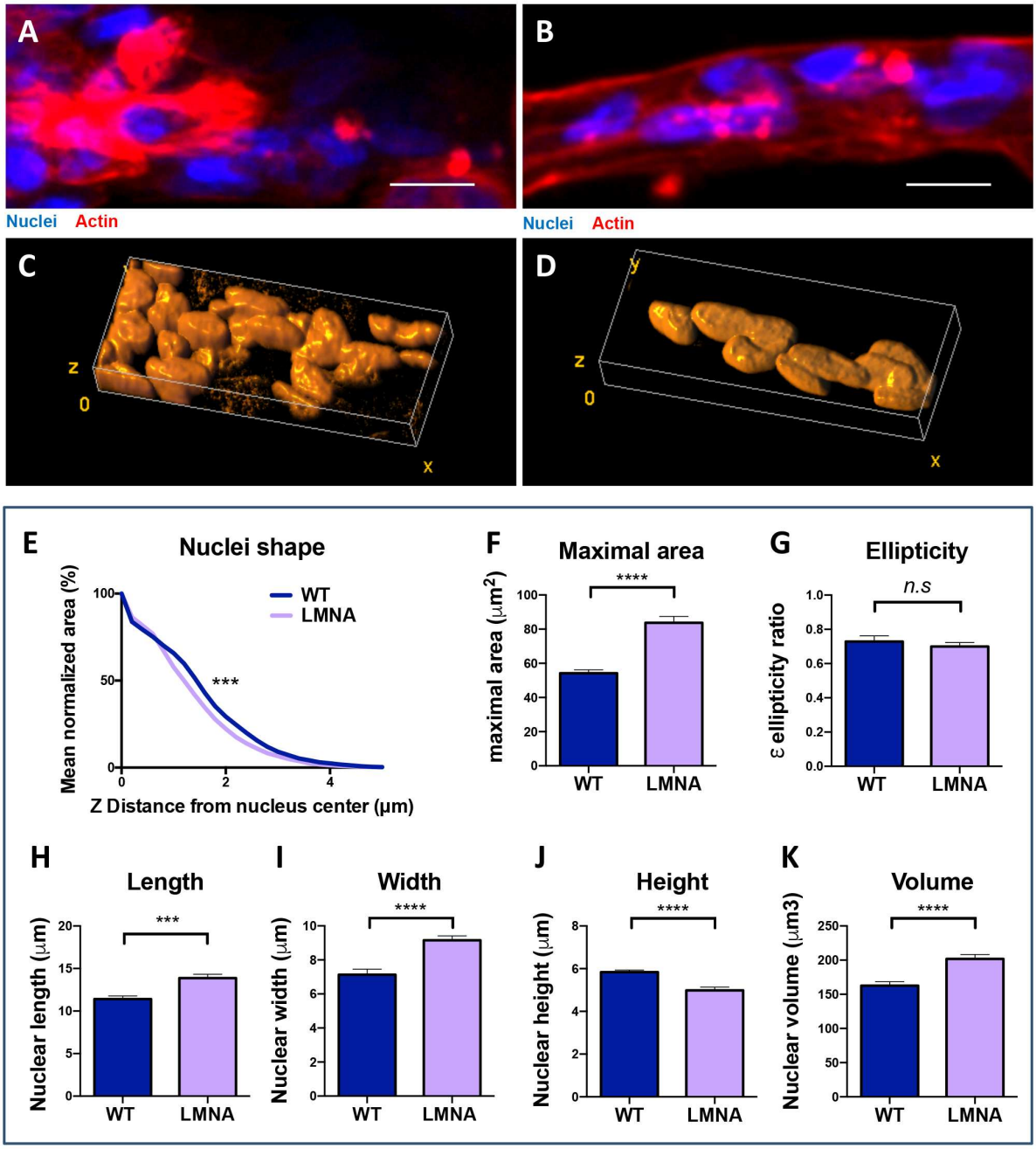

Figure 6: Effect of a LMNA gene mutation on nuclei morphology in patient 3D myotubes. A,B. Representative (top view) images of immunofluorescent stained 3D myotubes from control (A) and L-CMD (B) patients myoblasts after 7 days of differentiation (Hoechst (blue), phalloidin (red) scale bars = 25 µm, both images are later analyzed in C and D). **C,D.** Volume viewer of Hoechst-stained nuclei from tilted representative images of 3D myotubes from control (C) and L-CMD (D) patients myoblasts after 7 days of differentiation (rotations : x=150 ; y=15 ; x=10). **E.** Distributions of mean normalized areas calculated in 3D myotubes from control and L-CMD patients myoblasts after 7 days of differentiation. ***p<0.001 (Wilcoxon matched-pairs signed rank test), WT = 57 nuclei ; LMNA = 85 nuclei. **F.** Mean area at the central slice of the nuclei. ****p<0.0001 (Mann-Whitney unpaired test). **G.** Mean nuclear (xy) ellipticity in 3D myotubes from control and L-CMD patients myoblasts after 7 days of differentiation. *n.s* not significant (Unpaired *t* test), WT = 57 nuclei ; LMNA = 85 nuclei. **H,I,J,K.** Mean nuclear length (H), width (I), height (J) and volume (K) in 3D myotubes from control and L-CMD patients myoblasts after 7 days of differentiation. ***p<0.001 ; ****p<0.0001 (Mann-Whitney unpaired test), WT = 57 nuclei ; LMNA = 85 nuclei. (control myoblasts = 8220 line ; L-CMD myoblasts = EMD1365 line)

4. Discussion

We developed a Tissue-on-chip culture device allowing the assessment of forces generated by 3D myotubes from healthy donors or patients suffering muscular disorders. To our knowledge, light-induced molecular adsorption has never been used for mature skeletal muscle organoids. Using this technology allowed us to further downsize our system. Thereby, this work could inspire the implementation of this technology in myology research and organ-on-chip bioengineering for medical studies. This model might offer less versatility than other muscle constructs (Maffioletti et al., 2018) (Afshar et al., 2020) (Osaki et al., 2020), which recreate muscle-like beams of fiber bundles, and allow co-culture of vascular (Maffioletti et al., 2018) and neuronal (Afshar et al., 2020) (Osaki et al., 2020) tissues. Also, the presence of residual myocytes between patterned areas (Fig. 2E) could eventually bias bulk RNA and protein based molecular biology approaches performed with other models (Rao et al., 2018) (Mills et al., 2019).

However, we propose a culture device with an unprecedented cells-to-construct ratio designed to produce a great number of technical replicates with relatively few cells. Each 3D myotube requires 1 000 to 6 667 seeded myoblasts (considering that 100k cells are plated to obtain 100 myotube/chip in optimal conditions, whereas 200k cells are plated to obtain 30 myotube/chip in the worst conditions, such as the most severe mutant phenotype), depending on the cell type (primary or immortalized, control or mutant, etc…). For comparison purposes, 3D Artificial Muscles (Maffioletti et al., 2018) requires 1 million cells per construct ($x10^3$ more), MyoTACTIC (Afshar et al., 2020) uses gel suspension with 15 millions cell/mL, NMJ chip (Osaki et al., 2020) have an estimated biological cost of 84 000 cells per tissue and human skeletal micro muscles (Mills et al., 2019) need 30 000 cells per tissue ($x10^1$ more). Regarding downsizing, the system configuration can still be optimized to increase the pillar density and the 3D myotube culture yield.

The system worked with diverse cell lines (primary or immortalized myoblasts) from different muscle groups and various patients with diverging ages and phenotypes

(Supplementary table 1), and excellent 3D myotube survival rates (Fig. 3E) were obtained for the two healthy myogenic immortalized lineage cultured. There is a strong reproducibility between experiments performed with the same cell line, which ensures the reliability of this platform when used to study the effect of a therapeutical drug on a patient cell line. Nevertheless, there is an unequal yield (increasing with duration of culture) depending on the cell line (data not shown), most likely due to uneven adhesion capacity, passive resting tension and sarcomere-generated contraction forces. Consequently, the chip configuration should ideally be fine-tuned for each myogenic lineage. The calculation of force should be adapted accordingly to standardize the comparison of different biological replicates. We optimized the 3D myotube culture using two different pillar shapes (Fig. 3E). Counterintuitively, the tissue stability decreased as its width increased (Fig. 3D), suggesting that the higher surface given to the myotube to adhere does not protect from detachment. On the contrary, the wider myotubes seem to detach more easily, possibly due to increased contractile material. The relative small size of the 3D myotubes and pillars provide more control on physical parameters such as the stiffness constraints applied to the myotubes or the mechanical force generated by the tissue. This makes our contraction monitoring chip a great model for biophysics oriented research.

Addition of round caps or internal bending of pillar top is widely spread in other muscle culture models (Osaki et al., 2020) (Afshar et al., 2020). These are not strictly necessary as demonstrated by this study, but would certainly improve myotube stability and help to maximize the culture yield. That is undoubtly the first refinement to be incremented to our 3D myotube culture chip. Abstaining from the use of a hydrogel scaffold probably diminishes the tissue stability as well. Most 3D skeletal muscle in vitro models are indeed borne by gel-based scaffolds providing a structural support for cells to fuse and spread in all three spatial dimensions. The hosting matrix can be composed of various ECM components to imitate the microenvironment, such as fibrin gels (Chiron et al., 2012), fibronectin-gelatin nanofilms (Gribova et al., 2016), and most interestingly collagen-Matrigel mix (Mills et al., 2019). The gel suspension is also thought to provide the proliferating cells with a condition closer to the *in vivo* environment of early skeletal muscle regeneration, in terms of chemical interactions with the ECM proteins and the physical constraints mimicking a necrosed myofiber.

This method is not compatible with our micropatterned based downsized system, if not combined with use of recessed wells (as shown in the Fig. S2I), but the absence of preexisting hydrogel allows pre-alignment of the seeded myoblasts in the substrate striations, which results in a mono-cylindrical shape of the sarcomeric network. Indeed, the alignment in the axis of the pillars takes place in a steadier manner than in models using gel scaffolds (Sakar et al., 2012) (Cvetkovic et al., 2014) (Mills et al., 2019). This is beneficial since variability in myotube density and orientation within the gel construct might create biases of force measurement. In the here developed system gel-free seeded myoblasts would form more compact myotube bundles with straighter orientation, theoretically improving the quality of force measurement, with production of their own matrix by the cells.

Spontaneous twitch contractions in 3D myotubes derived from primary human myoblasts were observed, and the model is thus greatly simplified by the suppression of numerous protocol steps usually associated to the activation of contraction, notably during cell culture and contraction monitoring. Primary tissues obtained do not need optogenetical (Mills et al., 2019)(Afshar et al., 2020) nor electrophysiological (Rao et al., 2018) modifications to be used in our system and therefore this surely represent a powerful material to study contractions as cells can be used straight after biopsy from the patients. Interestingly, spontaneous contractions were also observed in immortalized myoblasts-derived 3D myotubes (data not shown). In comparison to activated contractions, spontaneous contractions are not systematically observed in every matured tissue, which is usually fixed by the use of drugs (Caffein, Calmodulin, Nocodazol, Rapamycin, Bosutinib, Reparixin, etc…), ions (Calcium, Potassium, etc…), and other molecular supports such as ATP (Osaki et al., 2020). This promising optimization remains to be performed to gain in efficiency and control. The addition of optogenetic and electrophysiological activation to the system would also be interesting to make it more complete while preserving the downsizing benefits.

The specific forces of the spontaneous contractions here observed are in the order of few mN/mm^2, which is comparable to the specific forces of twitch and tetanic contractions measured in other muscle constructs (Afshar et al., 2020) (Rao et al., 2018) (Mills et al., 2019) (Sakar et al., 2012). This value is particularly interesting due to the

spontaneous nature of the observed contractions, in opposition of the optogenetical or electrophysiological activated ones from the literature. This also shows that our model allows to sense subtle generated force thanks to the finely tunable spring constant of the pillars.

Our reduced-scale model allows to precisely image subcellular structure like nuclei, sarcomeric network and many others. As expected, in absence of direct physical constraints from the substrate, 3D myotube nuclei substantially lost their 2D flatness (Fig. 5). The nuclei kept a length superior to their width and height, which is most likely due to the longitudinal mechanical forces exerted within the myotube by the cytoskeleton. This nuclear phenotype could also be reproduced previously by exerting external force on gel-borne nuclei (Bertrand et al., 2014). Interestingly, the overall volume of 2D monolayer nuclei was found to be more important than the one of 3D myotubes (Fig. 5K), confirming the relative morphological aberrance caused by 2D culture and proving the need for three-dimensional systems of culture. We also found the nuclei from 3D myotube to display similar height (Fig. 5F) and width (Fig. 5H) (respectively 7.7 and 7 µm). This is consistent with the shape of *in vivo* myonuclei described in the literature (Bruusgaard *et al.* 2010)(Hastings *et al.* 2020), which makes our culture chip a relevant tool for the analysis of nuclei-linked pathology, such as laminopathies.

The importance of the lamin envelope for nuclei morphological integrity is well known. Mutation in the LMNA gene, coding for Lamin A and Lamin C proteins, is highly detrimental to nuclei organization as it causes deleterious nuclear defects such as chromatin protrusion and nuclear envelope rupture (Earle et al., 2020). LMNA-related Congenital Muscular Dystrophy (L-CMD), the most severe type of laminopathy, affects various tissues including the striated muscles (Bertrand et al., 2020). The ΔK32-P1 mutant myoblast lineage (Bertrand et al., 2014) we cultured into 3D myotube expressed the same nuclear phenotype (elongation in comparison to WT nuclei) that has been previously observed in preceding 3D skeletal muscle platforms (Maffioletti et al., 2018). As expected, LMNA mutated nuclei showed similar morphological aberrations such as increased flatness and volume. This proves that our 3D myotube culture chip is a reliable system to model such muscular disorders, with potential applications in terms of therapeutic molecular screening.

Supplementary data

Matrigel Micro-Patterned Chip Preparation and 3D Myotube Culture

(Manipulate PDMS chip and liquid reagents under Laminar Flow Cabinet)

Surface Passivisation

-Mold PDMS chips on silicon wafer and let 2hrs at 80°C.
-Cut the PDMS chips (around 1 cm^2) from the wafer (the edges must be neat to avoid liquid leakage).
-Hydrophilize PDMS chips with plasma cleaner (or deep UVs) at full power for 5min while preparing 1X PLL-PEG with PBS (100 uL per chip).
-Immediately after plasma cleaning, add PLL-PEG 1X (50-100 uL/chip) on the chips and leave it for 1hr.
-Rinse with PBS vigorously 3 times each PDMS chip to remove the PLL-PEG.
(From that point, do not let the chips dry up)

Patterning with Primo

(Keep the samples and reagents protected from the light)
-Put a chip on glass coverslip, remove excess of PBS without letting the chip drying up.
-Add 40uL of PLPP and mix to homogenize with remaining PBS.
-Put the cover slip on the Primo facility and pattern for 20 min maximum to keep the PLPP wet (Dose per pattern = 1200 mJ/mm2).
-Once the UV exposition done, rinse the PLPP very rigorously 5-6 times with PBS (go back and forth with the pipet at least 5 times for each rinsing).
-Add Matrigel 1mg/mL + 1:50 FN-Cy5 by washing 3 times 50uL each chip (remove as much PBS as possible to keep the Matrigel dilution as pure as possible).
-Let the matrigel at T°room for 1hr (from now on, keep the samples protected from the light).
-Rinse very gently the matrigel away with ddH2O.

Cell seeding and 3D myotube culture

-Rinse the chips with sterile PBS and transfer them in a new well plate. (do not let it dry)
-Plate 100k to 200k cells (depending on cell type) over the chip, do not mix with the medium. Spin 5min at 300g and leave it for an hour in incubation.
-Change medium to rinse out off-pattern cells while keeping the chips immerged in the medium
-Let the seeded chips in growth condition overnight and change to differentiation medium.
-After tissue formation, be careful and gentle while changing medium.
-To generate Acetylcholine receptors clusters, add Agrin (0.4μg/mL) the day before contraction assay.
-Gently add 1mL of pre-warmed fresh medium before videomicroscopy for contraction monitoring

Immunostaining

-Pipet out medium while keeping the chips immerged and gently add PFA 4% (repeat 2-3 times).
-Continue as a classic immunostaining.
-Prepare 35mm round slide in 60mm petri dish for each chip.
-Add 7.5μL of mounting medium on each petri dish (Do not put more)
-Once the staining done, pipet out and absorb all PBS form the chip and mount it upside down.
-Keep the petri dish containing chips sealed at 4°C.

Figure S1: Experimental protocol for micropatterned chip preparation and 3D myotube culture.

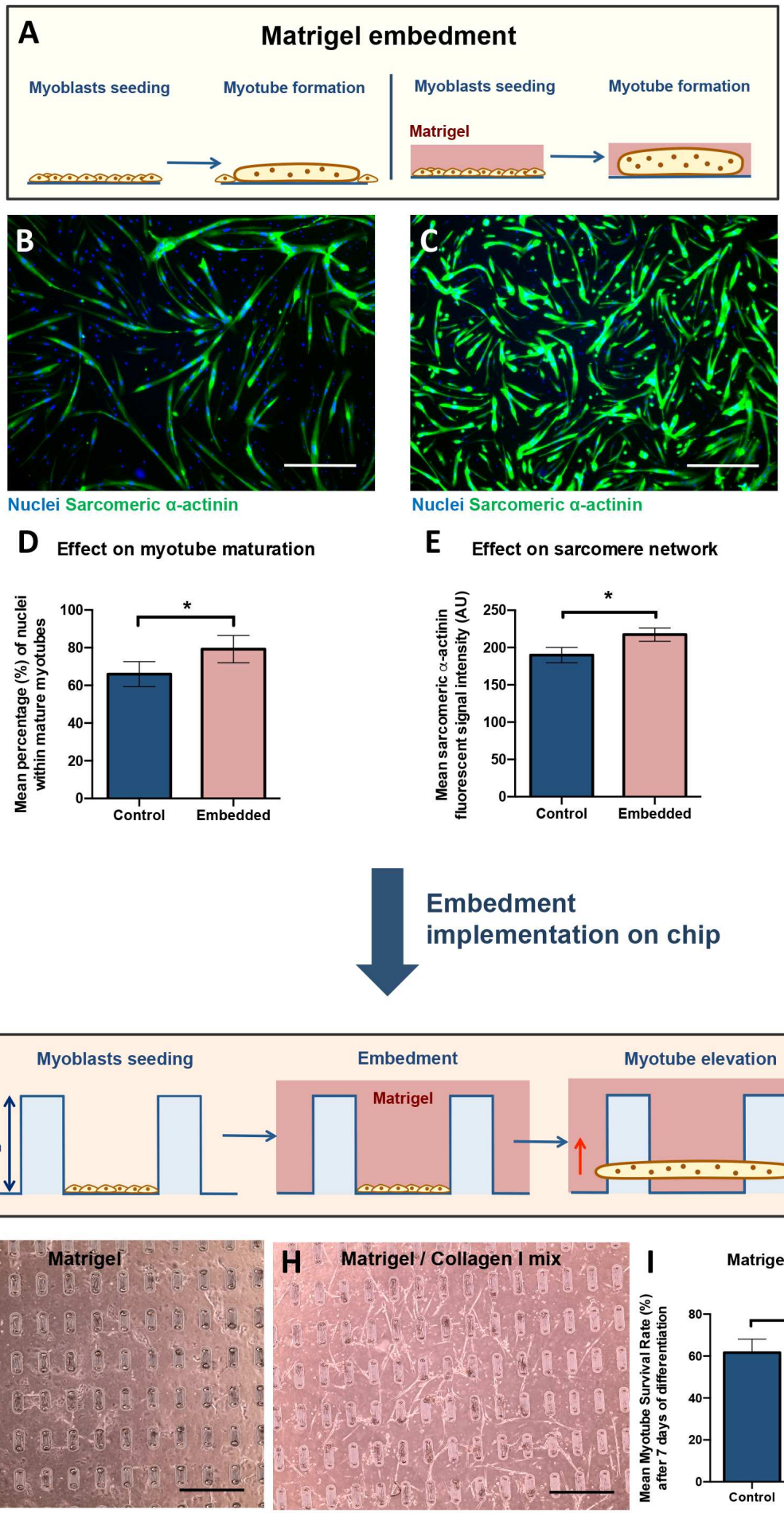
A
Matrigel embedment
Myoblasts seeding
Myotube formation
Myoblasts seeding
Myotube formation
Matrigel
B
C
Nuclei Sarcomeric α-actinin
Nuclei Sarcomeric α-actinin
D
Effect on myotube maturation
Mean percentage (%) of nuclei within mature myotubes
100
80
60
40
20
0
*
Control
Embedded
E
Effect on sarcomere network
Mean sarcomeric α-actinin fluorescent signal intensity (AU)
250
200
150
100
50
0
*
Control
Embedded
Embedment implementation on chip
F
Myoblasts seeding
Embedment
Myotube elevation
80 µm
Matrigel
G
Matrigel
H
Matrigel / Collagen I mix
I
Matrigel-Col I mix
Mean Myotube Survival Rate (%) after 7 days of differentiation
80
60
40
20
0
*
Control
Embedded

Figure S2: Incrementation of gel embedment methods in the system. A. Schematic representation of Matrigel embedment protocol (right) in comparison to classic 2D culture of myotubes (left). **B,C.** Representative images of immunofluorescent stained myotubes (from human immortalized myoblasts) after 6 days differentiation in normal 2D culture conditions (B) and Matrigel embedment conditions (C) (Sarcomeric α-actinin (green), nuclei (blue) scale bars = 500 µm). **D.** Mean percentage ± s.e.m. of nuclei located within mature (Sarcomeric α-actinin-expressing) myotubes (from human immortalized (8220 and AB1190) myoblasts) after 6 days of differentiation with or without Matrigel embedment. **p*<0.05 (Wilcoxon matched-pairs signed rank test), N=3. **E.** Mean fluorescent signal intensity (Arbitrary Unit) ± s.e.m. from labeled Sarcomeric α-actinin of myotubes (from human immortalized (8220 and AB1190) myoblasts) after 6 days of differentiation with or without Matrigel embedment. **p*<0.05 (Wilcoxon matched-pairs signed rank test), N=3. **F.** Schematic representation of Matrigel embedment protocol adapted to 3D myotube culture on chip. **G,H.** Transmitted light microscopic images of myotubes (from human immortalized (8220 and AB1190) myoblasts) after 7 days of differentiation with pure Matrigel (G), and Matrigel/Collagen I mix (H) embedments. Scale bars = 500 µm. **I.** Mean myotube (from human immortalized (8220 and AB1190) myoblasts) survival rate ± s.e.m. after 7 days of differentiation on chip in normal culture conditions or Matrigel/Collagen I mix embedment. **p*<0.05 (Mann-Whitney unpaired test), N=4.

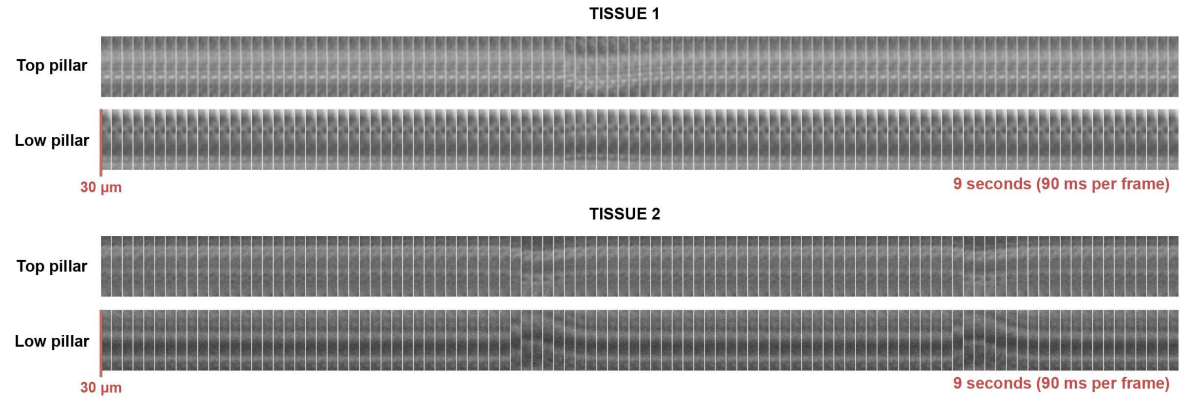

Figure S3: Kymographs. Transmitted light microscopic images of contracting 3D myotubes from human primary myoblasts after 9 days of differentiation.

Cell Line	Genotype	Phenotype	Lineage	Muscle	Sex	Age
8220	-	Healthy	Immortalized	Paraspinal	Male	12 yo
AB1190	-	Healthy	Immortalized	Paravertebral	Male	16 yo
EMD1365	LMNA AAG, pLys32del c. del94-96	LMNA related Congenital Muscular Dystrophy	Immortalized	Right gluteal	Male	13 yo
AB678C53Q	-	Healthy	Primary	Quadriceps	Male	53 yo

Table 1: Description table of cell lineages used in the presented figures.

Pattern n°	Striation	Shape	Minor axis (µm)	Major axis (µm)	Axial ratio	Height (µm)	k constant spring (µN/µm)
1	3.5 µm	Ellipse	57	80.7	1.4	148.5	1.2
2	3.5 µm	Ellipse	21.4	70.5	3.3	137	0.07
3	3.5 µm	round	57	-	1	138	1.06
4	3.5 µm	Ellipse	44	80	1.8	145	0.59
5	3.5 µm	Ellipse	30	54	1.8	130	0.18
6	3.5 µm	Ellipse	27	44.7	1.7	135	0.09
7	3.5 µm	Ellipse	42.4	81.5	1.9	145	
8	3.5 µm	Ellipse	57	-	1		

Table 2: Description table of PDMS microfabricated pillar patterns used in the presented figures.

Mechanosensitivity of satellite cells quiescence in early muscle regeneration

1. Materials and methods

- *1.1. Satellite cells isolation and primary myoblast lineage generation.*

Wild-type mice used in this project were 2 to 5 months-old C57Bl6/N mice purchased from Janvier Laboratories. Satellite cells were isolated by fluorescence-activated cell sorting, using the protocol from Liu et al. 2015 (Liu *et al.* 2015). Murine myoblast lineage were generated using Satellite Cell Isolation Kit MACS protocol (Miltenyi Biotec). Briefly, hindlimb muscles were dissected, minced and transfered in a 50mL falcon tube with 1000U/mL collagenase II. The mixture were first digested for 1hr30, and digested a second time with 100U/mL Collagenase II and 1.1U/mL solution for 30min. Each digestion was performed in a shaking bath at 37°C, and were followed by pipet trituration, centrifugation and rinsing of digestion solution. Digested samples were triturated with syringe (20G needles) and filtered in 40µm strainer. Isolation were performed by magnetic-activated cell sorting with satellite cell isolation antibodies kit. Satellite cells were amplified and used under 10 passages.

- *1.2. PEG hydrogels preparation and cell culture.*

PEG hydrogels were prepared following Gilbert lab protocol (described in Davoudi and Gilbert 2017) and coated with Matrigel matrix solution (1mg/mL in DMEM). Satellite cells and myoblasts were amplified in growth condition on collagen-coated Petri dish with Ham's F10 (complemented with 20% FBS, 1% Anti/anti and 2.5ng/ml of bFGF). Differentiation was induced by incubating cells in DMEM (complemented with 2% Horse serum and 1% penicillin/streptomycin).

- *1.3. RNA extraction and transcriptomic analysis.*

Myoblasts were plated on hydrogels, centrifuged (300g for 5min) and incubated for 24hrs at 37°C. Cells were then trypsinized and pelleted to be kept at -80°C. RNA was extracted using MiniPrep RNA extraction kit. Microarray analysis were performed (with

ClariomS Mouse chip, Ovation PicoSL v2 chemistry and Partek7.18 software) by Cochin Hospital's GENOM'IC platform.

- *1.4. Immunostaining and imaging.*

Samples were fixed 10min with 4% Paraformaldehyde (formaldehyde) aqueous solution, blocked with 4% Bovine Serum Albumin (BSA) in PBS (complemented with 0.2% TritonX-100, 2.5% Horse serum). Primary antibodies (diluted in blocking solution) were incubated overnight at 4°C (Pax7 1 :10, DSHB ; MyoD 1:100, sc-760), secondary antibodies 45min at room temperature (Alexa-Fluor-488/647-conjugated, Life technologies, 1 :500) and nuclei were stained with Hoechst 33342 (1:10 000 for 5min at room temperature). Images were acquired with EVOS FL Cell Imaging System microscope (Life Technologies) and treated with ImageJ.

2. Results

- *2.1. Satellite cells activation is facilitated by stiffening of the niche.*

First, we cultured primary murine myoblasts on PEG hydrogels with muscle-like Young's modulus of 12 and 40 kPa (Fig. 1A). Whether in proliferating (Fig. 1B) or differentiating (Fig. 1C) conditions, 40 kPa hydrogels displayed increased cell density compared to 12 kPa gels. Then, isolated satellite cells were directly plated on 12 and 40 kPa hydrogels and cultured 4 days in growth condition (Fig. 1D) to be fixed and stained with specific markers (Pax7 and MyoD).

As explained in the introduction (see chapter A.3), Pax7 is expressed in muscle stem cells and myoblasts nuclei, whereas MyoD is expressed in myoblasts nuclei through proliferation and commitment into myocyte. Therefore, it can be considered that Pax7-positive/MyoD-negative cells are quiescent muscle stem cells, Pax7-positive/MyoD-positive cells are proliferating myoblasts and Pax7-negative/MyoD-positive cells are commited into myocytes. Comparing these three classes (Fig. 1E-G), we found the proportion of Pax7-positive/MyoD-negative nuclei to be significantly decreased in cells cultured on 40 kPa gels, while the proportion of Pax7-positive/MyoD-positive nuclei were significantly increased in comparison to cells cultured on 12 kPa gels. This indicates a shift of quiescent muscle stem cells population toward proliferating myoblasts when cultured on 40 kPa gels compared to 12 kPa gels.

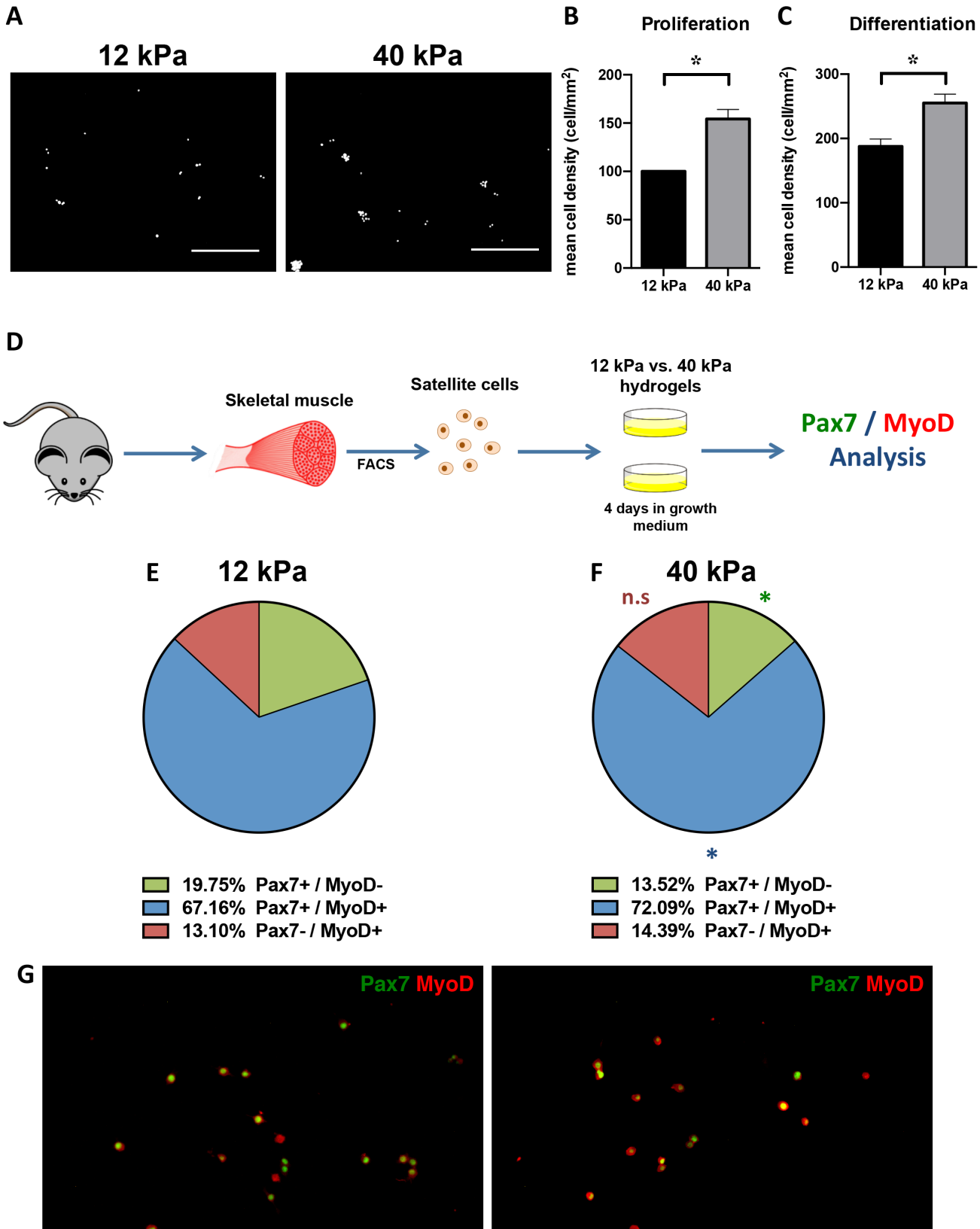
A
12 kPa
40 kPa
B
Proliferation
mean cell density (cell/mm²)
200
150
100
50
0
*
12 kPa
40 kPa
C
Differentiation
mean cell density (cell/mm²)
300
200
100
0
*
12 kPa
40 kPa
D
Skeletal muscle
FACS
Satellite cells
12 kPa vs. 40 kPa hydrogels
4 days in growth medium
Pax7 / MyoD Analysis
E
12 kPa
19.75% Pax7+ / MyoD-
67.16% Pax7+ / MyoD+
13.10% Pax7- / MyoD+
F
40 kPa
n.s
*
*
13.52% Pax7+ / MyoD-
72.09% Pax7+ / MyoD+
14.39% Pax7- / MyoD+
G
Pax7 MyoD
Pax7 MyoD

Figure 1: Transient muscle stiffness increase promotes satellite cells activation. A. Representative images of Hoechst-labeled nuclei from primary murine myoblasts on 12 kPa (left) or 40 kPa (right) hydrogels after 48 hours in growth medium. Scale bars = 100 µm. **B.** Mean normalized cell density per mm^2 ± s.e.m. of cells cultured on 12 kPa or 40 kPa hydrogels after 48 hours in growth medium. *p<0.05 (Normalized unpaired t-test). **C.** Mean cell density per mm^2 ± s.e.m. of cells cultured on 12 kPa or 40 kPa hydrogels after 10 days of differentiation *p<0.05 (Unpaired t-test). **D.** Experimental design (FACS = Fluorescence-activated cell sorting). **E,F.** Percentages of Pax7- and MyoD-positive FACS-isolated satellite cells after 4 days in growth culture on 12 kPa (E) or 40 kPa (F) hydrogels. Data are presented as a mean from at least three independent experiments. *p<0.05, *n.s*=not significant, compared to 12 kPa (Unpaired t-test). **G.** Representative images of immunofluorescent staining of Pax7 and MyoD on cells cultured on 12 kPa (left) or 40 kPa (right) hydrogels. Scale bars = 50 µm.

- *2.2. Influence of substrate stiffness on gene expression.*

To investigate the mechanisms underneath the promotion of satellite cells activation caused by the transient muscle stiffness increase, we performed a transcriptomic analysis of murine primary myoblast cultured on 12 and 40 kPa hydrogels beforehand (Fig. 2A). Among the transcripts differentially expressed (Fig. 2B), we found 18 which are known in the literature as quiescence signature genes (Supplementary Fig. S2). These genes are associated with satellite cell quiescent state, whether positively or negatively (ADAMTS2 and MCAT) (Fig. 2C).

Interestingly, we found differentially expressed transcripts (Alk2 receptor and Smad4 effector) from the Bone Morphogenetic Pathway (BMP) (Fig. 2B), which has been shown to influence myogenesis (Ono et al. 2011 ; Paris et al. 2016 ; Stanzou et al. 2017). We also found differentially expressed transcripts (FGF7 ligand and its specific receptor FGFR2) from Fibroblast Growth Factor (FGF7) pathway (Fig. 2B), whose role in muscle regeneration remains mainly unknown.

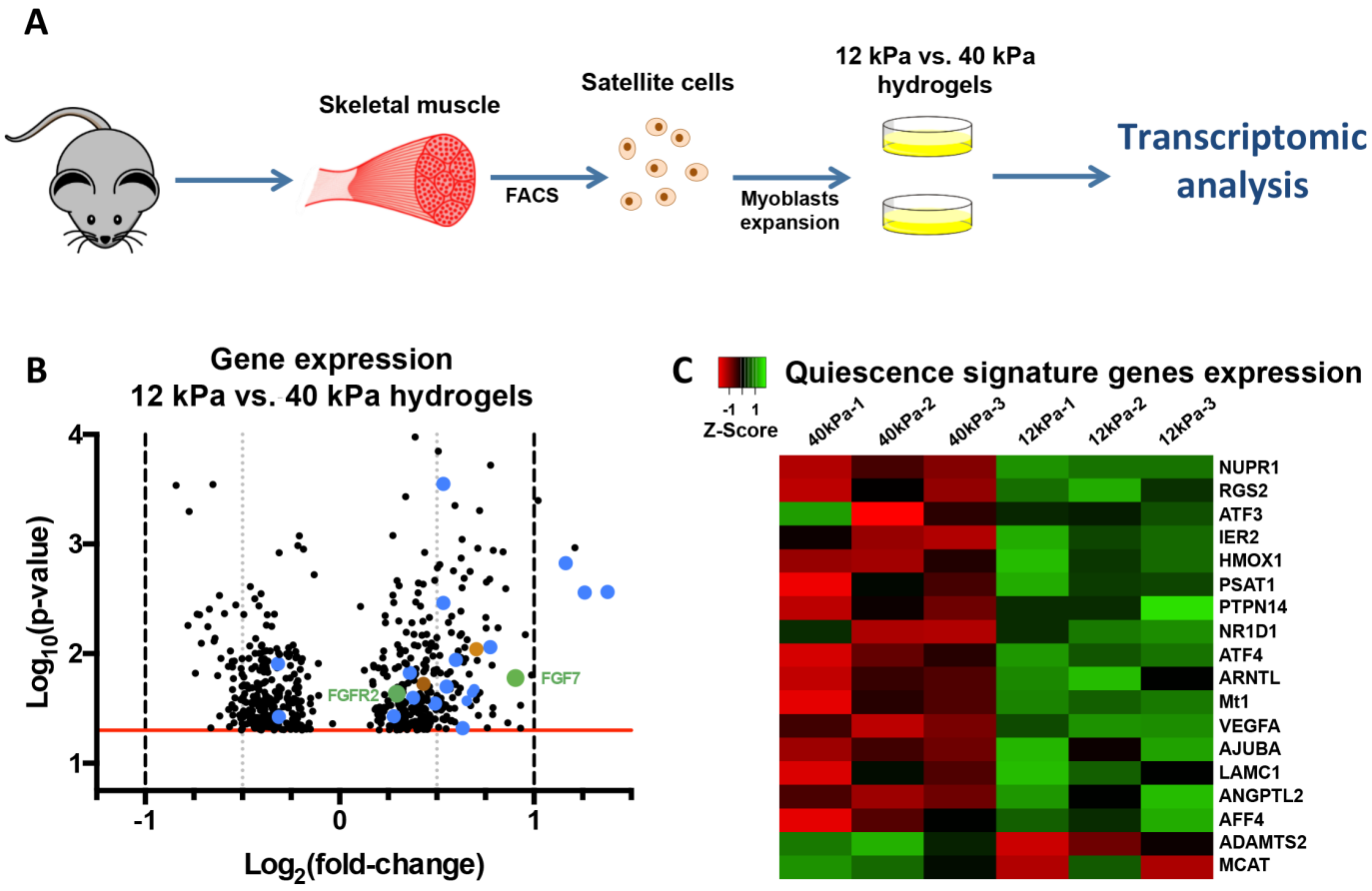

Figure 2: Transcriptomic analysis of the transient muscle stiffness effect on primary murine myoblasts. A. Schematic representation of the experimental design. **B**. Volcano plot of the 669 significantly differentially expressed genes (with a p-value<0.05, represented in red) on 12 kPa hydrogels compared to 40 kPa hydrogels (18 quiescence signature genes are represented by blue dots, 2 FGF7 pathway genes are represented by green dots, 2 BMP pathway genes are represented by orange dots). **C.** Heatmap of differentially expressed quiescence signature genes associated Z-scores (calculated with Heatmapper.ca Euclidean distance measurement method) from micro-array analysis of primary myoblasts cultured on 12 kPa and 40 kPa hydrogels.

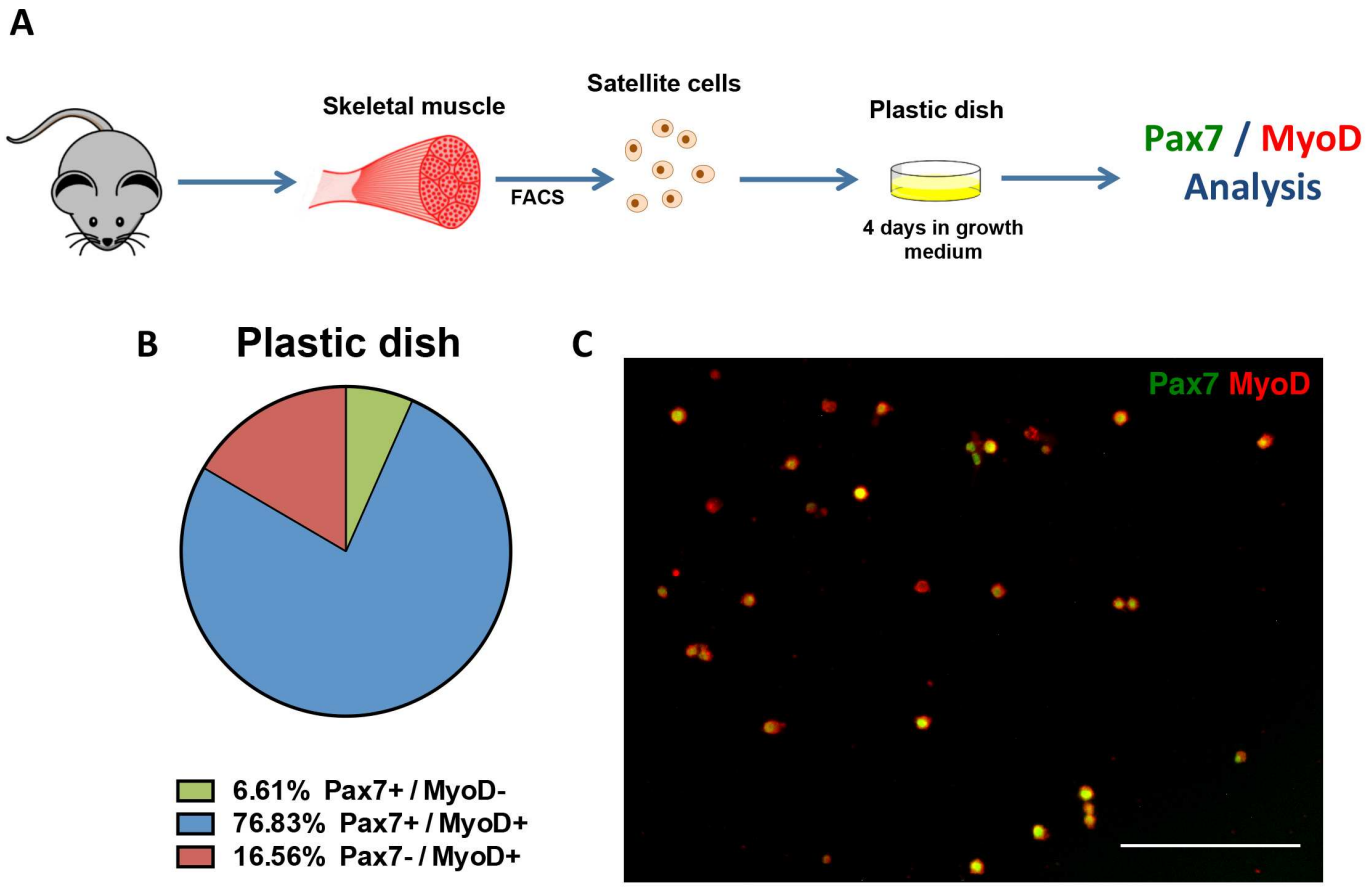

Figure S1: Plastic dish cultured satellite cells activation level. A. Experimental design (FACS = Fluorescence-activated cell sorting). **B.** Percentages of Pax7- and MyoD-positive FACS-isolated satellite cells after 4 days in growth culture on plastic. Data presented correspond to average values obtained from at least three independent experiments. **C.** Representative image of immunofluorescent staining of Pax7 and MyoD on cells cultured on plastic. Scale bar = 50 µm.

Over-expression	Transcript	Full name	Sources	Mechanisms
12 kPa gels	NUPR1	Nuclear protein 1, transcriptional regulator	Sambasivan *et al.* 2009	Cell cycle inhibitor, inducing differentiation in C2C12 cells
	RGS2	Regulator of G protein signaling 2	Fukada *et al.* 2007	Cell cycle inhibitor, upregulated in quiescent satellite cells and downregulated in activated ones
	ATF3	Activating transcription factor 3	Pietrosemoli *et al.* 2017	Quiescence signature
	IER2	Immediate early response 2	Pietrosemoli *et al.* 2017	Qiescence signature
	HMOX1	Heme oxygenase 1	Kozakowska *et al.* 2018	HO-1 deficient satellite cells are prone to activation
	PSAT1	Phosphoserine aminotransferase 1	Hwang *et al.* 2016	Promote the self-renewal of Embryonic Stem Cells
	PTPN14	Protein tyrosine phosphatase, non-receptor type 14	Michaloglou *et al.* 2013	Negative regulator of YAP (which promotes activation according to Judson et al. 2012)
	NR1D1	Nuclear receptor subfamily 1 group D member 1	Chatterjee *et al.* 2019	Inhibits both proliferation and myogenic progression (through Wnt/Bcat activation)
	ATF4	Activating transcription factor 4	Zismanov *et al.* 2016	Upregulated translation (through eIF2a's phosphorylation) in quiescent satellite cells compared to 3 days activated ones
	ARNTL	Aryl hydrocarbon receptor nuclear translocator like	Pietrosemoli *et al.* 2017	Quiescence signature
	Mt1	Metallothionein 1	Di Foggia *et al.* 2012	Improves sattelite cells pool
	VEGFA	Vascular endothelial growth factor A	Verma *et al.* 2018	Maintains quiescence
	AJUBA	Ajuba LIM protein	Judson *et al.* 2012	Inhibits YAP (which promotes activation according to Judson et al. 2012)
	LAMC1	Laminin subunit gamma 1	Bentzinger *et al.* 2014	More expressed in quiescent satellite cells
	ANGPTL2	Angiopoietin like 2	Zhao *et al.* 2018	Knock out of ANGPTL2 increases satellite cells activation
	AFF4	AF4/FMR2 family member 4	Gala *et al.* 2018	Represses G0-stalled genes ; AFF4 deletion leads to accelerated cell cycle progression
40 kPa gels	ADAMTS2	ADAM metallopeptidase with thrombospondin type 1 motif 2	Pallafacchina *et al.* 2010	Low in quiescent cells, increased during activation
	MCAT	Malonyl-CoA-acyl carrier protein transacylase	Judson *et al.* 2012	Downstream target of YAP (which promotes activation according to Judson et al. 2012)
		Quiescent state marker for satellite cells		
		Activated state marker for satellite cells		

Figure S2: List of quiescence signature genes differentially expressed between primary myoblasts cultured on 12 vs. 40 kPa hydrogels.

3. Discussion

Mimicking the mechanical properties of the satellite cell niche during early muscle regeneration permitted to assess the effect of microenvironment stiffness on muscle stem cell quiescence. Our results demonstrate the promotion of satellite cells activation by transient muscle stiffness increase in the first 3 days of regeneration. We propose that the evolution of the microenvironment mechanical properties helps to guide progenitor cells through myogenesis during early muscle regeneration and is essential to maintain the skeletal muscle regenerative capacity. Thus, the resting 12 kPa muscle stiffness promotes stem cell quiescence, the transient increase in the first 3 days post-injury triggers satellite cells activation and proliferation, and the decrease to normal stiffness level (12 kPa) at the 4th day post-injury facilitates the return to quiescence and self-renewal of the satellite cell pool.

Unlike satellite cell survival, which is facilitated on non injured muscle-like stiffness (12 kPa hydrogels) (Gilbert and Blau 2011), culture of myoblasts on 1 to 3 days post injury (d.p.i.) muscle-like stiffness (40 kPa hydrogels) resulted in higher cell densities in proliferation and differentiation conditions (Fig. 1A-C). This is most likely due to increased proliferation on substrates with post injury-like stiffness, as suggested by the cell clusters observed on 40kPa gels (Fig. 1A) and the promotion of activation observed in the Figure 1F. Moreover, the defect of cell attachment on hydrogels compared to standard culture condition in Petri dishes might be due to a lack of matrigel adhesion on the gels.

Interestingly, in a similar experiment I performed on regular plastic Petri dish (Supplementary Fig. S1) in the context of a collaboration (studying the effect of LSD1 protein inhibition on satellite cells activation) with Isabella Scionti (Laurent Schaeffer research team, Institut NeuroMyoGène), the proportion of Pax7-positive/MyoD-negative nuclei was much lower (6.61%) than on hydrogels (12 kPa: 19.75%; 40 kPa: 13.52%) (Fig. 1E-F). This proportion is consistent with the experiment previously performed on plastic dishes in the litterature (Judson *et al.* 2018). These results confirm that culture on muscle-like stiffness preserves satellite cells regenerative potential (Gilbert *et al.* 2010).

Transcriptomic analysis with freshly FACS-isolated satellite cells would have been more relevant, unfortunately the quantity of cellular content required to perform the microarray was too high in that experimental setting, especially with the defect of cell adhesion to the hydrogels compared to classic culture on plastic dish, accentuating the need to seed a massive amount of primary myoblasts. However, as shown in Monge *et al.* 2017, the mechanosensitivity of quiescence is reversible and myoblasts can be amplified on plastic before use on softer gels. Moreover, the quiescence signature could still be observed on 12 kPa gels (Fig. 2C).

We found FGF7 and FGFR2 transcripts to be overexpressed in cells cultured on 12 kPa hydrogels, which would need to be confirmed with RT-qPCR experiments. Firstly demonstrated in 1996 (Hannon *et al.* 1996), FGF7 expression by skeletal muscle cells and FGFR2 pathway activation during myogenesis has been poorly investigated ever since in comparison to other FGF family members (Sheenan *et al.* 1999 ; Kastner *et al.* 2000), such as βFGF. Yet, FGF7 ligand have a specific and restricted affinity to FGFR2 (Zinkle and Mohammadi 2019) and should therefore be studied distinctly.

For the continuation of the project, it would be interesting to add FGF7 recombinant protein on satellite cells and perform a Pax7/MyoD analysis (as in the Fig. 1D and S1A) to search for an effect on activation. Also, BrdU proliferation assay (as performed in Girardi *et al.* 2020) and reserve cell assay (Pax7 staining of myotubes after 3days differentiation) should be performed on FGF7-treated myoblasts. Overall, we found 669 transcripts differentially expressed between cells cultured on 12 and 40 kPa. This gives as many leads to be investigated to better understand the mechanisms underlying the mechanosensitivity of quiescence in skeletal muscle stem cells (pathways linked to mechanotransduction should be prioritized).

To conclude, we established a direct causality between the stiffness of the niche and the regulation of myogenesis during early muscle regeneration. Since the physical parameters of the niche are highly dependent on the extracellular matrix volume and composition, the increase of stiffness and other mechanical constraints in the context of dystrophic and aged-linked fibrosis cannot be neglected for the study of pathogenesis

and for the therapeutic approach. These aspects will be further examined in the conclusion chapter.

CONCLUSION

During this doctoral project, we investigated two different situations involving muscle mechanics study, one controlling the mechanical input applied to muscle cells by the niche, the second measuring the mechanical output generated by the muscle cells on the surrounding microenvironment. We recreated artificial niches and developed force-integrative approaches for mechanical interactions to be analyzed. In fact, we bioengineered new *ex vivo* models to answer a fundamental biology question, overcome a technical obstacle and get a deeper insight into cultured myotube organization and behaviour.

We cultured 3D myotubes using diverse cell lines from different muscle groups and various patients with diverging ages and phenotypes. However, the culture yields are cell lineage-dependent, which must be considered during the conception of experimental design. We bioengineered a force sensitive "Tissue-on-chip" device. Similar systems existed for other cell types such as fibroblasts (Legant *et al.* 2009) and cardiac cells (Boudou *et al.* 2012). But adapting such a technology to skeletal muscle is remarkably more worthy of interest since the skeletal muscle display more diversity of discrepancies in contraction pattern and force generation. Combining light-induced molecular adsorption technology and optimized micropatterned substrate design enabled us to outreach cell-to-constructs ratios previously obtained in the literature (1-6.7 kcell/3D construct ; for detailed comparison see Introduction Fig. 12E p.43).

Unlike the contractions triggered by electrophysiological and optogenetical activation currently assessed in other systems, spontaneous twitch contractions as obtained in this project are easier to monitor, and the generated forces displayed strong reproducibility (as shown in Fig. 4 p. 61). The specific forces of the spontaneous contractions are similar to the ones measured in other muscle constructs (few mN/mm^2) (Rao et al., 2018) (Mills et al., 2019) (Sakar et al., 2012). As mentioned in the Introduction, pre-suspension of myoblasts in gels can lead to misarrangement of 3D myotube, which affects force measurement. To that regard, our gel-free system associated to photopatterning and addition of striations (which are key components for myotube culture yield, as shown in

Fig. 3A p. 58) is a guarantee for compact myotube bundle formation and reliable force assessment. The finely tunable spring constant of the pillars and the miniature size of 3D myotubes provides more control on physical parameters such as the stiffness constraints applied to the myotubes or the mechanical force generated by the tissue.

This new *ex vivo* model can be used in multiple configurations with any kind of human myoblasts and skeletal muscle function might be investigated for nearly infinite different purposes:

-From understanding mechanisms of pathogenesis to screening therapeutic intervention for myopathies linked to various components of muscle fiber structure (Duchenne muscular dystrophy, oculopharyngeal muscular dystrophy, Dynamin 2-related centronuclear myopathy, etc…), laminopathies (LMNA-related Congenital Muscular Dystrophy, Emery-Dreifuss muscular dystrophies, striated muscle laminopathies, etc…), and other pathologies affecting the skeletal muscles such as myositis (primary inflammatory myopathy) or Pompe disease.

-Testing the reaction to different drugs, metabolites, ions and other types of treatments on contraction pattern and magnitude.

-Culturing 3D myotube from myoblasts with any given or induced genotype, issued from patients of any age and athletic background.

-Studying the effect of tissue length and substrate resistance on 3D myotube contraction pattern to give new insights on sarcomeric shortening and force generation.

As described in respective discussion sections of the two projects, there are still improvements to be incremented to get closer to *in vivo* condition and produce more reliable and ergonomic platforms. A noteworthy limitation of the doctoral project is the use of a single cell type (muscle stem cells and derived progeny). A potential perspective would consist in enriching these models with different progenitor cell types as it is done in other systems (Bakooshli *et al.* 2019, Osaki *et al*. 2019, Maffioletti *et al.* 2020). Indeed, prospective work might test the influence of transient muscle stiffness increase on gene expression and protein secretion of other cell types participating in early muscle regeneration, such as macrophages, fibroblasts, endothelial cells and many more.

In order to better comprehend muscle physiopathology, these two technologies represent a complementary approach to study both contraction patterns of patient-derived cells and myogenesis reaction to microenvironment stiffness variations. Ergo, they are intended to be used for large-scale applications in the field of myology studies, as well as therapy-oriented biomedical reasearches.

ANNEX

Annex 1 | Troubleshooting

The major project of my doctoral work mainly consisted in system development and protocol optimization. Thereby, many technical obstacles were encountered and had to be overcome.

In order to help the readers and future experimenters that would try to reproduce this method, our troubleshooting approach is described in the following table.

Troubleshooting	
ISSUE	**SOLUTION**
Silicon wafer type	Use a negative silicon wafer (with pillar-shape wells). Positive original wafers are more easily damaged and require to mold epoxy intermediate wafer, which lessens the final quality of microsubstrates. Check the pillars dimensions and integrity with electronic microscopy to have accurate contraction force measurement.
Silicon chip cutting	To avoid liquid leaks during incubations, the silicone chips must be neatly cut (without internal incisions).
PDMS hydrophilization	Give the chips appropriate exposure (5min) to plasma cleaning and add the PLL-PEG solution immediately after hydrophylization.
Photopatterning	Test a gradient of UV exposure on patterning efficacy. We found that 1000 mJ/ mm^2 dose to be the minimal for efficient matrigel adhesion (Fig. 2C) and we used 1200 mJ/ mm^2 exposure.
Matrigel patterning	To avoid excessive Matrigel dilution due to PBS remaining on the chip, add, homogenize and remove 50 µL of Matrigel solution (1 mg/mL in DMEM) from the chip 3 times.
Matrigel rinsing	Matrigel proteins can easily be washed away, use H_2O instead of PBS and rinse (with 100 µL) the chip only once, pipetting back and forth very gently.
Patterned chip usage	Do not let patterned chip overnight, seed the myoblasts in the following hours.
Chip detachment	Make sure the bottom of the chip is dry before plating it to the culture dish (wipe it if necessary) and avoid leaving air bubble between the chip and the receiving well.
Murine myoblasts	Murine myoblasts are much more difficult to culture as muscle microtissues in comparison to human myoblasts.
Choice of cell line	Myoblast lineages might display maturation and fusion discrepancies. These parameters must be checked in 2D culture first.
Myoblasts pre-culture	Use myoblasts with maximal confluency to obtain optimal 3D myotube formation.
Plated cell density	Add myoblasts in a small volume of medium and drop it above the chip before spinning the plate in the centrifuge (5min x 300g) to increase cell density and 3D myotube formation.
Medium change	Change the medium very gently and always keep the chip's surface immersed in medium.
Chip mounting	Use the appropriate amount of mounting medium. Excess of mounting medium might cause chip sliding and 3D myotube detachment, whereas lack of mounting medium might cause the pillars to be crushed against the coverslip.

Annex 2 | Muscle-tendon junction modelisation

During my PhD, I also participated in a project led by Clément Rieu and Léa Trichet from the Laboratoire de Chimie de la Matière Condensée de Paris, in collaboration with Fabien Le Grand's research team. This research project also aimed at developing a new *ex vivo* culture system, specifically to mimic the myotendinous junction.

In the pre-print article below, which has been posted on bioRχiv.org (doi: https://doi.org/10.1101/2020.05.12.091868) and submitted as a communication to Biomaterials Science, I performed the myoblasts and tenoblasts culture and immunostaining and part of the imaging, while Clément Rieu performed the thread extrusion, part of the imaging, data analysis and figure design.

In this work, collagen and fibrin threads were developed and used as culture substrates to model the myotendinous junction. Collagen threads displayed an increased stiffness compared to the fibrin ones, and mechanical properties were overall more similar between Collagen and Collagen/fibrin mixed threads. These latter thread compositions enable to decouple mechanical features from chemical properties by providing fibrin islands for the cells to adhere, together with the stiffness of the embedding collagen network. Both primary tenoblasts and myoblasts had the same behaviour on mixed and fibrin threads, rather than on Collagen, showing the importance of the chemical interaction with the extracellular matrix. However, myoblasts differentiated but did not fuse on threads, in contrary to 2D controls, which might be attributed to substrate curvature.

Differential myoblast and tenoblast affinity to collagen, fibrin and mixed threads in the prospect of muscle-tendon junction modelisation

Clément Rieu, Nicolas Rose, Anissa Taleb, Gervaise Mosser, Bernard Haye, Thibaud Coradin, Fabien Le Grand*, Léa Trichet*

Abstract

The myotendinous junction transfers forces from muscle to tendon. As such, it must hold two tissues of completely different biological and cellular compositions as well as mechanical properties (kPa-MPa to MPa-GPa) and is subject to frequent stresses of high amplitude. This region remains a weak point of the muscle-tendon unit and is involved in frequent injuries. We here produce fibrin (40 mg/mL, E0 =0.10 ± 0.02 MPa) and collagen (60 mg/mL, E0=0.57 ± 0.05 MPa) threads as well as mixed collagen:fibrin threads (3:2 in mass, E0 = 0.33 ± 0.05 MPa) and investigate the difference of affinity between primary murine myoblasts and tenoblasts. We demonstrate a similar behavior of cells on mixed and fibrin threads with high adherence of tenoblasts and myoblasts, in comparison to collagen threads that promote high adherence and proliferation of tenoblasts but not of myoblasts. Besides, we show that myoblasts on threads differentiate but do not fuse, on the contrary to 2D control substrates, raising the question of the effect of substrate curvature on the ability of myoblasts to fuse *in vitro*.

Introduction

Tendons are connective tissues that anchor skeletal muscles to the bones, transmitting the force generated by the muscles to the skeletal structure. As such, tendons play an obvious role in everyday movement and posture control. In case of injury, partly due to their low vascularization, they exhibit poor regeneration capacity resulting in loss of mobility, pain, *etc.* Injury of the muscle-tendon unit often occurs in the junction area as reported in many articles [1–5]. In particular, muscle injuries are often located close to the junction [6,7], leading to the rupture of the myofibres rather than the tearing of the collagen fibres from the sarcolemma. Tensile tests on whole muscle-tendon units from rabbits also highlighted the weakness of the myo-tendinous junction (MTJ) area [6]. As muscles often taper in contact with the tendon, stress concentration increases with decreasing cross-section [8].

During muscle regeneration process, quiescent muscle stem cells called satellite cells activate, and give rise to proliferating myoblasts destined to differentiate into myocytes able to fuse with one another or with injured myofibres [9]. Up to date both the intrinsic transcription factors and the extrinsic cell-to-cell signaling pathways controlling muscle stem cells and myoblasts functions are well characterized. However, an emerging body of evidence supports the notion that myogenic cells integrate biochemical factors together with biomechanical cues that may control their cell fate[10].
Muscles and tendons have completely different composition and structure, resulting in radically different mechanical properties: muscles are soft materials with Young moduli

between 0.005 and 3 MPa while tendons are much stiffer, with Young moduli ranging from 500 to 1850 MPa [11]. Junctions between materials with such a difference in mechanical properties may result in high interfacial stress and are likely to fail first during mechanical solicitation all the more since the stress borne by the MTJ reaches several tens of kPa [12]. The increase of the contact surface between tendon and muscle by a factor 10 to 20, with finger-like structures, enables to decrease this stress [13]. Along the myofibers the repeating sarcomeric units consist of an overlap of myosin and actin filaments, with Z-lines acting as anchoring points of the actin filaments and delineating the sarcomeric segments. In the peripheral finger-like structures, the last Z line is linked to the interdigitated sarcolemma through actin filament bundles. These actin filaments bind to transmembrane protein complexes containing integrins, and interact with the collagen IV and laminin-rich basal membrane and the extra-cellular matrix of tendons, rich in collagen I. Rebuilding the MTJ following muscle injury may thus subject progenitor cells to highly different environmental stiffnesses that promote divergent cellular responses.

For both muscular and tendon sides, reconstruction of the MTJ is relevant to help reconstruction in case of damaged MTJ or for better integration of the neo-tissue. For instance, in the hypothetical case of the grafting of a tendon *de novo*, integration at the muscular level through a new MTJ may be more effective and rapid as muscle is highly vascularized and is rich in satellite cells. MTJ structure is much less documented than muscle or tendon ones, and attempts to reproduce the MTJ are also scarce. We can cite the work reported by Ladd *et al.* [11] in which two different polymers are electrospun with collagen the poly(L lactic acid), being stiffer, for the tendon part and poly(ε -caprolactone) for the muscle part. Merceron *et al.* [14] used co-printing of two synthetic polymers polyurethane (PU) and poly(ε-caprolactone) (PCL) together with a bio-ink based on hyaluronic acid, fibrinogen and gelatin. The bio-ink contained C2C12 myoblasts on the PU side while the bio-ink on the stiffer PCL side contained NIH/3T3 cells. Both works used two materials with different mechanical properties to mimic the tendon and the muscle sides.

Mechanical properties of the substrate have been highlighted as key factors to control cell migration [15,16] and differentiation [17,18]. In particular, substrate stiffness has been shown to play a role in muscle stem cells self-renewal [19], as well as in myotubes differentiation [20]. Substrate stiffness has also been shown to promote tendon progenitor cells (here called tenoblasts) differentiation [21,22]. Besides cell interactions with structural proteins have been shown to influence cell phenotype [23,24]. Among them, collagen and fibrin are among the preferential proteins used in tissue engineering.

Type I collagen is an ubiquitous fibrillar protein found in most of the connective tissues *in vivo* [25]. It is widely used in biomaterials [26] as it is a relatively stiff body protein [27] that bears multiple adhesion sites [28,29] for integrin receptors [30]. In particular, it is the major component of tendons, reaching 55 to 80 % of tendon's dry weight [31]. On the other hand, fibrin is a major player in haemostasis, and polymerizes to form a clot after activation of its precursor, the blood-born fibrinogen, by thrombin [32]. This fibrillar protein exhibits high deformability [33] and direct integrin adhesion sites [34–36], making it a material of choice for various applications such as for cardiovascular remediation [37–39] or cartilage repair [40–42]. It is particularly favored for muscular reconstruction [43–45].

In this work, we investigate the effect of collagen I, fibrin and of mixed collagen:fibrin materials on mouse primary tenoblasts and myoblasts. Given the differing mechanical properties of the constitutive proteins, such scaffolds, composed only of biopolymers, might represent new types of tools to screen the respective influence of compositional and mechanical features on cell behavior. As a first step and in the prospect of musculotendinous junction modelisation, the capacity of highly concentrated collagen to offer a proper environment for tenoblasts, and of softer fibrin to favour muscular development, will be tested, as well as the influence of a mixed material. For this purpose, collagen, fibrin and "mix" threads are extruded. Mechanical properties and structure of threads are characterized and primary myoblasts and tenoblasts extracted from mice hind limbs are seeded on the threads.

Material & Methods

Extrusion

Threads were produced based on protocols developed in [Rieu tb free]. Briefly, collagen solutions (extracted from rat tail tendons) were concentrated at 60 mg/mL in 3 mM HCl 0.8 mM citrate. Fibrinogen solutions were made from fibrinogen stock solutions (Merck) at 40 mg/mL by addition of HCl to reach 60 mM HCl. To obtain fibrin solutions, the acidic fibrinogen solution was supplemented with $CaCl_2$ (10 mM final) and thrombin (Sigma, 20 U/mL final). Such solution was either directly mixed with collagen at a ratio 1:1 (volume:volume) to prepare mix solution, or incubated 10 mn to reach suitable viscosity for pure fibrin extrusion.

Solutions were then transferred to a 1 mL syringe and centrifugated for 8 mn at 3000 x g to remove bubbles. They were then extruded in 100 mM HEPES 2.5 w.% PEG solutions, pH 7.4, through a 370 µm needle. The resulting threads (Fig.1.A) were left for at least 10 days in the HEPES/PEG solution and then rinsed at least three times with cell culture medium and left in it for 24 hours to remove PEG.

Tensile Testing

Tensile testing was done on an Instron 3343 machine equipped with a 10N load-cell and a watertight column to perform the tests in hydrated conditions. Tests were performed in PBS 1X, to mimic physiological conditions and thus give an idea of the possible mechanical behavior *in vivo*. Threads were immobilized into clamps with Velcro tape to prevent sliding of the threads. Strain was calculated with the displacement of the clamps.

Transmission Electron Microcopy

Hydrated samples, crosslinked with PFA, glutaraldehyde and osmium tetroxide 4 wt. %, were subsequently dehydrated using baths with increasing concentrations in ethanol. They were then progressively transferred to propylene oxide and to araldite resin prior to full embedding in pure araldite. After inclusion, 70 nm ultrathin sections (Leica microtome) were made and contrasted with uranyl acetate and observed on a transmission electron microscope FEI Tecnai Spirit G2 operating at 120 kV. Images were recorded on a Gatan Orius CCD camera.

Cell isolation

Satellite cells were extracted from the hindlimb muscles (hamstring muscle group, quadriceps,

tibialis, extensor digitorum longus, gastrocnemius, soleus, gluteus) of 2 to 3 months-old mice while tenoblasts were extracted from the mice Achilles tendons.

Muscles were dissected and minced to a pulp using forceps then digested with collagenase B solution (0.75 U/mL final, from Roche) with dispase II (1.2 U/mL final, from Roche) and CaCl2 (2.5 mM) at 37 °C for 40 minutes. Preparations were washed twice in culture media, filtered through a 70 µm cell strainer and subjected to immunomagnetic cell sorting using a "satellite cell isolation" kit and a MACS "midi" column (Miltenyi Biotech).

Tendons were either digested in 600 U/mL of collagenase II (Worthington) or in 1.5 U/mL of collagenase B (Roche) at 37°C for 18 hours, mechanically destroyed by up and down pipetting and filtered through a 100 µm cell strainer.

Primary myoblasts and tenoblasts were then amplified and cultured on collagen-coated plates for several passages.

Thread seeding

Threads were cut in approximately 1-cm-long pieces. They were seeded with myoblasts or tenoblasts at 10^5 cell/cm^2 in 24-well plates. Cells used were between P5 and P10 for both types. For tenoblasts, 3 threads of each condition were seeded with a first cell line and 1 thread with a different one. For myoblasts, two threads were seeded with a first line and two others with a second one.

Growth medium (high-serum medium - 79 % Hams F-10 from Gibco, 20 % fetal bovine serum, 1 % antibiotic-antimycotic Gibco, with 2.5 ng/mL recombinant human fibroblast growth factor R&D Systems) and fusion medium (low-serum medium - 94 % Dulbecco's Modified Eagle's Medium, Gibco, 5 % horse serum, 1 % antibiotic/ antimycotic Gibco) were changed every other day. Unless specified, the differentiation process involves 7 days of proliferation in the growth medium, followed by differentiation in the fusion medium. Aminocaproic acid (6-aminohexanoic acid, Sigma) at a final concentration of 2 mg/mL was added to both media. Recombinant human Wnt7a (Chinese Hamster Ovary cell line-derived, R&D Systems) at a concentration of 50 ng/mL was used for the culture displayed on Supp.Fig.1.

2D culture

Culture of myoblasts in 2D was performed in 24 well plates coated with the different materials. Plates were coated with collagen, mix and fibrin with the same solutions as the ones used for extrusion. A thin layer of the solution was deposited, with further addition of growth medium to trigger fibrillation. Matrigel-coated plates, used to promote fusion, were seeded as a reference (BD Biosciences). They were prepared by incubation at 37°C for 30 mn of a thin layer of Matrigel at 1 mg/mL and subsequent drying under the hood. They were then rehydrated using growth medium. Each well was seeded with a density of $2x10^4$ cells/cm^2, with triplicates per material, and left 1 day in proliferation medium for the myoblasts to attach and then cultured in fusion medium for 6 days. Aminocaproic acid at a final concentration of 2 mg/mL was added to both media.

Fluorescence microscopy

To be observed the seeded threads were rinsed with PBS 1X and then fixed with 4 % PFA for 15 minutes at room temperature. After a blocking step with BSA 4% for 45 minutes, cells were stained using primary (Myosin heavy chain: primary hybridoma mouse IgG2b; Myogenin: myogenin antibody (5FD) Santa Cruz biology;) and secondary antibodies (Red: Alexa Fluor 546 goat anti-mouse IgG2b, In vitrogen; Magenta: A647 anti-rabbit, Life Technology). Nuclei were stained with Hoechst (Life Technology). Observations were made on a calibrated EvosR fluorescence inverted microscope.

To assess homogeneity of mix threads, fibrinogen-FITC was used. To label fibrinogen, 20 mg of FITC CeliteR was dissolved in 3 mL of 0.13 M carbonate buffer pH 9.2. Fibrinogen stock solution at 40 mg/mL was then mixed to the FITC solution at a ratio 1:3. The resulting solution was then dialysed 48 hours against 2 L of a solution of 20 mM citrate pH 7.4, with regular changes of the dialysing bath. Final solution was aliquoted and stored at -80°C. For extrusion, 10% in volume of FITC-labelled fibrinogen [Fbg-FITC] was added to fibrinogen stock solution, before addition of HCl, and following the usual protocol afterwards.

Statistical analysis

For statistical analysis, imaging of every part of the threads was carried out at 4x magnification to minimize deviation due to image sampling. ImageJ software was used to measure cell density. An area taking only the central part of the thread was outlined and measured using ImageJ. The central area was chosen to be approximately two thirds of the thread width. This was done for two reasons. First, the projected area measured on the picture in 2D was smaller than the actual area in 3D, due to the curvature of the threads. For a ratio r = 2/3, the relative error made is around 8% which is reasonable. Second, due to the curvature of the thread, the cells outside
the central part tend to appear as cell aggregates and are more difficult to distinguish and count. Cells inside the outlined area were manually counted using the cell counter plug-in from ImageJ. To count cells positive to MF20, a composite picture was used with both the blue channel (Hoechst, nuclei) and the red channel (MF20, heavy chain myosin).

Prism software was used to draw the whisker boxes as well as to perform Mann Whitney tests to compare two distributions.

Results

Mechanical properties

Results of mechanical tests are displayed on Fig.1.B. First, we noticed that the three types of threads exhibit a strain stiffening behavior. Two Young moduli were then measured: at low strain, noted E_0, and during strain-stiffening, written E_1 (Fig.1.B.1). For both moduli, the difference between collagen and fibrin stands out: collagen is much stiffer (E_0 = 0.57 ± 0.05 MPa, E_1 = 1.11 ± 0.13 MPa) than fibrin (E_0 = 0.10 ± 0.02 MPa, E_1 = 0.21 ± 0.06 MPa). Mix threads exhibit intermediate stiffness (E_0 = 0.33 ± 0.05 MPa, E_1 = 0.83 ± 0.19 MPa) between collagen and fibrin.

Fibrin threads exhibit higher strain at break than collagen (251 ± 63 % *vs.* 75 ± 15 %) (Fig.1.B.2) but lower ultimate tensile strength (0.33 ± 0.04 MPa vs. 0.70 ± 0.11 MPa) (Fig.1.B.3). Interestingly, mix threads seem to break at even lower strain than collagen (57 ± 21 %) with an ultimate tensile strength slightly higher than for fibrin (0.42± 0.2 MPa).

Structure

Investigation of the microstructure of threads was performed on ultrathin transverse sections of threads using Transmission Electron Microscopy (Fig.1.C). Collagen threads are made of thin fibers with different orientations, among which a significant part is pointing toward the direction of observation, *i.e.* along the thread axis (blue arrow, Fig.1.C.1). Fibrin threads exhibit dense aggregate-like structures with some fibrous-like structures on the outside (red arrow, Fig.1.C.3). Mix threads structure is composed of small islands of fibrin materials (noted F on Fig.1.C.2), embedded into a collagen matrix (C Fig.1.C.2), made of thicker fibers than the ones observed in collagen alone.

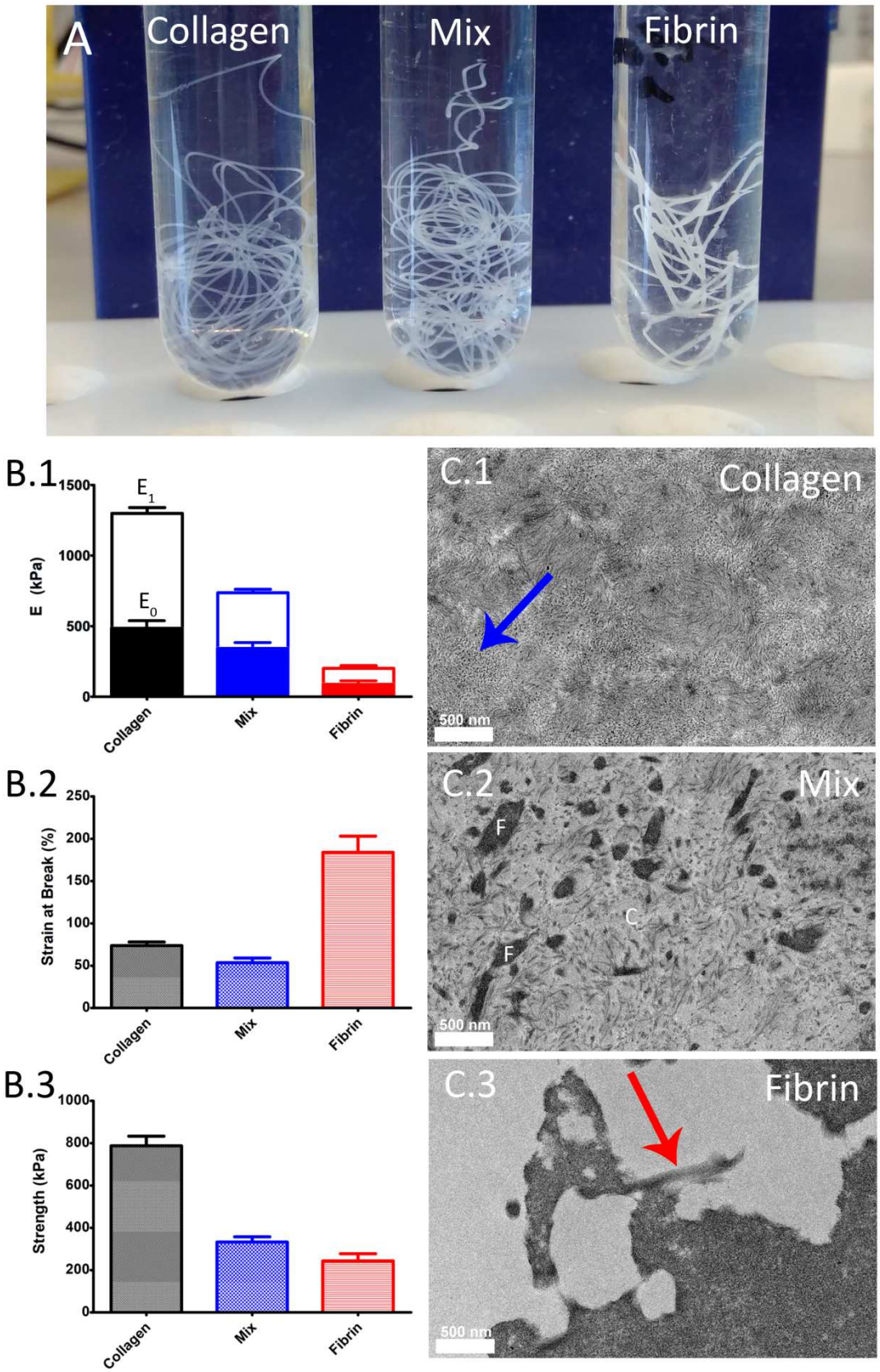

Figure 1 : Threads structural & mechanical properties. (A) Macroscopic photos of the three types of threads: collagen, mix and fibrin. (B) Mechanical properties of the three types of threads: (B.1) low-strain E_0 (full histogram) and high-strain E_1 (empty

histogram) moduli, (B.2) strain at break, (B.3) ultimate tensile strength (UTS). Cross sections of the (C.1) collagen, (C.2) mix and (C.3) fibrin threads as observed by transmission electron microscopy. Blue arrow points at collagen fibers aligned along the thread. Red arrow points at the fibrous-like structure at the surface of the fibrin aggregates.

Tenoblasts culture on threads

Tenoblasts were seeded on the three types of threads and observed after 4 days in high-serum medium (Fig.2.A) and after 7 days in high-serum medium plus 3 days in low-serum medium (Fig.2.B). After 4 days, we observed that tenoblasts on collagen threads would form cell "crusts" that detached from the thread (Fig.2.A.1). On mix and fibrin threads, tenoblasts cover threads with high cell density, without cell crust detaching from them (Fig.2.A.2 & A.3 resp.). The detachment of cells causes the cell density to drop on collagen (median ≈ 200 cell/mm^2) compared to mix (med. ≈ 1100 cell/mm^2, p=0.012) and fibrin (med. ≈ 1000 cell/mm^2, p=0.006) threads, with no significant difference between mix and fibrin (Fig.2.A.4).

After 7 days in high-serum medium plus 3 days in low-serum medium, few cells remain on collagen threads (Fig.2.B.1) while mix and fibrin threads still appear covered with cells (Fig.2.B.2 & B.3 resp.). On both types of threads, cells seem to align along the main axis of the threads. Cell density is extremely low on collagen threads (med. < 100 cell/mm^2), much below the ones on mix threads (med. ≈ 700 cell/mm^2, p<0.0001) and fibrin threads (med. ≈ 350 cell/mm^2, p=0.020) (Fig.2.B.4). Compared to cell density after 4 days in high-serum medium, a decrease is observed on mix threads (p=0.0014) and even more on fibrin threads (p=0.0016), resulting in a lower density on fibrin than on mix threads (p=0.0059). The decrease occurs during the low-serum culture, as no significant change in cell density could be observed for both types of threads at day 7 (data not shown).

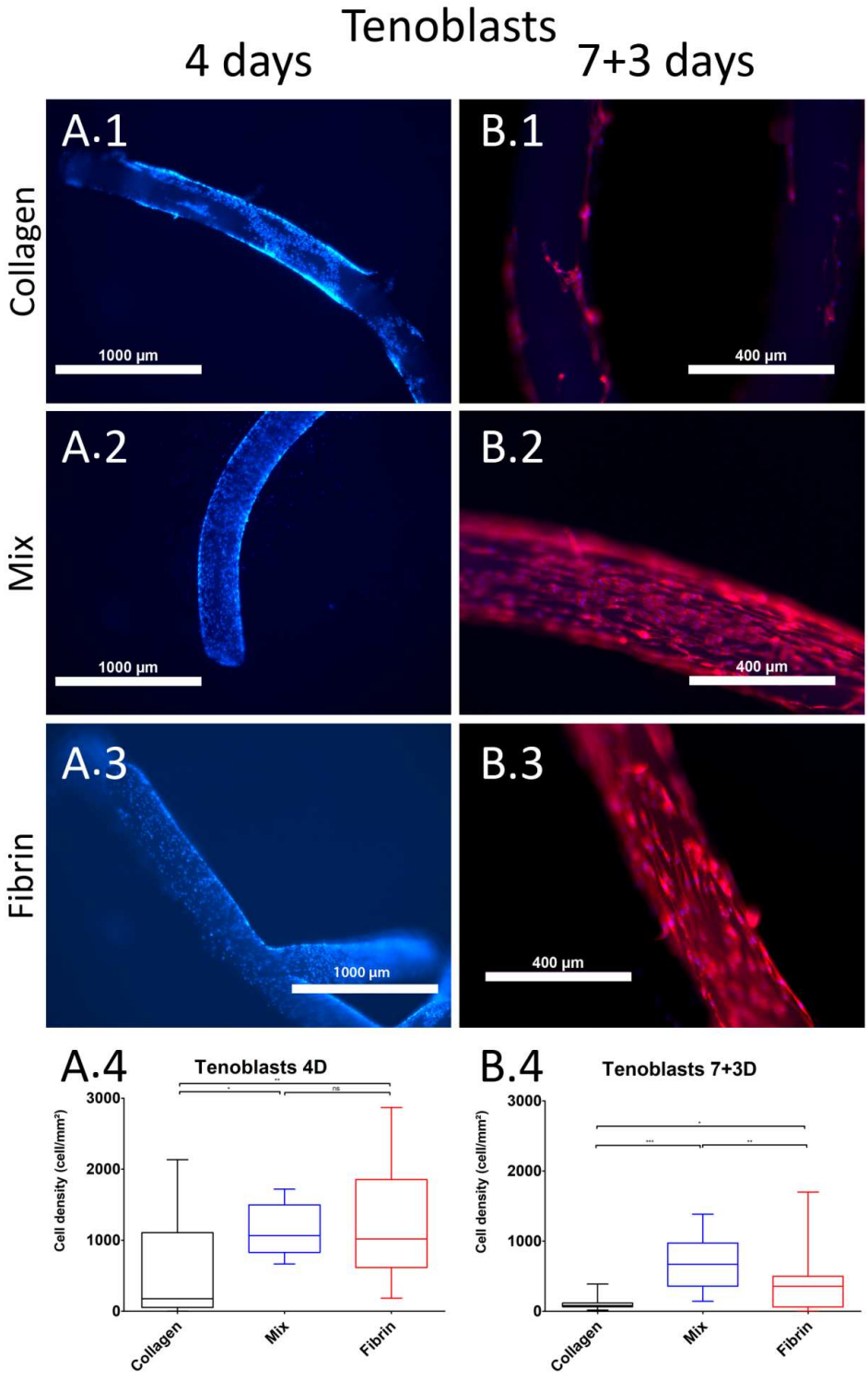

Figure 2: Tenoblast colonization of the three types of threads after day 4 (A) and 7+3 (B). Fluorescence microscope images of a collagen, mix and fibrin threads after 4 days in high-serum medium (A.1, A.2 and A.3 resp) and after 7 days in high-serum medium and 3 days in low serum medium (B.1, B.2 and B.3 resp.), and the resulting tenoblasts densities at day 4 (A.4) and day 7+3 (B.4). Blue staining: Hoechst; red: F-actin.

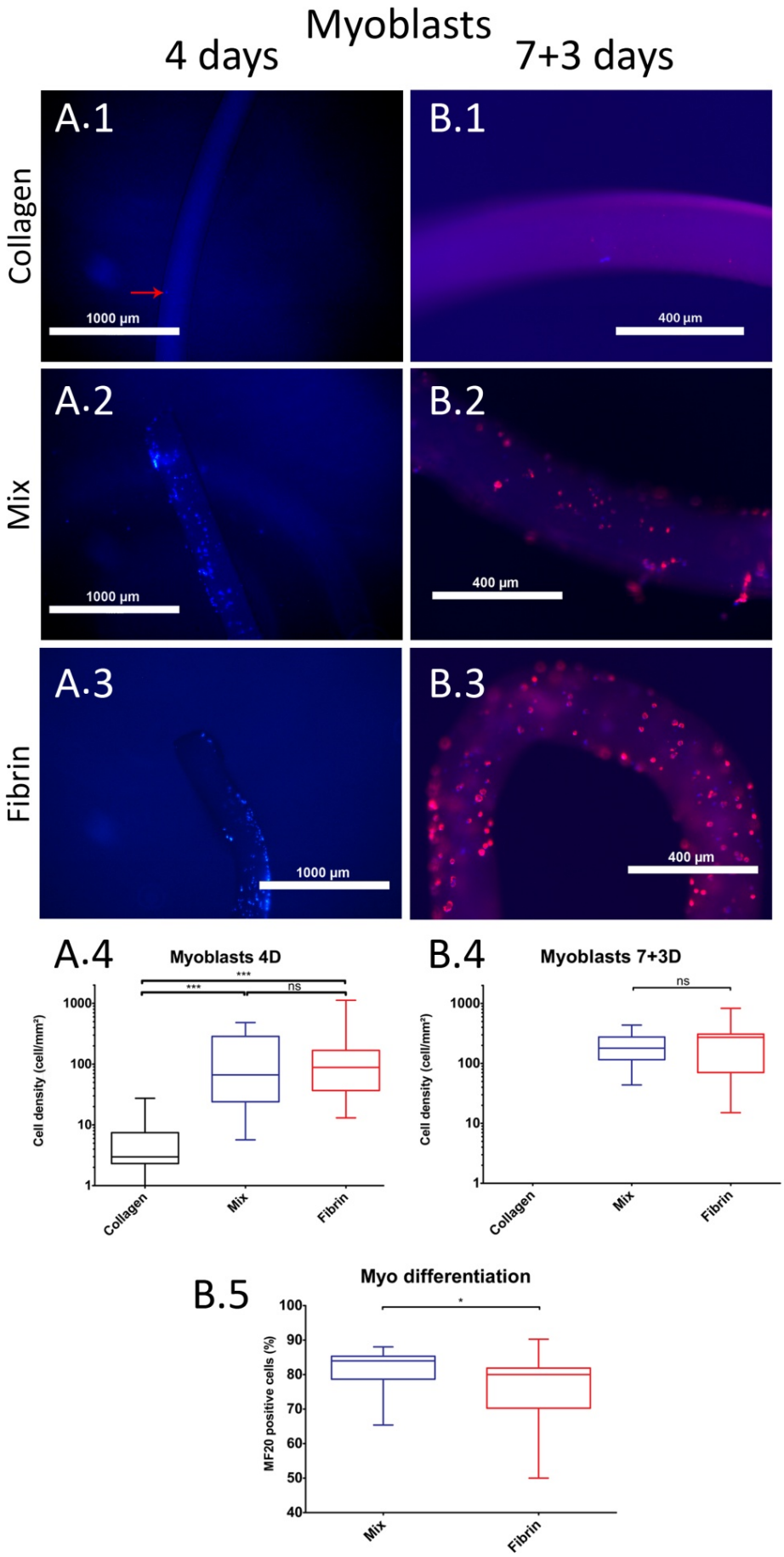
Myoblasts
4 days
7+3 days
Collagen
Mix
Fibrin
A.1
B.1
A.2
B.2
A.3
B.3
1000 µm
400 µm
A.4
Myoblasts 4D
B.4
Myoblasts 7+3D
Cell density (cell/mm²)
***
ns
Collagen
Mix
Fibrin
B.5
Myo differentiation
MF20 positive cells (%)
*

Figure 3: Myoblast colonization of the three types of threads after day 4 (A) and 7+3 (B). Fluorescence microscope images of a collagen, mix and fibrin threads after 4 days in high-serum medium (A.1, A.2 and A.3 resp.) and after 7 days in high-serum medium plus 3 days in low serum medium (B.1, B.2 and B.3 resp.), and the resulting myoblasts densities at day 4 (A.4) and day 7+3 (B.4). (B.5) Proportion of MF20 positive myoblasts over the whole number of myoblasts on mix and collagen threads. Blue staining: Hoechst; red: F-actin. Staining Blue: Hoechst, Red: myosin heavy chains MF20.

Myoblasts culture on threads

Seeding of myoblasts on the three types of threads resulted in a poor adhesion of the cells on collagen threads after 4 days in high-serum medium (Fig.3.A.1) while mix and fibrin threads were well colonized (Fig.A.2 & A.3 resp.). Same trend was observed after 3 days of differentiation, with rare cells found on collagen (Fig.3.B.1) and well colonized mix and fibrin threads (Fig.3.B.2 & B.3 resp.). Most myoblasts on mix and fibrin threads were positive to MF20 staining exhibiting production of myosin heavy chains, a late-differentiation marker. Quantitatively, after 4 days, cell density was dramatically lower on collagen (med. = 3 cell/mm^2) than on mix (med. ≈70 cell/mm^2, $p<0.001$) and fibrin threads (med. ≈ 90 cell/mm^2, $p<0.001$) (Fig.3.A.4). After 3 days of differentiation, cellular densities exhibited higher median value on both mix (med. ≈200 cell/mm^2 $p=0.035$) and fibrin (med. ≈ 300 cell/mm^2, ns) compared to 4 days of proliferation. Myoblasts on collagen were too scarce to enable statistically relevant count. No significant difference in cell density between mix and fibrin could be observed either after 4 days of proliferation or 3 days in differentiation. A slight difference in MF20 positive myoblast ratio was however noticed with 84 % of MF20+ cells on mix compared to the 80% on threads ($p=0.015$) (day 7+3). Interestingly, myoblasts remained round-shaped on both types of threads and no trace of spindle-shaped or fused cells could be observed. Prolonged culture in low-serum medium (5 days) and in presence of Wnt7a at 50 ng/mL fostered faint spindle shape but no fusion as seen on Supp. Fig. 1.A &B. As a reference, same line cultured on a 2D substrate coated with Matrigel exhibited high number of myotubes (Supp. Fig. 1.C), in spite of the same cellular density (Supp. Fig. 1.D).

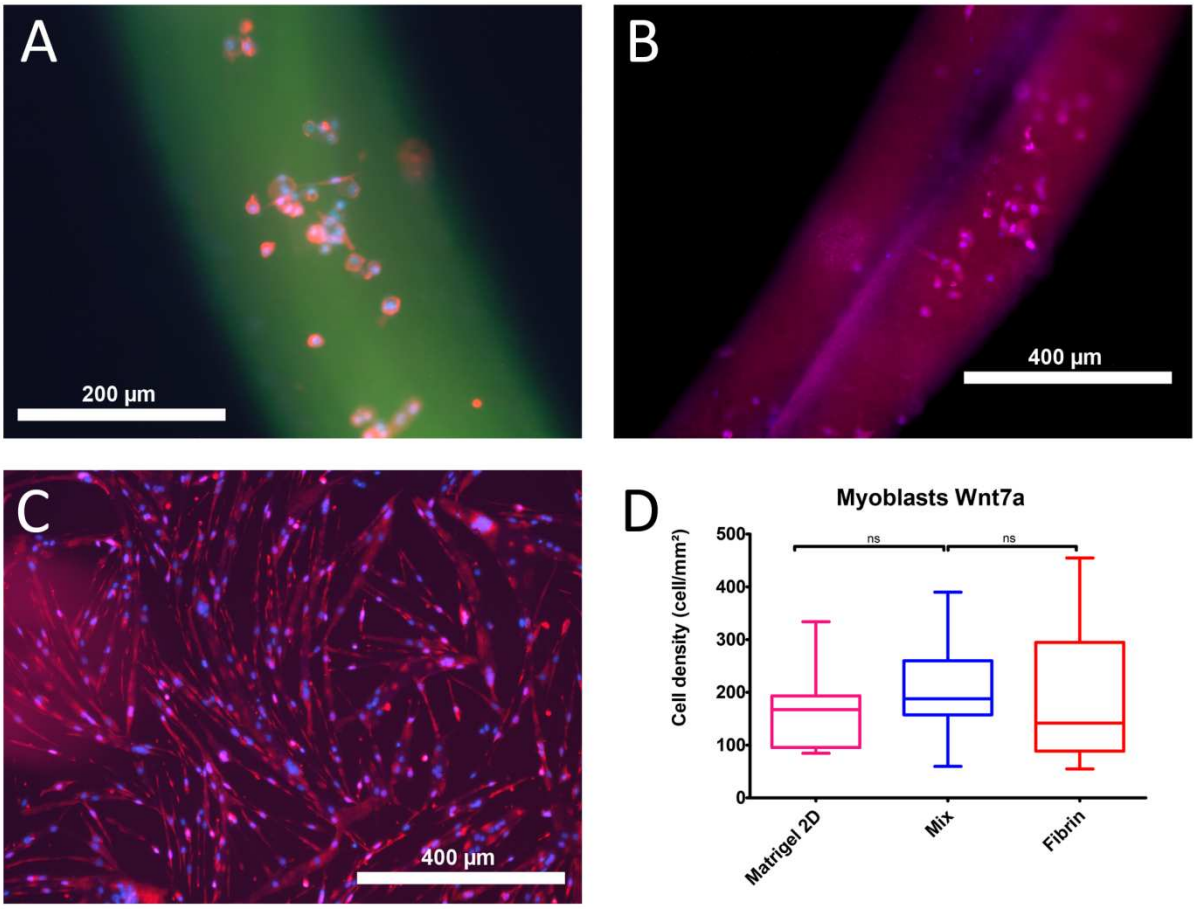

Supp. Fig. 1: Primary myoblasts cultured for 7 days in proliferation and 5 days in differentiation with Wnt7a at 50 ng/mL. Immunofluorescence staining images of myoblasts on mix (A) and fibrin (B) threads and on Matrigel®-coated plates (C) (blue: Hoechst, red: myosin heavy chains, magenta: myogenin, green: fibrin marked FITC). (D) Resulting cell densities on plates and threads.

Myoblast culture in 2D

To investigate the role played by the threads substrates on myoblasts fusion, compared to 2D substrates, the same solutions as the ones used for thread production were coated on well-plates. Myoblasts were also seeded on Matrigel-coated wells as a control. As seen on Fig.4, several features stand out. Myoblasts seeded on collagen exhibited scarce spindle shapes and extremely low numbers of fused cells (Fig.4.A). On the contrary, myoblasts cultured on mix (Fig.4.B) and fibrin wells (Fig.4.C) could elongate and formed myotubes, with an apparent number of myotubes being higher on mix. Myoblasts on Matrigel formed many more and much larger myotubes (Fig.4.C).

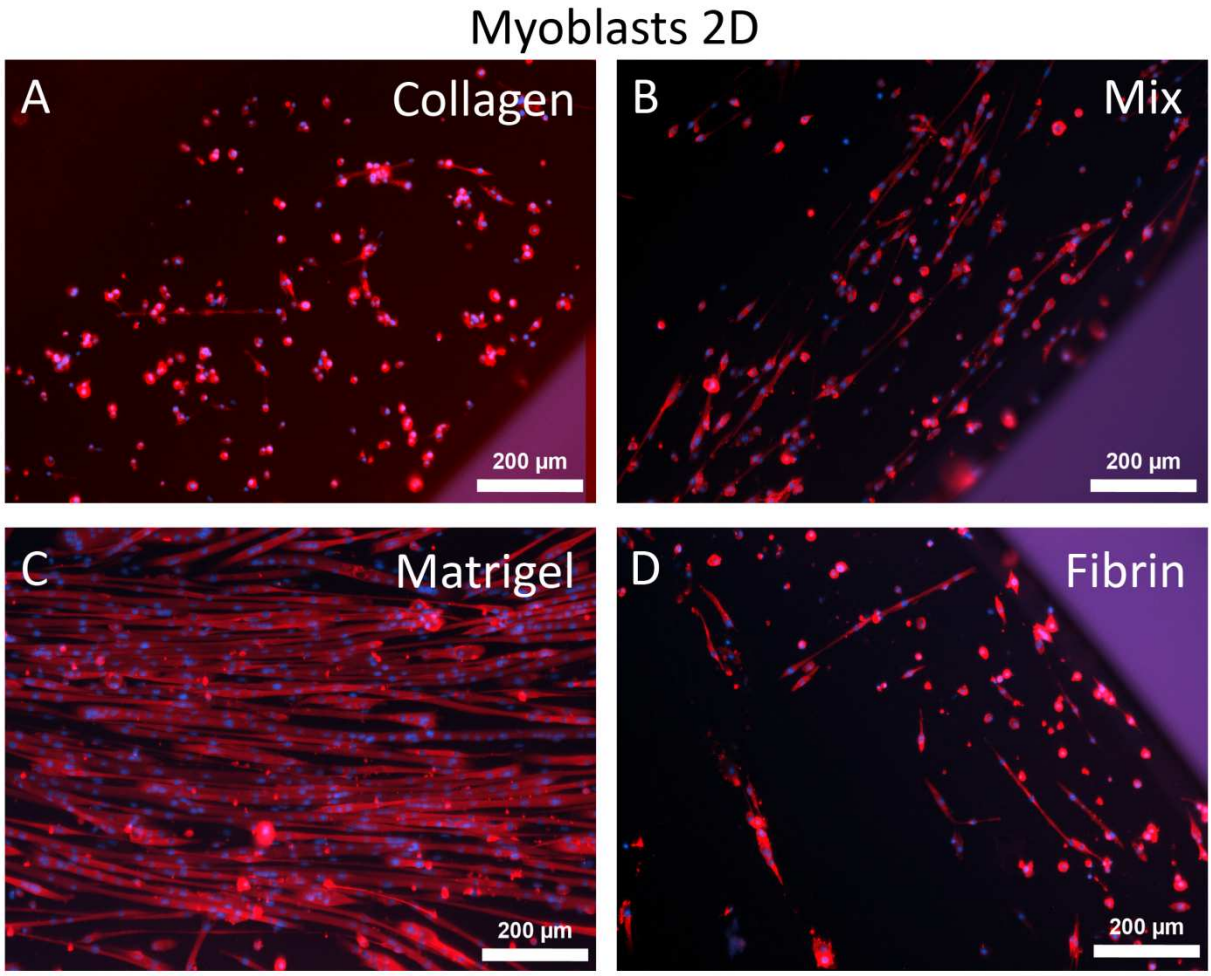

Figure 4: Primary myoblasts cultured for 1 day in proliferation and 6 days in differentiation . Immunofluorescence staining images of myoblasts on collagen (A), mix (B), Matrigel® (C) and fibrin (D) coated plates (blue: Hoechst, red: myosin heavy chains

Discussion

We have produced in this work three types of threads, one made of pure collagen, one of pure fibrin and the last one of a mix of collagen and fibrin at a ratio 3:2 in mass. These threads differing in terms of chemical composition present also different mechanical properties.

Mechanical properties

In tensile testing, we noticed that the three types of threads exhibit a strain stiffening behavior characteristic of fibrin and collagen materials [46]. As expected, collagen threads exhibited stiffer behavior, with higher strength, and lower strain at break compared to fibrin, which could be stretched up to approximately 250%. In accordance with first intuitions, mix threads had intermediate stiffness and strength between fibrin and collagen. Mix threads had however lower strain at break than collagen.

Interestingly, our results are consistent with the ones obtained by Lai *et al.* [47] who studied mechanical properties of lower concentration (2 to 3 mg/mL in proteins)

collagen/fibrin gels with different proportions from 100 % collagen to 100 % fibrin to understand the nature of the networks and their relationships in fibrin/collagen composites. The reported values of modulus and strain at failure of composites at 60 % collagen are closer to those for pure collagen than for pure fibrin. They demonstrated that such behavior could not be explained by a simple parallel (*i.e.* non interacting networks) or series (*i.e.* co-dependent networks) model of collagen and fibrin materials. They partially explained mechanical properties obtained in this study in a second article using a model of non-percolating network in which islands of the diluted protein are embedded in the concentrated one [48]. Such conclusion is in total agreement with the structure observed in mix threads, with islands of fibrin inside the collagen matrix (Fig.1.C.2). While mix threads are macroscopically homogeneous as observed on threads made from FITC-labelled fibrinogen, it seems that a phase separation occurs microscopically, resulting in islands of fibrin in a collagen matrix, for the ratio collagen:fibrin used here.
Structure of collagen threads with small fibrils with local orientation is typical of highly concentrated collagen scaffolds [49] and was already observed in threads extruded in high osmotic pressure buffer [50]. Fibrin's structure is similar to the structure we observed in fibrin threads extruded in Dulbecco's Modified Eagle Medium with a fibrillar structure on the outside of the aggregates instead of the thin bridging fibers, probably due to high osmotic pressure exerted by the high PEG concentration in the extrusion buffer. Same structure is observed for fibrin islands in mix threads. The small size of islands and the low distance between them (<1µm) ensure that cells can access both collagen and fibrin materials. It may be interesting to think about the "clustering" effect of these islands on cellular response, compared to a situation where collagen and fibrin would be thouroughly mixed, as clustering effect has shown to have paramount effect on cellular response.

Tenoblasts
Several features stood out from the culture of tenoblasts on collagen, mix and fibrin threads. First, tenoblasts rapidly proliferated rapidly on collagen threads, due to high affinity, and rapidly formed a crust around the threads, made of interconnected tenoblasts and secreted ECM [51,52]. After only 4 days in culture the crust detached from collagen threads suggesting that collagen is not a suitable substrate to enable long-term culture of tenoblasts. The difference in mechanical properties as well as the tendency of cells to contract their surrounding matrix may cause the observed crust-detaching effect.

Second, the cell density drops on mix and especially on fibrin threads between day 7 and day 7+3. This drop is likely to be caused by the switch from high-serum to low-serum medium. While mix and fibrin had similar densities at day 4 and 7, cell density is lower at day 7+3 on fibrin than on mix. The combination of collagen and fibrin thus seems beneficial to maintain tenoblasts survival in low serum.

On fibrin threads, cell density seems rather stable during the 7 days of proliferation. After 7 days (data not shown), some small cell plaques seem to detach but without significantly affecting cell density when compared to density at day 4. After 3 days in differentiation medium, cell density decreased. This may be due to the change to low serum- content medium, or to the detachment due to confluence in a similar fashion as for collagen.

Third, tenoblasts seem to spontaneously align along the direction of the thread on both mix and fibrin threads. This may be explained by a minimization of the stress on internal structure due to bending as already pointed out [53].

Myoblasts

The observed low adherence of myoblasts on collagen threads may appear surprising as primary myoblasts are routinely cultured on collagen-coated plates for proliferation [54]. Actually, on collagen-coated dishes myoblasts adopt a round shape demonstrating low affinity to collagen whereas they strongly adhere on coating containing laminin and/or fibronectin such as Matrigel® and adopt tapered shape [55]. In fact, myoblasts do not bind directly to collagen but through fibronectin [30], and the one provided by the addition of serum is supposed to be sufficient to permit adhesion of myoblasts [56].

Given the higher densities on mix and fibrin threads, myoblasts seemed to adhere more on fibrin. Myoblasts can bind directly to fibrin through integrin receptors [57]. The cell density on mix threads was each time comparable to the one on fibrin. It is surprising that mix threads induced similar response as pure fibrin, given the relatively low content in fibrin compared to collagen. Fibrin islands contained in mix threads were thus sufficient to provide similar adhesion of cells to threads as on pure fibrin. Given the absence of adhesion of myoblasts on collagen threads, we can hypothesize that myoblasts attach to fibrin islands instead of collagen matrix, and thus "feel" a fibrin composition. However, given the small size of islands embedded in the collagen matrix, it is probable that cells, when pulling on focal adhesion, rather "feel" the stiffness of the collagen matrix. Mix materials may then appear as a way to decouple the composition and mechanical properties of the substrate and thus show that the lack of adherence of myoblasts to collagen threads is rather due to the poor binding to collagen compared to fibrin, rather than a too high stiffness of the substrate.

Concentration of proteins in threads may also play a role. Gerard *et al.* [58] reported that concentration of fibrin had an effect on myoblasts entrapped in a fibrin gel. They demonstrated that loose gels (3mg/mL) promoted higher proliferation and metabolic activity compared to 50 mg/mL gels.

The absence of fusion of myoblasts into myotubes was unexpected as fibrin has been widely used for muscle constructs [43–45,59] and is believed to be the gold-standard material [60]. However, myoblasts on threads expressed myogenin and heavy myosin chains, two markers of muscle cell terminal differentiation. The high density of multinucleated myotubes on 2D Matrigel control proves that the absence of fusion on the threads is not due to low cellular density or to an inability of the primary myoblasts we used to fuse. We tested on differentiated cells on threads the stimulation by Wnt7a that, as previously reported, is an inducer of muscle cell fusion [61]. We only observed a modest effect on cell sprawling and polarization [62], still too low to enable cell fusion. Given the fact that most cells expressed were terminally differentiated, and kept a round "myoblastic" shape on threads, it seemed that the absence of fusion is due to a problem of adhesion of cells to the matrix.

The comparison between culture on threads and 2D culture on coated wells enables to point out two distinct reasons that seem to play a role in the absence of fusion of myoblasts. The first is due to the composition of the thread. Collagen alone seems to be particularly non-permissive to myocyte fusion. Differentiation of myoblasts without fusion has already been observed on collagen-coated plates [63]. On the contrary to collagen, fibrin-coated plates comports multiple myotubes. The combination of collagen and fibrin in mix plates may have a synergetic effect and as they seem to promote even more myotube fusion. Number and size of myotubes are however much lower than on Matrigel, which contains multiple ECM components. The lack of fusion may thus result from the lack of certain components of the ECM such as laminin, shown to be paramount for cell fusion [64] and often used to promote myoblasts adhesion and fusion [65,66].

A clear difference could however be observed between myoblasts seeded on 2D fibrin or mix, compared to myoblasts seeded on threads. Multiple myotubes and spindle-shaped cells could be observed in 2D while no fusion was witnessed on threads, and cell polarization and elongation was tediously and limitedly obtained using Wnt7a. As the materials used in 2D and threads are identical, the absence of fusion is likely to be due to the topology of the threads, *ie.* the curvature. Curvature has already been reported to influence cell migration and differentiation [67] but to our knowledge, no study has shown that substrate curvature inhibited myoblast fusion. In 1994, Rovensky *et al.* reported that cells with straight actin filament such as fibroblasts tend to align in the direction of lower curvature to minimize stress [53]. We can hypothesize that the myoblasts do not fuse and do not even elongate because they are highly sensitive to internal stress.

It is known that muscle satellite cells do not fuse on an isolated myofibre while they fuse once plated on a Matrigel®-coated plate [68]. The shape and curvature of the substrate may then inhibit fusion. Myoblasts on our threads seemed to behave in the same fashion as satellite cells on isolated myofibres, adopting the same shape and unable to fuse. The topological inhibition is surprising given the difference of dimension compared to myofibers with diameters of a few tens of micrometers [69,70]. The curvature inhibition may prevent differentiation of satellite cells at the surface of undamaged myofibers.

The threads developed may then represent an interesting model of isolated myofibers. This is also encouraging for muscular reconstruction as satellite cells adopt such a behavior when anchored to an isolated fiber but behave differently in a 3D environment, in the niche comprised between multiple fibers. Use of multiple braided threads for instance, possibly held together by a loose gel, may then form a niche model for myoblasts and effectively promote myotube formation and muscle reconstruction.

Conclusion

We developed here collagen, fibrin and mixed threads and used them as substrates of different mechanical properties, collagen threads being stiffer than fibrin ones. Mix threads demonstrated properties similar to collagen due to their non percolating fibrin island network in the collagen matrix. Such substrates enable to decouple mechanical properties from chemical interaction by providing fibrin islands for the cells to adhere with the stiffness of the embedding collagen network. Both primary tenoblasts and myoblasts on mix threads behave similarly to fibrin threads, rather than collagen, highlighting the importance of the chemical nature of the cell/matrix interaction.

Even though myoblasts differentiated on mix and fibrin threads, they did not fuse. Investigations carried out seem to point out a possible inhibition of fusion due to substrate curvature. Further characterization of such phenomenon should be undertaken as it may provide a better understanding of the satellite cells differentiation commitment all the more since prevention of satellite cell differentiation is a challenge for muscular reconstruction [71]. Indeed, surface curvature seems to be a parameter of choice to foster or not the differentiation of satellite cells and ensure differentiation only upon fiber damage.

The work reported here is a first step toward myo-tendinous junction modelisation. The next step would be to co-culture both tenoblasts and myoblasts on our substrates, as we demonstrated their viability in the same medium, to understand the cooperative role they may play. As fibrin, collagen and mix threads are produced in the same conditions, collagen:fibrin ratio of mix threads can be tuned to investigate cell response to substrate and find the optimal composition for tenoblasts and myoblasts. Even further, pluripotent stem cells could be used and composition of mix threads adapted to favor tenogenic or myogenic commitment.

1. Armfield, D. R., Kim, D. H.-M., Towers, J. D., Bradley, J. P. & Robertson, D. D. Sports-Related Muscle Injury in the Lower Extremity. *Clin. Sports Med.* **25**, 803–842 (2006).

2. Palmer, W. E., Kuong, S. J. & Elmadbouh, H. M. MR imaging of myotendinous strain. *Am. J. Roentgenol.* **173**, 703–709 (1999).

3. Tavernier, Th., Walch, G., Barthelemy, R., Nove-Josserand, L. & Liotard, J. P. Lésion isolée de l'infra-épineux à la jonction myotendineuse : une nouvelle lésion. *J. Radiol.* **87**, 1875–1882 (2006).

4. Hertel, R. & Lambert, S. M. Supraspinatus rupture at the musculotendinous junction. **7**, 4 (1998).

5. Taneja, A. K. *et al.* MRI Findings of Rotator Cuff Myotendinous Junction Injury. *Am. J. Roentgenol.* **203**, 406–411 (2014).

6. Garrett, W. E., Nikolaou, P. K., Ribbeck, B. M., Glisson, R. R. & Seaber, A. V. The effect of muscle architecture on the biomechanical failure properties of skeletal muscle under passive extension. *Am. J. Sports Med.* **16**, 7–12 (1988).

7. Woo, S. L.-Y. & Buckwalter, J. A. Injury and repair of the musculoskeletal soft tissues. Savannah, Georgia, June 18–20, 1987. *J. Orthop. Res.* **6**, 907–931 (1988).

8. Sharafi, B., Ames, E. G., Holmes, J. W. & Blemker, S. S. Strains at the myotendinous junction predicted by a micromechanical model. *J. Biomech.* **44**, 2795–2801 (2011).

9. Zammit, P. S., Partridge, T. A. & Yablonka-Reuveni, Z. The Skeletal Muscle Satellite Cell: The Stem Cell That Came in From the Cold. *J. Histochem. Cytochem.* **54**, 1177–1191 (2006).

10. Li, E. W., McKee-Muir, O. C. & Gilbert, P. M. Cellular Biomechanics in Skeletal Muscle Regeneration. in *Current Topics in Developmental Biology* **126**, 125–176 (Elsevier, 2018).

11. Ladd, M. R., Lee, S. J., Stitzel, J. D., Atala, A. & Yoo, J. J. Co-electrospun dual scaffolding system with potential for muscle–tendon junction tissue engineering. *Biomaterials* **32**, 1549–1559 (2011).

12. Charvet, B., Ruggiero, F. & Le Guellec, D. The development of the myotendinous junction. A review. *MLTJ Muscles Ligaments Tendons J.* **2**, 53–63 (2012).

13. Knudsen, A. B. *et al.* The human myotendinous junction: An ultrastructural and 3D analysis study: The human myotendinous junction. *Scand. J. Med. Sci. Sports* **25**, e116–e123 (2015).

14. Merceron, T. K. *et al.* A 3D bioprinted complex structure for engineering the muscle–tendon unit. *Biofabrication* **7**, 035003 (2015).

15. Vincent, L. G., Choi, Y. S., Alonso-Latorre, B., Álamo, J. C. del & Engler, A. J. Mesenchymal stem cell durotaxis depends on substrate stiffness gradient strength. *Biotechnol. J.* **8**, 472–484 (2013).

16. Isenberg, B. C., DiMilla, P. A., Walker, M., Kim, S. & Wong, J. Y. Vascular Smooth Muscle Cell Durotaxis Depends on Substrate Stiffness Gradient Strength. *Biophys. J.* **97**, 1313–1322 (2009).

17. Engler, A. J., Sen, S., Sweeney, H. L. & Discher, D. E. Matrix Elasticity Directs Stem Cell Lineage Specification. *Cell* **126**, 677–689 (2006).

18. Trumbull, A., Subramanian, G. & Yildirim-Ayan, E. Mechanoresponsive musculoskeletal tissue differentiation of adipose-derived stem cells. *Biomed. Eng. Online* **15**, 1 (2016).

19. Gilbert, P. M. *et al.* Substrate Elasticity Regulates Skeletal Muscle Stem Cell Self-Renewal in Culture. *Science* **329**, 1078–1081 (2010).

20. Engler, A. J. *et al.* Myotubes differentiate optimally on substrates with tissue-like stiffness: pathological implications for soft or stiff microenvironments. *J. Cell Biol.* **166**, 877–887 (2004).

21. Liu, C. *et al.* Matrix stiffness regulates the differentiation of tendon-derived stem cells through FAK-ERK1/2 activation. *Exp. Cell Res.* **373**, 62–70 (2018).

22. Patel, D., Sharma, S., Screen, H. R. C. & Bryant, S. J. Effects of cell adhesion motif, fiber stiffness, and cyclic strain on tenocyte gene expression in a tendon mimetic fiber composite hydrogel. *Biochem. Biophys. Res. Commun.* **499**, 642–647 (2018).

23. Keselowsky, B. G., Collard, D. M. & García, A. J. Integrin binding specificity regulates biomaterial surface chemistry effects on cell differentiation. *Proc. Natl. Acad. Sci.* **102**, 5953–5957 (2005).

24. Vicente-Manzanares, M., Ma, X., Adelstein, R. S. & Horwitz, A. R. Non-muscle myosin II takes centre stage in cell adhesion and migration. *Nat. Rev. Mol. Cell Biol.* **10**, 778–790 (2009).

25. Portier, F. *et al.* Stabilization of Collagen Fibrils by Gelatin Addition: A Study of Collagen/Gelatin Dense Phases. *Langmuir* **33**, 12916–12925 (2017).

26. Rieu, C., Picaut, L., Mosser, G. & Trichet, L. From Tendon Injury to Collagen-based Tendon Regeneration: Overview and Recent Advances. *Curr. Pharm. Des.* 3483–3506 (2017).

27. Wegst, U. G. K., Bai, H., Saiz, E., Tomsia, A. P. & Ritchie, R. O. Bioinspired structural materials. *Nat. Mater.* **14**, 23–36 (2014).

28. Barczyk, M., Carracedo, S. & Gullberg, D. Integrins. *Cell Tissue Res* **339**, 269–280 (2010).

29. Jokinen, J. *et al.* Integrin-mediated cell adhesion to type I collagen fibrils. *J. Biol. Chem.* **279**, 31956–31963 (2004).

30. Kleinman, H. K. Role of collagenous matrices in the adhesion and growth of cells. *J. Cell Biol.* **88**, 473–485 (1981).

31. Screen, H. R. C., Berk, D. E., Kadler, K. E., Ramirez, F. & Young, M. F. Tendon Functional Extracellular Matrix: tendon functional extracellular matrix. *J. Orthop. Res.* **33**, 793–799 (2015).

32. Semple, J. W., Italiano, J. E. & Freedman, J. Platelets and the immune continuum. *Nat. Rev. Immunol.* **11**, 264–274 (2011).

33. Litvinov, R. I. & Weisel, J. W. Fibrin mechanical properties and their structural origins. *Matrix Biol.* (2016). doi:10.1016/j.matbio.2016.08.003

34. Bayless, K. J., Salazar, R. & Davis, G. E. RGD-Dependent Vacuolation and Lumen Formation Observed during Endothelial Cell Morphogenesis in Three-Dimensional Fibrin Matrices Involves the αvβ3 and α5β1 Integrins. *Am. J. Pathol.* **156**, 1673–1683 (2000).

35. Lishko, V. K. *et al.* Multiple Binding Sites in Fibrinogen for Integrin $\alpha_M \beta_2$ (Mac-1). *J. Biol. Chem.* **279**, 44897–44906 (2004).

36. Flick, M. J. *et al.* Leukocyte engagement of fibrin(ogen) via the integrin receptor $\alpha_M\beta_2$/Mac-1 is critical for host inflammatory response in vivo. *J. Clin. Invest.* **113**, 1596–1606 (2004).

37. Jockenhoevel, S. *et al.* Fibrin gel – advantages of a new scaffold in cardiovascular tissue engineering. *Eur. J. Cardiothorac. Surg.* **19**, 424–430 (2001).

38. Long, J. L. & Tranquillo, R. T. Elastic fiber production in cardiovascular tissue-equivalents. *Matrix Biol.* **22**, 339–350 (2003).

39. Ross, J. J. & Tranquillo, R. T. ECM gene expression correlates with in vitro tissue growth and development in fibrin gel remodeled by neonatal smooth muscle cells. *Matrix Biol.* **22**, 477–490 (2003).

40. Fussenegger, M. *et al.* Stabilized Autologous Fibrin-Chondrocyte Constructs for Cartilage Repair in Vivo. *Ann. Plast. Surg.* **51**, 493 (2003).

41. Hunter, C. J., Mouw, J. K. & Levenston, M. E. Dynamic compression of chondrocyte-seeded fibrin gels: effects on matrix accumulation and mechanical stiffness. *Osteoarthritis Cartilage* **12**, 117–130 (2004).

42. Sims, C. D. *et al.* Tissue engineered neocartilage using plasma derived polymer substrates and chondrocytes. *Plast. Reconstr. Surg.* **101**, 1580–1585 (1998).

43. Page, R. L. *et al.* Restoration of Skeletal Muscle Defects with Adult Human Cells Delivered on Fibrin Microthreads. *Tissue Eng. Part A* **17**, 2629–2640 (2011).

44. Kang, H.-W. *et al.* A 3D bioprinting system to produce human-scale tissue constructs with structural integrity. *Nat. Biotechnol.* **34**, 312–319 (2016).

45. Huang, Y.-C., Dennis, R. G., Larkin, L. & Baar, K. Rapid formation of functional muscle in vitro using fibrin gels. *J. Appl. Physiol.* **98**, 706–713 (2005).

46. Munster, S. *et al.* Strain history dependence of the nonlinear stress response of fibrin and collagen networks. *Proc. Natl. Acad. Sci.* **110**, 12197–12202 (2013).

47. Lai, V. K., Lake, S. P., Frey, C. R., Tranquillo, R. T. & Barocas, V. H. Mechanical behavior of collagen-fibrin co-gels reflects transition from series to parallel interactions with increasing collagen content. *J. Biomech. Eng.* **134**, 011004 (2012).

48. Nedrelow, D. S., Bankwala, D., Hyypio, J. D., Lai, V. K. & Barocas, V. H. Mechanics of a two-fiber model with one nested fiber network, as applied to the collagen-fibrin system. *Acta Biomater.* **72**, 306–315 (2018).

49. Gobeaux, F. *et al.* Fibrillogenesis in Dense Collagen Solutions: A Physicochemical Study. *J. Mol. Biol.* **376**, 1509–1522 (2008).

50. Picaut, L. *et al.* Pure dense collagen threads from extrusion to fibrillogenesis stability. *Biomed. Phys. Eng. Express* **4**, 035008 (2018).

51. Stoll, C. *et al.* Extracellular matrix expression of human tenocytes in three-dimensional air-liquid and PLGA cultures compared with tendon tissue: Implications for tendon tissue engineering. *J. Orthop. Res.* **28**, 1170–1177 (2010).

52. Subramanian, A. & Schilling, T. F. Tendon development and musculoskeletal assembly: emerging roles for the extracellular matrix. *Development* **142**, 4191–4204 (2015).

53. Rovensky, Y. A. & Samoilov, V. I. Morphogenetic response of cultured normal and transformed fibroblasts, and epitheliocytes, to a cylindrical substratum surface. 9 (1994).

54. Le Grand, F. *et al.* Six1 regulates stem cell repair potential and self-renewal during skeletal muscle regeneration. *J. Cell Biol.* **198**, 815–832 (2012).

55. Lukjanenko, L. *et al.* Loss of fibronectin from the aged stem cell niche affects the regenerative capacity of skeletal muscle in mice. *Nat. Med.* **22**, 897–905 (2016).

56. Chiquet, M., Puri, E. C. & Turner, D. C. Fibronectin mediates attachment of chicken myoblasts to a gelatin-coated substratum. *J. Biol. Chem.* **254**, 5475–5482 (1979).

57. Chiron, S. *et al.* Complex Interactions between Human Myoblasts and the Surrounding 3D Fibrin-Based Matrix. *PLOS ONE* **7**, e36173 (2012).

58. Gerard, C., Forest, M. A., Beauregard, G., Skuk, D. & Tremblay, J. P. Fibrin Gel Improves the Survival of Transplanted Myoblasts ,
Fibrin Gel Improves the Survival of Transplanted Myoblasts. *Cell Transplant.* **21**, 127–138 (2012).

59. Bian, W. & Bursac, N. Engineered skeletal muscle tissue networks with controllable architecture. *Biomaterials* **30**, 1401–1412 (2009).

60. Koning, M., Harmsen, M. C., van Luyn, M. J. A. & Werker, P. M. N. Current opportunities and challenges in skeletal muscle tissue engineering. *J. Tissue Eng. Regen. Med.* **3**, 407–415 (2009).

61. Lacour, F. *et al.* R-spondin1 Controls Muscle Cell Fusion through Dual Regulation of Antagonistic Wnt Signaling Pathways. *Cell Rep.* **18**, 2320–2330 (2017).

62. Le Grand, F., Jones, A. E., Seale, V., Scimè, A. & Rudnicki, M. A. Wnt7a Activates the Planar Cell Polarity Pathway to Drive the Symmetric Expansion of Satellite Stem Cells. *Cell Stem Cell* **4**, 535–547 (2009).

63. Heino, J. The collagen family members as cell adhesion proteins. *BioEssays* **29**, 1001–1010 (2007).

64. Goody, M. F., Sher, R. B. & Henry, C. A. Hanging on for the ride: Adhesion to the extracellular matrix mediates cellular responses in skeletal muscle morphogenesis and disease. *Dev. Biol.* **401**, 75–91 (2015).

65. Larkin, L. M., Calve, S., Kostrominova, T. Y. & Arruda, E. M. Structure and functional evaluation of tendon-skeletal muscle constructs engineered in vitro. *Tissue Eng.* **12**, 3149–3158 (2006).

66. Lam, M. T., Huang, Y.-C., Birla, R. K. & Takayama, S. Microfeature guided skeletal muscle tissue engineering for highly organized 3-dimensional free-standing constructs. *Biomaterials* **30**, 1150–1155 (2009).

67. Werner, M. *et al.* Surface Curvature Differentially Regulates Stem Cell Migration and Differentiation via Altered Attachment Morphology and Nuclear Deformation. *Adv. Sci.* **4**, 1600347 (2017).

68. Zammit, P. S. *et al.* Muscle satellite cells adopt divergent fates: a mechanism for self-renewal? *J. Cell Biol.* **166**, 347–357 (2004).

69. Harber, M. P. *et al.* Aerobic exercise training improves whole muscle and single myofiber size and function in older women. *Am. J. Physiol.-Regul. Integr. Comp. Physiol.* **297**, R1452–R1459 (2009).

70. Collins, C. A. *et al.* Stem Cell Function, Self-Renewal, and Behavioral Heterogeneity of Cells from the Adult Muscle Satellite Cell Niche. *Cell* **122**, 289–301 (2005).

71. Quarta, M. *et al.* An artificial niche preserves the quiescence of muscle stem cells and enhances their therapeutic efficacy. *Nat. Biotechnol.* **34**, 752–759 (2016).

BIBLIOGRAPHY

Afshar, M.E., Abraha, H.Y., Bakooshli, M.A., Davoudi, S., Thavandiran, N., Tung, K., Ahn, H., Ginsberg, H.J., Zandstra, P.W., and Gilbert, P.M. (2020). A 96-well culture platform enables longitudinal analyses of engineered human skeletal muscle microtissue strength. Sci Rep *10*, 6918.

Afshar Bakooshli, M., Lippmann, E.S., Mulcahy, B., Iyer, N., Nguyen, C.T., Tung, K., Stewart, B.A., van den Dorpel, H., Fuehrmann, T., Shoichet, M., et al. (2019). A 3D culture model of innervated human skeletal muscle enables studies of the adult neuromuscular junction. ELife *8*, e44530.

Akiyama, H., Ito, A., Kawabe, Y., and Kamihira, M. (2009). Fabrication of complex three-dimensional tissue architectures using a magnetic force-based cell patterning technique. Biomed Microdevices *11*, 713–721.

Barcellos-Hoff, M.H., Aggeler, J., Ram, T.G., and Bissell, M.J. (1989). Functional differentiation and alveolar morphogenesis of primary mammary cultures on reconstituted basement membrane. Development *105*, 223–235.

Bentzinger, C.F., Wang, Y.X., von Maltzahn, J., Soleimani, V.D., Yin, H., and Rudnicki, M.A. (2013). Fibronectin Regulates Wnt7a Signaling and Satellite Cell Expansion. Cell Stem Cell *12*, 75–87.

Bertrand, A.T., Ziaei, S., Ehret, C., Duchemin, H., Mamchaoui, K., Bigot, A., Mayer, M., Quijano-Roy, S., Desguerre, I., Laine, J., et al. (2014). Cellular microenvironments reveal defective mechanosensing responses and elevated YAP signaling in LMNA-mutated muscle precursors. Journal of Cell Science *127*, 2873–2884.

Bertrand, A.T., Brull, A., Azibani, F., Benarroch, L., Chikhaoui, K., Stewart, C.L., Medalia, O., Ben Yaou, R., and Bonne, G. (2020). Lamin A/C Assembly Defects in LMNA-Congenital Muscular Dystrophy Is Responsible for the Increased Severity of the Disease Compared with Emery–Dreifuss Muscular Dystrophy. Cells *9*, 844.

Bian, W., and Bursac, N. (2009). Engineered skeletal muscle tissue networks with controllable architecture. Biomaterials *30*, 1401–1412.

Bian, W., Liau, B., Badie, N., and Bursac, N. (2009). Mesoscopic hydrogel molding to control the 3D geometry of bioartificial muscle tissues. Nat Protoc *4*, 1522–1534.

Bischoff, R. (1975). Regeneration of single skeletal muscle fibers in vitro. Anat. Rec. *182*, 215–235.

Bloch, R.J., and Gonzalez-Serratos, H. (2003). Lateral Force Transmission Across Costameres in Skeletal Muscle: Exercise and Sport Sciences Reviews *31*, 73–78.

Boudou, T., Legant, W.R., Mu, A., Borochin, M.A., Thavandiran, N., Radisic, M., Zandstra, P.W., Epstein, J.A., Margulies, K.B., and Chen, C.S. (2012). A Microfabricated Platform to Measure and Manipulate the Mechanics of Engineered Cardiac Microtissues. Tissue Engineering Part A *18*, 910–919.

Braun, T., and Gautel, M. (2011). Transcriptional mechanisms regulating skeletal muscle differentiation, growth and homeostasis. Nat Rev Mol Cell Biol *12*, 349–361.

Bruusgaard, J.C., Johansen, I.B., Egner, I.M., Rana, Z.A., and Gundersen, K. (2010). Myonuclei acquired by overload exercise precede hypertrophy and are not lost on detraining. Proceedings of the National Academy of Sciences *107*, 15111–15116.

Carrel, A., and Burrows, M.T. (1911). CULTIVATION OF TISSUES IN VITRO AND ITS TECHNIQUE. Journal of Experimental Medicine *13*, 387–396.

Charest, J.L., García, A.J., and King, W.P. (2007). Myoblast alignment and differentiation on cell culture substrates with microscale topography and model chemistries. Biomaterials *28*, 2202–2210.

Chatterjee, S., Yin, H., Li, W., Lee, J., Yechoor, V.K., and Ma, K. (2019). The Nuclear Receptor and Clock Repressor Rev-erb α Suppresses Myogenesis. Sci Rep *9*, 4585.

Cheung, T.H., and Rando, T.A. (2013). Molecular regulation of stem cell quiescence. Nat Rev Mol Cell Biol *14*, 329–340.

Chiron, S., Tomczak, C., Duperray, A., Lainé, J., Bonne, G., Eder, A., Hansen, A., Eschenhagen, T., Verdier, C., and Coirault, C. (2012). Complex Interactions between Human Myoblasts and the Surrounding 3D Fibrin-Based Matrix. PLoS ONE *7*, e36173.

Choi, J.S., Lee, S.J., Christ, G.J., Atala, A., and Yoo, J.J. (2008). The influence of electrospun aligned poly(ε-caprolactone)/collagen nanofiber meshes on the formation of self-aligned skeletal muscle myotubes. Biomaterials *29*, 2899–2906.

Clark, P., Coles, D., and Peckham, M. (1997). Preferential Adhesion to and Survival on Patterned Laminin Organizes Myogenesisin Vitro. Experimental Cell Research *230*, 275–283.

Clevers, H. (2016). Modeling Development and Disease with Organoids. Cell *165*, 1586–1597.

Collins, C.A., Olsen, I., Zammit, P.S., Heslop, L., Petrie, A., Partridge, T.A., and Morgan, J.E. (2005). Stem Cell Function, Self-Renewal, and Behavioral Heterogeneity of Cells from the Adult Muscle Satellite Cell Niche. Cell *122*, 289–301.

Comai, G., and Tajbakhsh, S. (2014a). Molecular and cellular regulation of skeletal myogenesis. Curr Top Dev Biol *110*, 1–73.

Comai, G., and Tajbakhsh, S. (2014b). Molecular and Cellular Regulation of Skeletal Myogenesis. In Current Topics in Developmental Biology, (Elsevier), pp. 1–73.

Cosgrove, B.D., Gilbert, P.M., Porpiglia, E., Mourkioti, F., Lee, S.P., Corbel, S.Y., Llewellyn, M.E., Delp, S.L., and Blau, H.M. (2014). Rejuvenation of the muscle stem cell population restores strength to injured aged muscles. Nat Med *20*, 255–264.

Cummings, C.L., Gawlitta, D., Nerem, R.M., and Stegemann, J.P. (2004). Properties of engineered vascular constructs made from collagen, fibrin, and collagen–fibrin mixtures.

Biomaterials *25*, 3699–3706.

Cvetkovic, C., Raman, R., Chan, V., Williams, B.J., Tolish, M., Bajaj, P., Sakar, M.S., Asada, H.H., Saif, M.T.A., and Bashir, R. (2014). Three-dimensionally printed biological machines powered by skeletal muscle. Proceedings of the National Academy of Sciences *111*, 10125–10130.

Davoudi, S., and Gilbert, P.M. (2017). Optimization of Satellite Cell Culture Through Biomaterials. In Muscle Stem Cells, E. Perdiguero, and D. Cornelison, eds. (New York, NY: Springer New York), pp. 329–341.

Dennis, R.G., and Kosnik, P.E. (2000). Excitability and isometric contractile properties of mammalian skeletal muscle constructs engineered in vitro. In Vitro Cell Dev Biol Anim *36*, 327–335.

Di Foggia, V., Zhang, X., Licastro, D., Gerli, M.F.M., Phadke, R., Muntoni, F., Mourikis, P., Tajbakhsh, S., Ellis, M., Greaves, L.C., et al. (2014). Bmi1 enhances skeletal muscle regeneration through MT1-mediated oxidative stress protection in a mouse model of dystrophinopathy. Journal of Experimental Medicine *211*, 2617–2633.

Earle, A.J., Kirby, T.J., Fedorchak, G.R., Isermann, P., Patel, J., Iruvanti, S., Moore, S.A., Bonne, G., Wallrath, L.L., and Lammerding, J. (2020). Mutant lamins cause nuclear envelope rupture and DNA damage in skeletal muscle cells. Nat Mater *19*, 464–473.

Elwood, R.W., Barr, S., and Patterson, L. (2009). Pain and stress in crustaceans? Applied Animal Behaviour Science *118*, 128–136.

Engler, A.J., Griffin, M.A., Sen, S., Bönnemann, C.G., Sweeney, H.L., and Discher, D.E. (2004). Myotubes differentiate optimally on substrates with tissue-like stiffness. Journal of Cell Biology *166*, 877–887.

European Commission. Joint Research Centre. Institute for Health and Consumer Protection. (2014). Alternative methods for regulatory toxicology: a state of the art review. (LU: Publications Office).

Eyckmans, J., and Chen, C.S. (2017). 3D culture models of tissues under tension. J Cell Sci *130*, 63–70.

Faustino Martins, J.-M., Fischer, C., Urzi, A., Vidal, R., Kunz, S., Ruffault, P.-L., Kabuss, L., Hube, I., Gazzerro, E., Birchmeier, C., et al. (2020). Self-Organizing 3D Human Trunk Neuromuscular Organoids. Cell Stem Cell *26*, 172-186.e6.

Fischer, M., Rikeit, P., Knaus, P., and Coirault, C. (2016). YAP-Mediated Mechanotransduction in Skeletal Muscle. Front. Physiol. *7*.

Fukada, S., Uezumi, A., Ikemoto, M., Masuda, S., Segawa, M., Tanimura, N., Yamamoto, H., Miyagoe-Suzuki, Y., and Takeda, S. (2007). Molecular Signature of Quiescent Satellite Cells in Adult Skeletal Muscle. Stem Cells *25*, 2448–2459.

Gala, H.P., Saha, D., Venugopal, N., Aloysius, A., and Dhawan, J. (2018). RNA polymerase II pausing regulates a quiescence-dependent transcriptional program, priming cells for cell

cycle reentry (Developmental Biology).

Ghibaudo, M., Di Meglio, J.-M., Hersen, P., and Ladoux, B. (2011). Mechanics of cell spreading within 3D-micropatterned environments. Lab Chip *11*, 805–812.

Gilbert, P.M., and Blau, H.M. (2011). Engineering a stem cell house into a home. Stem Cell Res Ther *2*, 3.

Gilbert, P.M., and Weaver, V.M. (2017). Cellular adaptation to biomechanical stress across length scales in tissue homeostasis and disease. Seminars in Cell & Developmental Biology *67*, 141–152.

Gilbert, P.M., Havenstrite, K.L., Magnusson, K.E.G., Sacco, A., Leonardi, N.A., Kraft, P., Nguyen, N.K., Thrun, S., Lutolf, M.P., and Blau, H.M. (2010). Substrate Elasticity Regulates Skeletal Muscle Stem Cell Self-Renewal in Culture. Science *329*, 1078–1081.

Gillies, A.R., and Lieber, R.L. (2011). Structure and function of the skeletal muscle extracellular matrix: Skeletal Muscle ECM. Muscle Nerve *44*, 318–331.

Giordani, L., He, G.J., Negroni, E., Sakai, H., Law, J.Y.C., Siu, M.M., Wan, R., Corneau, A., Tajbakhsh, S., Cheung, T.H., et al. (2019). High-Dimensional Single-Cell Cartography Reveals Novel Skeletal Muscle-Resident Cell Populations. Molecular Cell *74*, 609-621.e6.

Girardi, F., Taleb, A., Giordani, L., Cadot, B., Datye, A., Ebrahimi, M., Gamage, D.G., Millay, D.P., Gilbert, P.M., and Grand, F.L. (2019). TGF β signaling curbs cell fusion and muscle regeneration (Cell Biology).

Goel, A.J., Rieder, M.-K., Arnold, H.-H., Radice, G.L., and Krauss, R.S. (2017). Niche Cadherins Control the Quiescence-to-Activation Transition in Muscle Stem Cells. Cell Reports *21*, 2236–2250.

Goodman, C.A., Hornberger, T.A., and Robling, A.G. (2015). Bone and skeletal muscle: Key players in mechanotransduction and potential overlapping mechanisms. Bone *80*, 24–36.

Gribova, V., Liu, C.-Y., Nishiguchi, A., Matsusaki, M., Boudou, T., Picart, C., and Akashi, M. (2016). Construction and myogenic differentiation of 3D myoblast tissues fabricated by fibronectin-gelatin nanofilm coating. Biochemical and Biophysical Research Communications *474*, 515–521.

Griffin, M.A. (2004). Adhesion-contractile balance in myocyte differentiation. Journal of Cell Science *117*, 5855–5863.

Grounds, M.D., Sorokin, L., and White, J. (2005). Strength at the extracellular matrix-muscle interface. Scand J Med Sci Sports *15*, 381–391.

Guilluy, C., and Burridge, K. (2015). Nuclear mechanotransduction: Forcing the nucleus to respond. Nucleus *6*, 19–22.

Hannon, K., Kudla, A.J., McAvoy, M.J., Clase, K.L., and Olwin, B.B. (1996). Differentially expressed fibroblast growth factors regulate skeletal muscle development through

autocrine and paracrine mechanisms. Journal of Cell Biology *132*, 1151–1159.

Hastings, R.L., Massopust, R.T., Haddix, S.G., Lee, Y. il, and Thompson, W.J. (2020). Exclusive vital labeling of myonuclei for studying myonuclear arrangement in mouse skeletal muscle tissue. Skeletal Muscle *10*, 15.

Heo, S.-J., Thorpe, S.D., Driscoll, T.P., Duncan, R.L., Lee, D.A., and Mauck, R.L. (2015). Biophysical Regulation of Chromatin Architecture Instills a Mechanical Memory in Mesenchymal Stem Cells. Sci Rep *5*, 16895.

Huang, N.F., Lee, R.J., and Li, S. (2010). Engineering of aligned skeletal muscle by micropatterning. Am J Transl Res *2*, 43–55.

Hwang, I.-Y., Kwak, S., Lee, S., Kim, H., Lee, S.E., Kim, J.-H., Kim, Y.A., Jeon, Y.K., Chung, D.H., Jin, X., et al. (2016). Psat1-Dependent Fluctuations in α-Ketoglutarate Affect the Timing of ESC Differentiation. Cell Metabolism *24*, 494–501.

Iaizzo, P.A., and Durfee, W.K. (2011). Functional Force Assessment of Skeletal Muscles. In Springer Handbook of Medical Technology, R. Kramme, K.-P. Hoffmann, and R.S. Pozos, eds. (Berlin, Heidelberg: Springer Berlin Heidelberg), pp. 273–287.

Iskratsch, T., Wolfenson, H., and Sheetz, M.P. (2014). Appreciating force and shape — the rise of mechanotransduction in cell biology. Nat Rev Mol Cell Biol *15*, 825–833.

Jaalouk, D.E., and Lammerding, J. (2009). Mechanotransduction gone awry. Nat Rev Mol Cell Biol *10*, 63–73.

Juban, G., and Chazaud, B. (2017). Metabolic regulation of macrophages during tissue repair: insights from skeletal muscle regeneration. FEBS Lett *591*, 3007–3021.

Judson, R.N., Tremblay, A.M., Knopp, P., White, R.B., Urcia, R., De Bari, C., Zammit, P.S., Camargo, F.D., and Wackerhage, H. (2012). The Hippo pathway member Yap plays a key role in influencing fate decisions in muscle satellite cells. Journal of Cell Science *125*, 6009–6019.

Judson, R.N., Quarta, M., Oudhoff, M.J., Soliman, H., Yi, L., Chang, C.K., Loi, G., Vander Werff, R., Cait, A., Hamer, M., et al. (2018). Inhibition of Methyltransferase Setd7 Allows the In Vitro Expansion of Myogenic Stem Cells with Improved Therapeutic Potential. Cell Stem Cell *22*, 177-190.e7.

Juhas, M., Engelmayr, G.C., Fontanella, A.N., Palmer, G.M., and Bursac, N. (2014). Biomimetic engineered muscle with capacity for vascular integration and functional maturation in vivo. Proceedings of the National Academy of Sciences *111*, 5508–5513.

Kalman, B., Picart, C., and Boudou, T. (2016). Quick and easy microfabrication of T-shaped cantilevers to generate arrays of microtissues. Biomed Microdevices *18*, 43.

Kästner, S., Elias, M.C., Rivera, A.J., and Yablonka-Reuveni, Z. (2000). Gene expression patterns of the fibroblast growth factors and their receptors during myogenesis of rat satellite cells. J Histochem Cytochem *48*, 1079–1096.

Kim, J.H., Seol, Y.-J., Ko, I.K., Kang, H.-W., Lee, Y.K., Yoo, J.J., Atala, A., and Lee, S.J. (2018). 3D Bioprinted Human Skeletal Muscle Constructs for Muscle Function Restoration. Sci Rep *8*, 12307.

Kjær, M. (2004). Role of Extracellular Matrix in Adaptation of Tendon and Skeletal Muscle to Mechanical Loading. Physiological Reviews *84*, 649–698.

Kozakowska, M., Pietraszek-Gremplewicz, K., Ciesla, M., Seczynska, M., Bronisz-Budzynska, I., Podkalicka, P., Bukowska-Strakova, K., Loboda, A., Jozkowicz, A., and Dulak, J. (2018). Lack of Heme Oxygenase-1 Induces Inflammatory Reaction and Proliferation of Muscle Satellite Cells after Cardiotoxin-Induced Skeletal Muscle Injury. The American Journal of Pathology *188*, 491–506.

Kuang, S., Kuroda, K., Le Grand, F., and Rudnicki, M.A. (2007). Asymmetric Self-Renewal and Commitment of Satellite Stem Cells in Muscle. Cell *129*, 999–1010.

Kural, M.H., and Billiar, K.L. (2013). Regulating tension in three-dimensional culture environments. Experimental Cell Research *319*, 2447–2459.

Lam, M.T., Sim, S., Zhu, X., and Takayama, S. (2006). The effect of continuous wavy micropatterns on silicone substrates on the alignment of skeletal muscle myoblasts and myotubes. Biomaterials *27*, 4340–4347.

Lancaster, M.A., Renner, M., Martin, C.-A., Wenzel, D., Bicknell, L.S., Hurles, M.E., Homfray, T., Penninger, J.M., Jackson, A.P., and Knoblich, J.A. (2013). Cerebral organoids model human brain development and microcephaly. Nature *501*, 373–379.

Lazure, F., Blackburn, D.M., Corchado, A.H., Sahinyan, K., Karam, N., Sharanek, A., Nguyen, D., Lepper, C., Najafabadi, H.S., Perkins, T.J., et al. (2020). Myf6/MRF4 is a myogenic niche regulator required for the maintenance of the muscle stem cell pool. EMBO Rep e49499.

Le Grand, F., Jones, A.E., Seale, V., Scimè, A., and Rudnicki, M.A. (2009). Wnt7a Activates the Planar Cell Polarity Pathway to Drive the Symmetric Expansion of Satellite Stem Cells. Cell Stem Cell *4*, 535–547.

Leckband, D.E., and de Rooij, J. (2014). Cadherin Adhesion and Mechanotransduction. Annu. Rev. Cell Dev. Biol. *30*, 291–315.

Legant, W.R., Pathak, A., Yang, M.T., Deshpande, V.S., McMeeking, R.M., and Chen, C.S. (2009). Microfabricated tissue gauges to measure and manipulate forces from 3D microtissues. Proceedings of the National Academy of Sciences *106*, 10097–10102.

Lepper, C., Partridge, T.A., and Fan, C.-M. (2011). An absolute requirement for Pax7-positive satellite cells in acute injury-induced skeletal muscle regeneration. Development *138*, 3639–3646.

Liu, L., Cheung, T.H., Charville, G.W., and Rando, T.A. (2015). Isolation of skeletal muscle stem cells by fluorescence-activated cell sorting. Nat Protoc *10*, 1612–1624.

Lluís, F., Roma, J., Suelves, M., Parra, M., Aniorte, G., Gallardo, E., Illa, I., Rodríguez, L., Hughes, S.M., Carmeliet, P., et al. (2001). Urokinase-dependent plasminogen activation is

required for efficient skeletal muscle regeneration in vivo. Blood *97*, 1703–1711.

Low, B.C., Pan, C.Q., Shivashankar, G.V., Bershadsky, A., Sudol, M., and Sheetz, M. (2014). YAP/TAZ as mechanosensors and mechanotransducers in regulating organ size and tumor growth. FEBS Letters *588*, 2663–2670.

Maffioletti, S.M., Sarcar, S., Henderson, A.B.H., Mannhardt, I., Pinton, L., Moyle, L.A., Steele-Stallard, H., Cappellari, O., Wells, K.E., Ferrari, G., et al. (2018). Three-Dimensional Human iPSC-Derived Artificial Skeletal Muscles Model Muscular Dystrophies and Enable Multilineage Tissue Engineering. Cell Reports *23*, 899–908.

Mann, C.J., Perdiguero, E., Kharraz, Y., Aguilar, S., Pessina, P., Serrano, A.L., and Muñoz-Cánoves, P. (2011). Aberrant repair and fibrosis development in skeletal muscle. Skeletal Muscle *1*, 21.

Martiel, J.-L., Leal, A., Kurzawa, L., Balland, M., Wang, I., Vignaud, T., Tseng, Q., and Théry, M. (2015). Measurement of cell traction forces with ImageJ. In Methods in Cell Biology, (Elsevier), pp. 269–287.

Mauro, A. (1961). SATELLITE CELL OF SKELETAL MUSCLE FIBERS. The Journal of Biophysical and Biochemical Cytology *9*, 493–495.

McKinnell, I.W., Ishibashi, J., Le Grand, F., Punch, V.G.J., Addicks, G.C., Greenblatt, J.F., Dilworth, F.J., and Rudnicki, M.A. (2008). Pax7 activates myogenic genes by recruitment of a histone methyltransferase complex. Nat Cell Biol *10*, 77–84.

Michaloglou, C., Lehmann, W., Martin, T., Delaunay, C., Hueber, A., Barys, L., Niu, H., Billy, E., Wartmann, M., Ito, M., et al. (2013). The Tyrosine Phosphatase PTPN14 Is a Negative Regulator of YAP Activity. PLoS ONE *8*, e61916.

Mills, R.J., Parker, B.L., Monnot, P., Needham, Elise.J., Vivien, C.J., Ferguson, C., Parton, R.G., James, D.E., Porrello, E.R., and Hudson, J.E. (2019). Development of a human skeletal micro muscle platform with pacing capabilities. Biomaterials *198*, 217–227.

Monge, C., DiStasio, N., Rossi, T., Sébastien, M., Sakai, H., Kalman, B., Boudou, T., Tajbakhsh, S., Marty, I., Bigot, A., et al. (2017). Quiescence of human muscle stem cells is favored by culture on natural biopolymeric films. Stem Cell Res Ther *8*, 104.

Mounier, R., Lantier, L., Leclerc, J., Sotiropoulos, A., Pende, M., Daegelen, D., Sakamoto, K., Foretz, M., and Viollet, B. (2009). Important role for AMPKalpha1 in limiting skeletal muscle cell hypertrophy. FASEB J *23*, 2264–2273.

Nakano, T., Ando, S., Takata, N., Kawada, M., Muguruma, K., Sekiguchi, K., Saito, K., Yonemura, S., Eiraku, M., and Sasai, Y. (2012). Self-Formation of Optic Cups and Storable Stratified Neural Retina from Human ESCs. Cell Stem Cell *10*, 771–785.

Ono, Y., Calhabeu, F., Morgan, J.E., Katagiri, T., Amthor, H., and Zammit, P.S. (2011). BMP signalling permits population expansion by preventing premature myogenic differentiation in muscle satellite cells. Cell Death Differ *18*, 222–234.

Osaki, T., Uzel, S.G.M., and Kamm, R.D. (2020). On-chip 3D neuromuscular model for drug

screening and precision medicine in neuromuscular disease. Nat Protoc *15*, 421–449.

Pallafacchina, G., François, S., Regnault, B., Czarny, B., Dive, V., Cumano, A., Montarras, D., and Buckingham, M. (2010). An adult tissue-specific stem cell in its niche: A gene profiling analysis of in vivo quiescent and activated muscle satellite cells. Stem Cell Research *4*, 77–91.

Paris, N.D., Soroka, A., Klose, A., Liu, W., and Chakkalakal, J.V. (2016). Smad4 restricts differentiation to promote expansion of satellite cell derived progenitors during skeletal muscle regeneration. ELife *5*, e19484.

Passier, R., Orlova, V., and Mummery, C. (2016). Complex Tissue and Disease Modeling using hiPSCs. Cell Stem Cell *18*, 309–321.

Penton, C.M., Badarinarayana, V., Prisco, J., Powers, E., Pincus, M., Allen, R.E., and August, P.R. (2016). Laminin 521 maintains differentiation potential of mouse and human satellite cell-derived myoblasts during long-term culture expansion. Skeletal Muscle *6*, 44.

Pietrosemoli, N., Mella, S., Yennek, S., Baghdadi, M.B., Sakai, H., Sambasivan, R., Pala, F., Di Girolamo, D., and Tajbakhsh, S. (2017). Comparison of multiple transcriptomes exposes unified and divergent features of quiescent and activated skeletal muscle stem cells. Skeletal Muscle *7*, 28.

Pimentel, M.R., Falcone, S., Cadot, B., and Gomes, E.R. (2017). In Vitro Differentiation of Mature Myofibers for Live Imaging. JoVE 55141.

Plotnikov, S.V., Sabass, B., Schwarz, U.S., and Waterman, C.M. (2014). High-Resolution Traction Force Microscopy. In Methods in Cell Biology, (Elsevier), pp. 367–394.

Polio, S.R., Stasiak, S.E., Jamieson, R.R., Balestrini, J.L., Krishnan, R., and Parameswaran, H. (2019). Extracellular matrix stiffness regulates human airway smooth muscle contraction by altering the cell-cell coupling. Sci Rep *9*, 9564.

Potter, C.M.F., Lao, K.H., Zeng, L., and Xu, Q. (2014). Role of Biomechanical Forces in Stem Cell Vascular Lineage Differentiation. Arterioscler Thromb Vasc Biol. *34*, 2184–2190.

Powell, C.A., Smiley, B.L., Mills, J., and Vandenburgh, H.H. (2002). Mechanical stimulation improves tissue-engineered human skeletal muscle. American Journal of Physiology-Cell Physiology *283*, C1557–C1565.

Pratt, S.J.P., and Lovering, R.M. (2014). A stepwise procedure to test contractility and susceptibility to injury for the rodent quadriceps muscle. J Biol Methods *1*.

Quarta, M., Brett, J.O., DiMarco, R., De Morree, A., Boutet, S.C., Chacon, R., Gibbons, M.C., Garcia, V.A., Su, J., Shrager, J.B., et al. (2016). An artificial niche preserves the quiescence of muscle stem cells and enhances their therapeutic efficacy. Nat Biotechnol *34*, 752–759.

Rao, L., Qian, Y., Khodabukus, A., Ribar, T., and Bursac, N. (2018). Engineering human pluripotent stem cells into a functional skeletal muscle tissue. Nat Commun *9*, 126.

Ravasio, A., Vaishnavi, S., Ladoux, B., and Viasnoff, V. (2015). High-resolution imaging of cellular processes across textured surfaces using an indexed-matched elastomer. Acta Biomaterialia *14*, 53–60.

Rodgers, J.T., King, K.Y., Brett, J.O., Cromie, M.J., Charville, G.W., Maguire, K.K., Brunson, C., Mastey, N., Liu, L., Tsai, C.-R., et al. (2014). mTORC1 controls the adaptive transition of quiescent stem cells from G0 to GAlert. Nature *510*, 393–396.

Romanazzo, S., Forte, G., Ebara, M., Uto, K., Pagliari, S., Aoyagi, T., Traversa, E., and Taniguchi, A. (2012). Substrate stiffness affects skeletal myoblast differentiation *in vitro*. Science and Technology of Advanced Materials *13*, 064211.

Ronaldson-Bouchard, K., and Vunjak-Novakovic, G. (2018). Organs-on-a-Chip: A Fast Track for Engineered Human Tissues in Drug Development. Cell Stem Cell *22*, 310–324.

Rozo, M., Li, L., and Fan, C.-M. (2016). Targeting β1-integrin signaling enhances regeneration in aged and dystrophic muscle in mice. Nat Med *22*, 889–896.

Rudnicki, M.A., Le Grand, F., McKinnell, I., and Kuang, S. (2008). The Molecular Regulation of Muscle Stem Cell Function. Cold Spring Harbor Symposia on Quantitative Biology *73*, 323–331.

Safaee, H., Bakooshli, M.A., Davoudi, S., Cheng, R.Y., Martowirogo, A.J., Li, E.W., Simmons, C.A., and Gilbert, P.M. (2017). Tethered Jagged-1 Synergizes with Culture Substrate Stiffness to Modulate Notch-Induced Myogenic Progenitor Differentiation. Cel. Mol. Bioeng. *10*, 501–513.

Sakar, M.S., Neal, D., Boudou, T., Borochin, M.A., Li, Y., Weiss, R., Kamm, R.D., Chen, C.S., and Asada, H.H. (2012). Formation and optogenetic control of engineered 3D skeletal muscle bioactuators. Lab Chip *12*, 4976.

Sambasivan, R., Cheedipudi, S., Pasupuleti, N., Saleh, A., Pavlath, G.K., and Dhawan, J. (2009). The small chromatin-binding protein p8 coordinates the association of anti-proliferative and pro-myogenic proteins at the myogenin promoter. Journal of Cell Science *122*, 3481–3491.

Sambasivan, R., Yao, R., Kissenpfennig, A., Van Wittenberghe, L., Paldi, A., Gayraud-Morel, B., Guenou, H., Malissen, B., Tajbakhsh, S., and Galy, A. (2011). Pax7-expressing satellite cells are indispensable for adult skeletal muscle regeneration. Development *138*, 4333–4333.

Schiaffino, S., and Reggiani, C. (2011). Fiber Types in Mammalian Skeletal Muscles. Physiological Reviews *91*, 1447–1531.

Schneider, A., Francius, G., Obeid, R., Schwinté, P., Hemmerlé, J., Frisch, B., Schaaf, P., Voegel, J.-C., Senger, B., and Picart, C. (2006). Polyelectrolyte Multilayers with a Tunable Young's Modulus: Influence of Film Stiffness on Cell Adhesion. Langmuir *22*, 1193–1200.

Shamir, E.R., and Ewald, A.J. (2014). Three-dimensional organotypic culture: experimental models of mammalian biology and disease. Nat Rev Mol Cell Biol *15*, 647–664.

Sheehan, S.M., and Allen, R.E. (1999). Skeletal muscle satellite cell proliferation in response to members of the fibroblast growth factor family and hepatocyte growth factor. J Cell Physiol *181*, 499–506.

Simian, M., and Bissell, M.J. (2017). Organoids: A historical perspective of thinking in three dimensions. Journal of Cell Biology *216*, 31–40.

Sneddon, L.U. (2003). The evidence for pain in fish: the use of morphine as an analgesic. Applied Animal Behaviour Science *83*, 153–162.

Stantzou, A., Schirwis, E., Swist, S., Alonso-Martin, S., Polydorou, I., Zarrouki, F., Mouisel, E., Beley, C., Julien, A., Le Grand, F., et al. (2017). BMP signaling regulates satellite cell-dependent postnatal muscle growth. Development *144*, 2737–2747.

Steward, A.J., and Kelly, D.J. (2015). Mechanical regulation of mesenchymal stem cell differentiation. J. Anat. *227*, 717–731.

Stoecklin, C., Yue, Z., Chen, W.W., de Mets, R., Fong, E., Studer, V., and Viasnoff, V. (2018). A New Approach to Design Artificial 3D Microniches with Combined Chemical, Topographical, and Rheological Cues. Adv. Biosys. *2*, 1700237.

Strale, P.-O., Azioune, A., Bugnicourt, G., Lecomte, Y., Chahid, M., and Studer, V. (2016). Multiprotein Printing by Light-Induced Molecular Adsorption. Adv. Mater. *28*, 2024–2029.

Strzyz, P. (2016). May the force be with you. Nat Rev Mol Cell Biol *17*, 533–533.

Sun, Z., Guo, S.S., and Fässler, R. (2016). Integrin-mediated mechanotransduction. Journal of Cell Biology *215*, 445–456.

Swasdison, S., and Mayne, R. (1992). Formation of highly organized skeletal muscle fibers in vitro. Comparison with muscle development in vivo. J Cell Sci *102 (Pt 3)*, 643–652.

Tan, Q., Choi, K.M., Sicard, D., and Tschumperlin, D.J. (2017). Human airway organoid engineering as a step toward lung regeneration and disease modeling. Biomaterials *113*, 118–132.

Trensz, F., Lucien, F., Couture, V., Söllrald, T., Drouin, G., Rouleau, A.-J., Grandbois, M., Lacraz, G., and Grenier, G. (2015). Increased microenvironment stiffness in damaged myofibers promotes myogenic progenitor cell proliferation. Skeletal Muscle *5*, 5.

Trichet, L., Le Digabel, J., Hawkins, R.J., Vedula, S.R.K., Gupta, M., Ribrault, C., Hersen, P., Voituriez, R., and Ladoux, B. (2012). Evidence of a large-scale mechanosensing mechanism for cellular adaptation to substrate stiffness. Proceedings of the National Academy of Sciences *109*, 6933–6938.

Uhler, C., and Shivashankar, G.V. (2017). Regulation of genome organization and gene expression by nuclear mechanotransduction. Nat Rev Mol Cell Biol *18*, 717–727.

Urciuolo, A., Quarta, M., Morbidoni, V., Gattazzo, F., Molon, S., Grumati, P., Montemurro,

F., Tedesco, F.S., Blaauw, B., Cossu, G., et al. (2013). Collagen VI regulates satellite cell self-renewal and muscle regeneration. Nat Commun *4*, 1964.

Verma, M., Asakura, Y., Murakonda, B.S.R., Pengo, T., Latroche, C., Chazaud, B., McLoon, L.K., and Asakura, A. (2018). Muscle Satellite Cell Cross-Talk with a Vascular Niche Maintains Quiescence via VEGF and Notch Signaling. Cell Stem Cell *23*, 530-543.e9.

Walker, M., Godin, M., and Pelling, A.E. (2018). A vacuum-actuated microtissue stretcher for long-term exposure to oscillatory strain within a 3D matrix. Biomed Microdevices *20*, 43.

Weiswald, L.-B., Bellet, D., and Dangles-Marie, V. (2015). Spherical Cancer Models in Tumor Biology. Neoplasia *17*, 1–15.

Yin, H., Price, F., and Rudnicki, M.A. (2013). Satellite Cells and the Muscle Stem Cell Niche. Physiological Reviews *93*, 23–67.

Zhang, C., and Gao, Y. (2014). Effects of aging on the lateral transmission of force in rat skeletal muscle. Journal of Biomechanics *47*, 944–948.

Zhao, J., Tian, Z., Kadomatsu, T., Xie, P., Miyata, K., Sugizaki, T., Endo, M., Zhu, S., Fan, H., Horiguchi, H., et al. (2018). Age-dependent increase in angiopoietin-like protein 2 accelerates skeletal muscle loss in mice. J. Biol. Chem. *293*, 1596–1609.

Zinkle, A., and Mohammadi, M. (2019). Structural Biology of the FGF7 Subfamily. Front. Genet. *10*, 102.

Zismanov, V., Chichkov, V., Colangelo, V., Jamet, S., Wang, S., Syme, A., Koromilas, A.E., and Crist, C. (2016). Phosphorylation of eIF2 α Is a Translational Control Mechanism Regulating Muscle Stem Cell Quiescence and Self-Renewal. Cell Stem Cell *18*, 79–90.